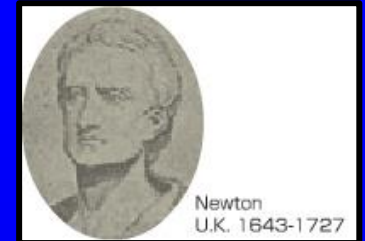


Princípios de óptica do tecido para terapia e diagnóstico

Martha Simões Ribeiro
Laboratório de Terapia Óptica
Centro de Lasers e Aplicações
IPEN-CNEN/SP

Breve histórico



- Século 17: Sir Isaac Newton mostrou que a luz branca é feita de diferentes cores (teoria corpuscular)





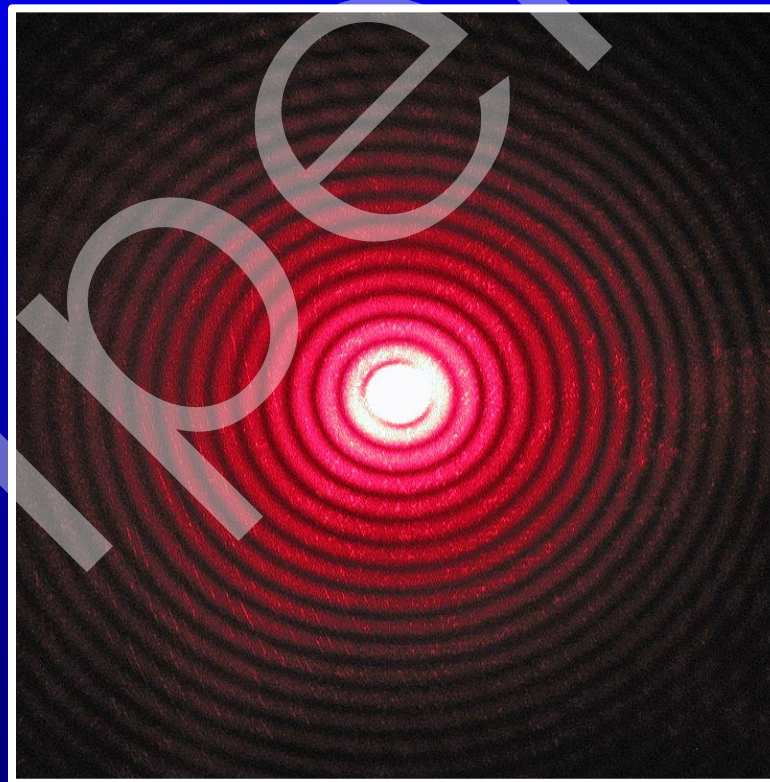
Huygens
Netherlands 1629-1695



Young
U.K. 1773-1829

Breve histórico

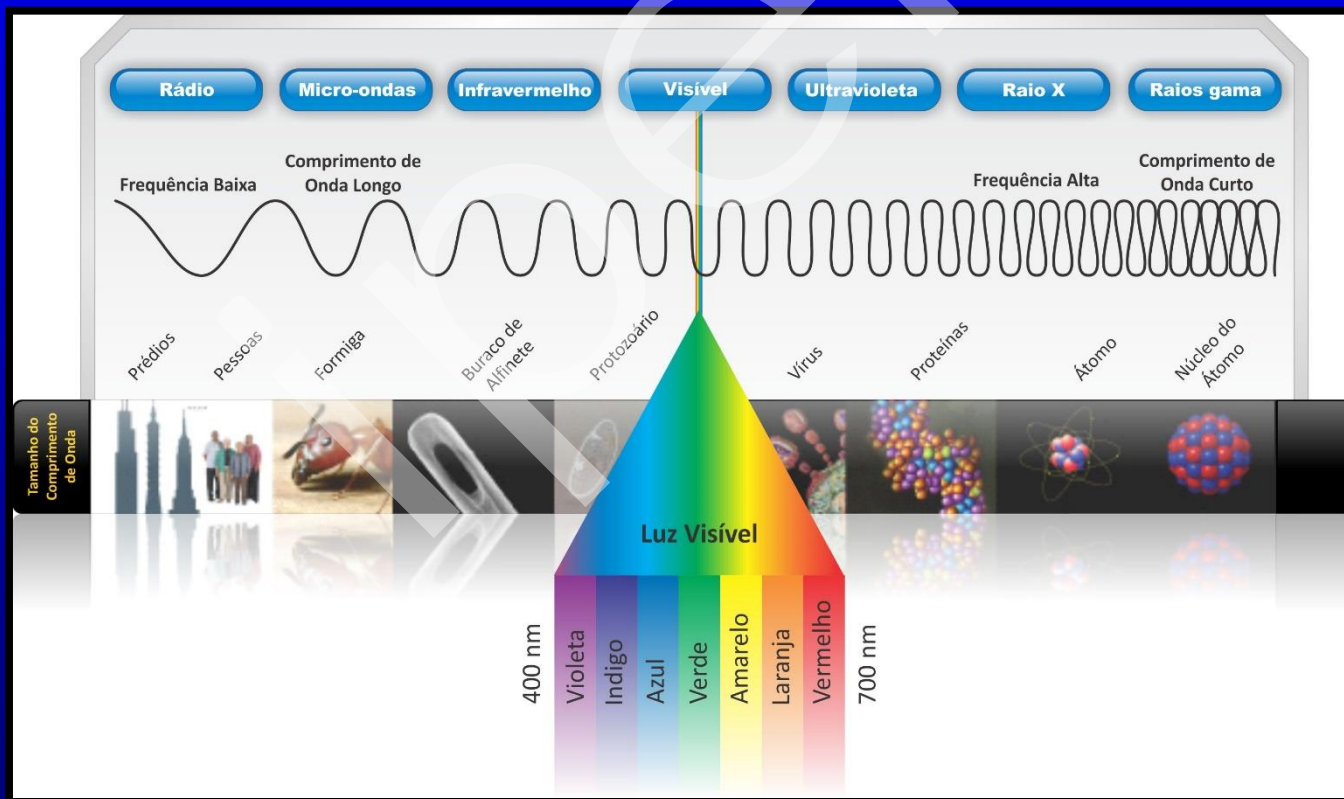
- Século 18: Huygens, Fresnel e Young mostraram que luz se comportava como onda



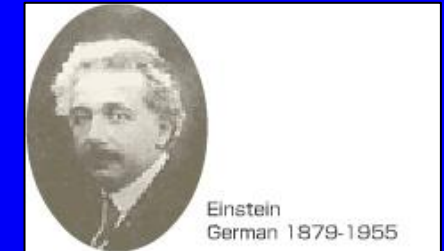
Breve histórico



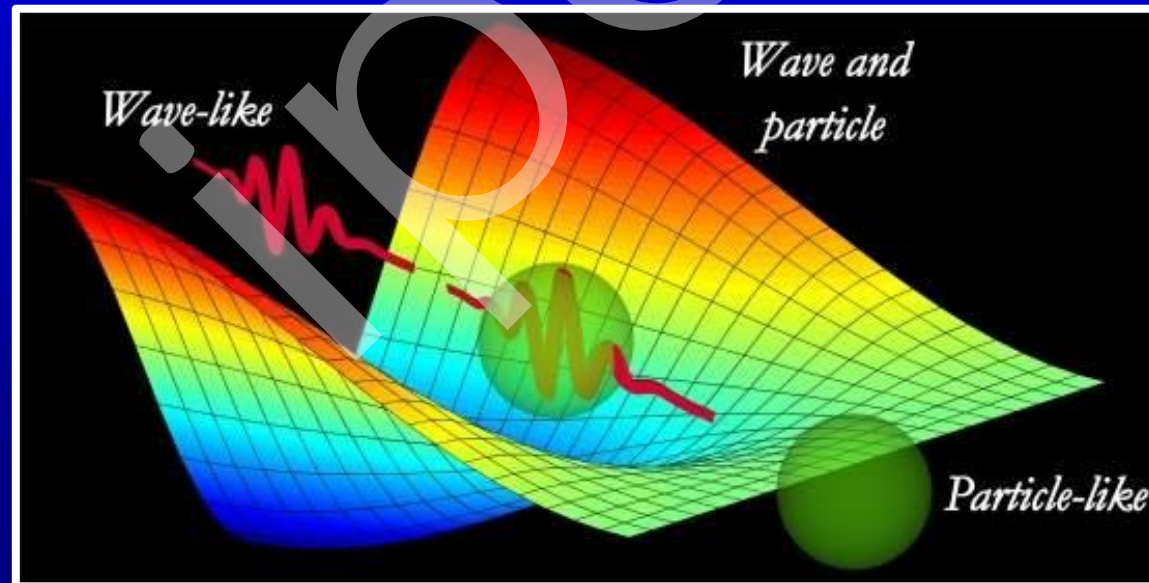
- Século 19: Luz é onda eletromagnética !!!!
(Maxwell)



Breve histórico



- Início do século 20: Max Planck e, mais tarde, Albert Einstein propõem que a luz era uma onda, bem como uma partícula (dualidade na natureza da luz)



Atualmente...

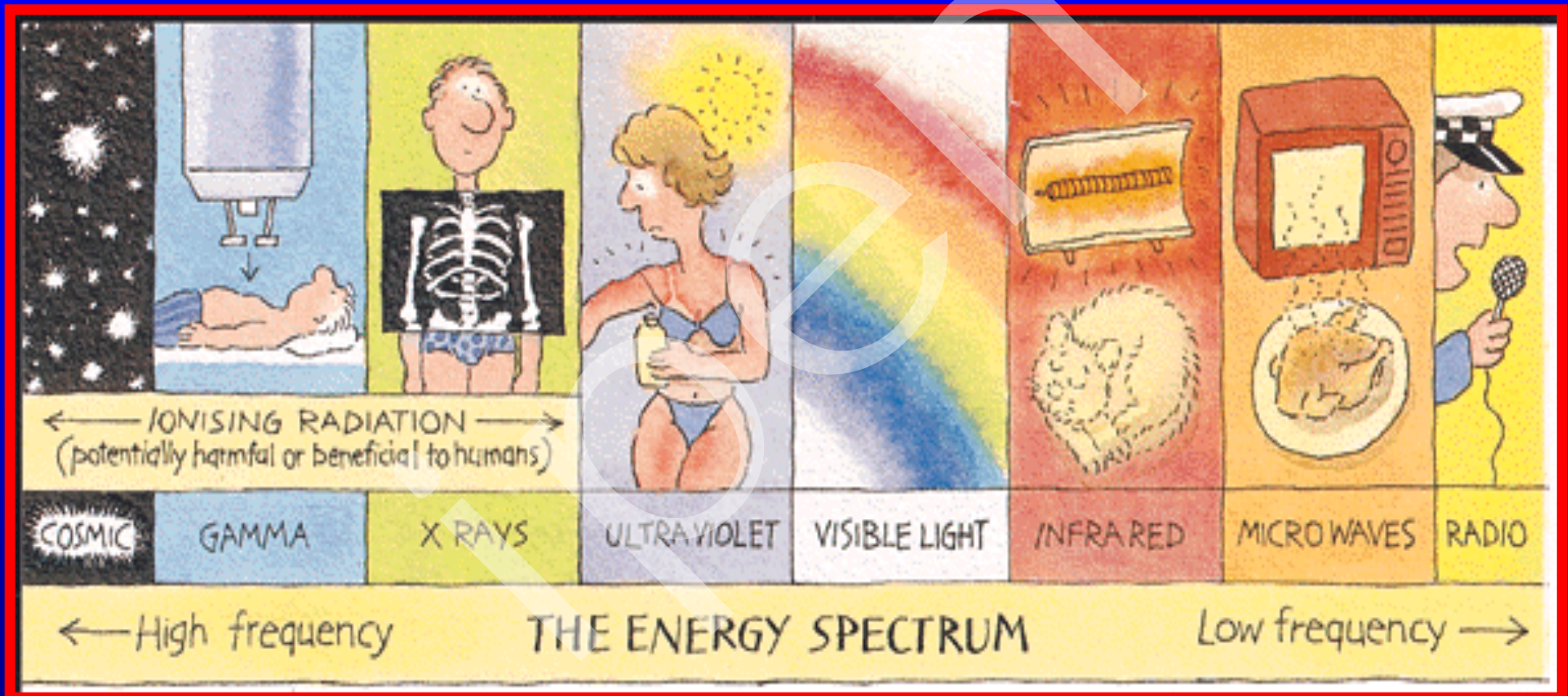


Fios de cobre: 10 Mb/s → downloads 1,25 MB/s
Fibra óptica: 10 Gb/s → downloads 1,25 MB/s

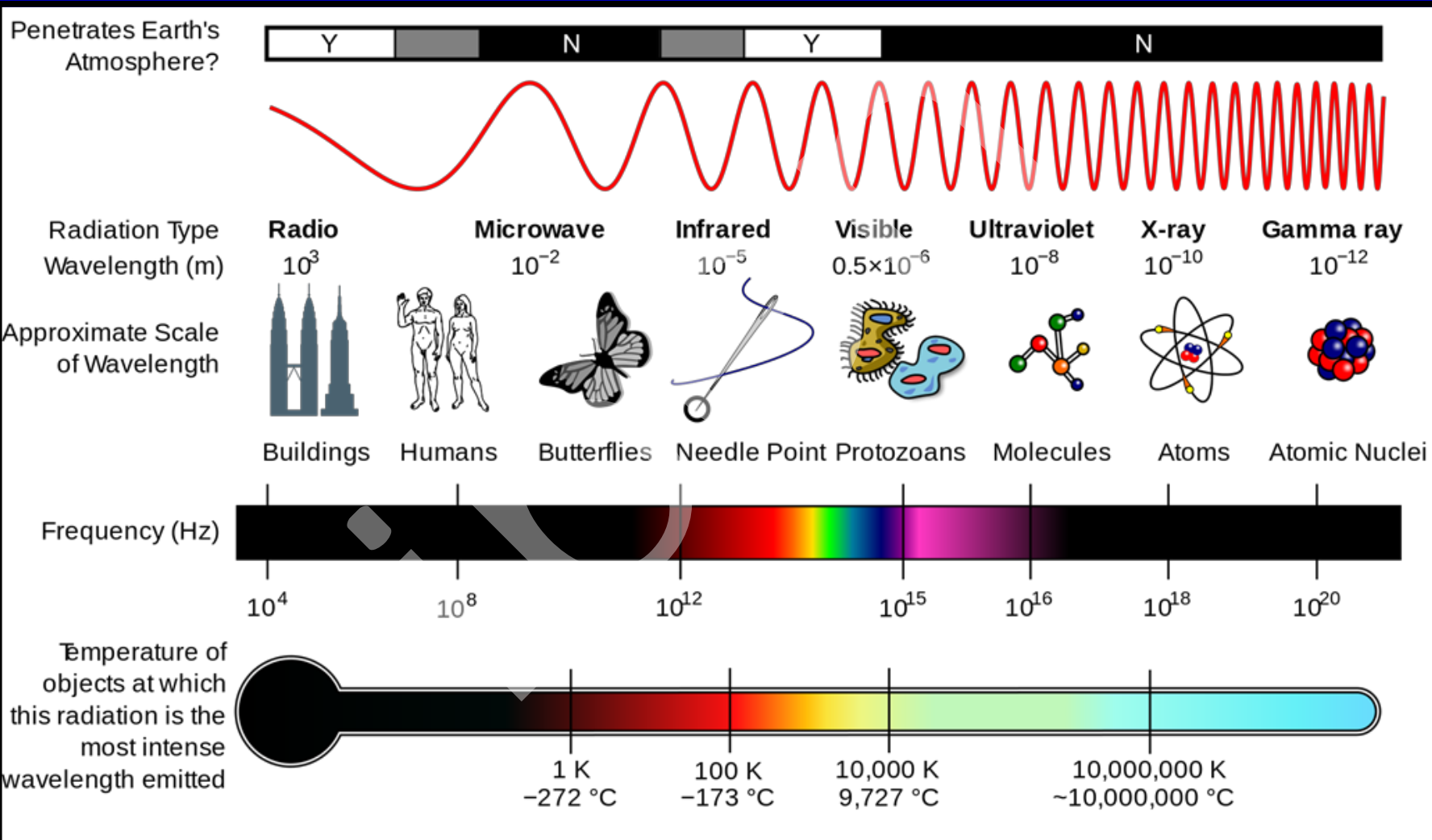
Tipos de Radiação

- *Corpuscular*: gerada por partículas com velocidade muito alta que carregam energia devido ao seu movimento (energia cinética). Ex: partículas α , β , neutrons (geradas por aceleradores lineares, ciclotrons, etc).
- *Eletromagnética*: gerada por fótons (ou quanta), que são pacotes de pequenas unidades de energia. Não contém matéria (não possui massa ou peso).

Radiação Eletromagnética



Radiação Eletromagnética



Características da radiação EM

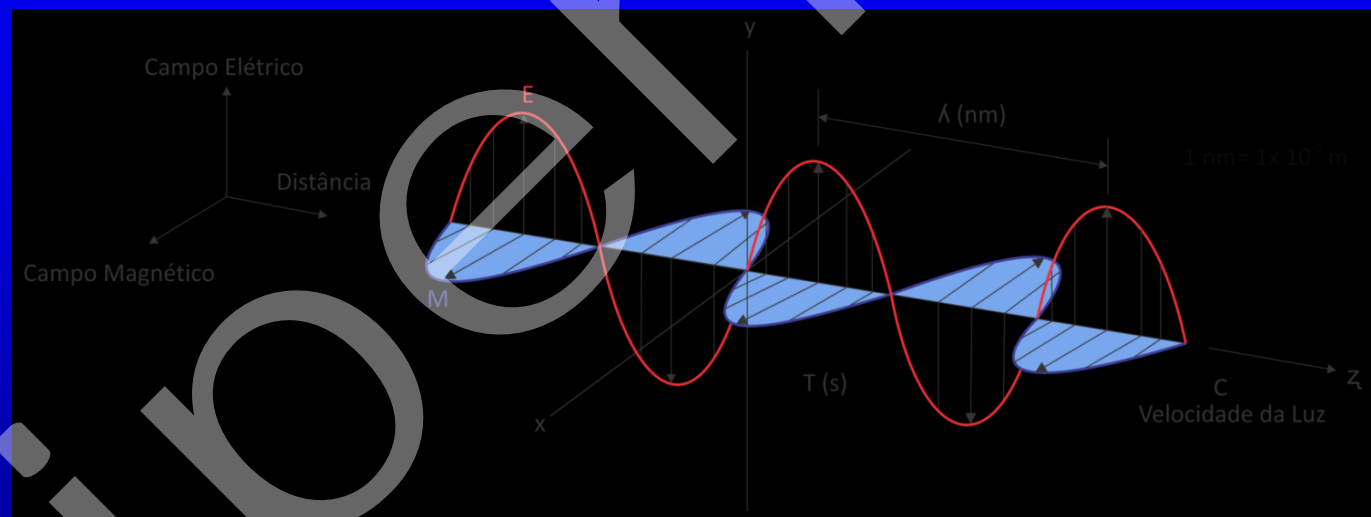
$$E = h \cdot v$$

($h=6,626 \times 10^{-34} \text{ J.s}$ ou $4,136 \times 10^{-15} \text{ eV.s}$)

Frequência (v) [Hz]

$$v = c/\lambda$$

$$E [\text{Kev}] = 1.24/\lambda [\text{nm}]$$



Comprimento de onda (m)

$$\lambda = c/v = c.h/E$$

$$\text{Velocidade (c)} = 3 \cdot 10^8 \text{ m/s}$$

ESPECTRO ELETROMAGNÉTICO

Tipo de radiação	Freqüência (Hz)	Comprimento de onda	Tipo de transição
raios gama	$10^{20} - 10^{24}$	< 10^{-12} m	nuclear
raios x	$10^{17} - 10^{20}$	1 nm - 1 pm	elétron mais interno
ultravioleta	$10^{15} - 10^{17}$	400 - 1 nm	elétron mais externo
visível	$4 - 7,5 \times 10^{14}$	750 - 400 nm	elétron mais externo
infravermelho próximo	$1 \times 10^{14} - 4 \times 10^{14}$	2,5 nm - 750 nm	elétron mais externo, vibrações moleculares
infravermelho	$10^{13} - 10^{14}$	25 - 2,5 mm	vibrações moleculares
microondas	$3 \times 10^{11} - 10^{13}$	1 mm - 25 mm	rotações moleculares, inversão de paridade do spin eletrônico
ondas de rádio	< 3×10^{11}	> 1 mm	inversão de paridade do spin nuclear

↑
ionização

dissociação

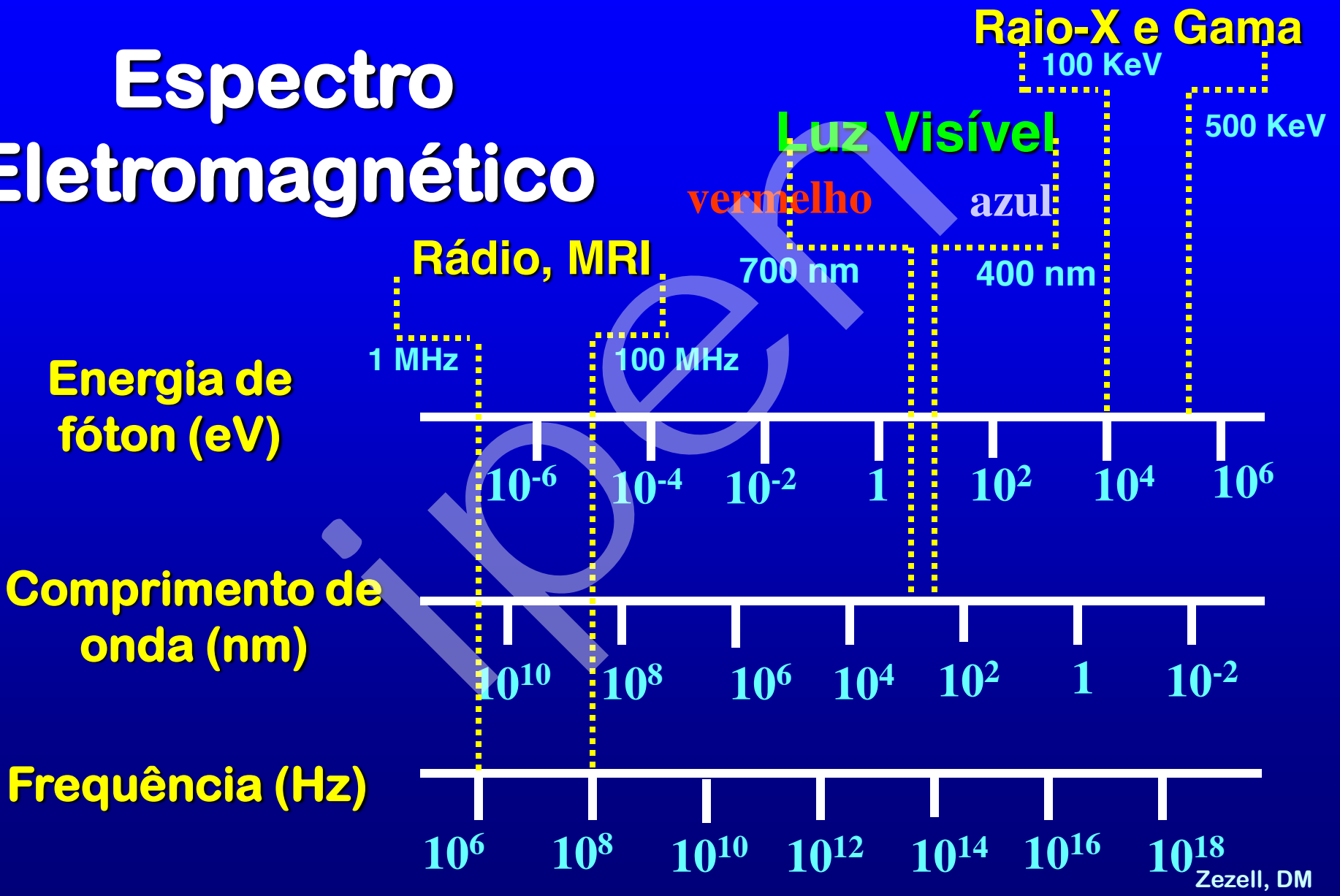
Energias de excitação eletrônica

Energias de vibração

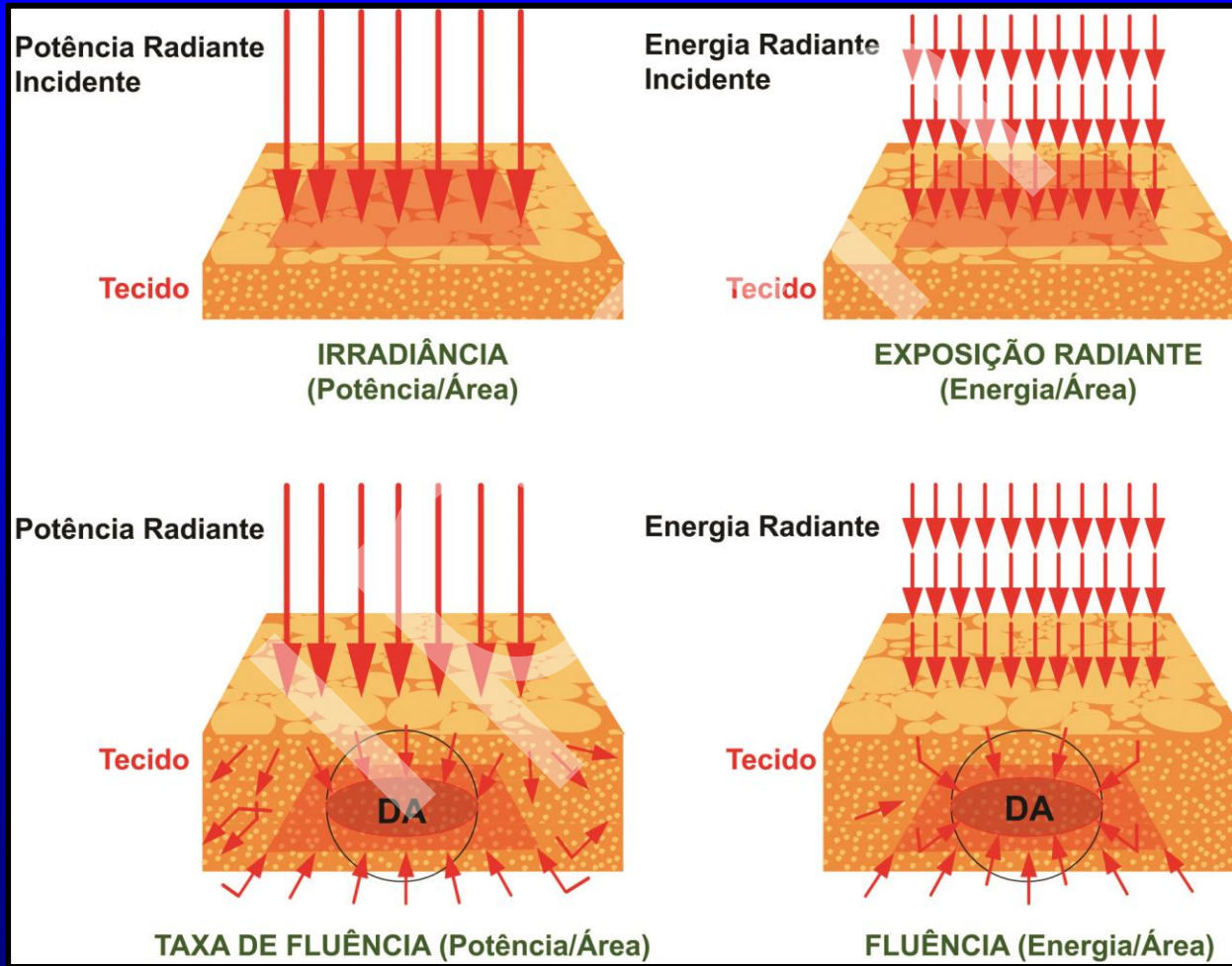
Energias de rotação

* níveis de energia separados por um campo magnético

Espectro Eletromagnético



Conceitos radiométricos



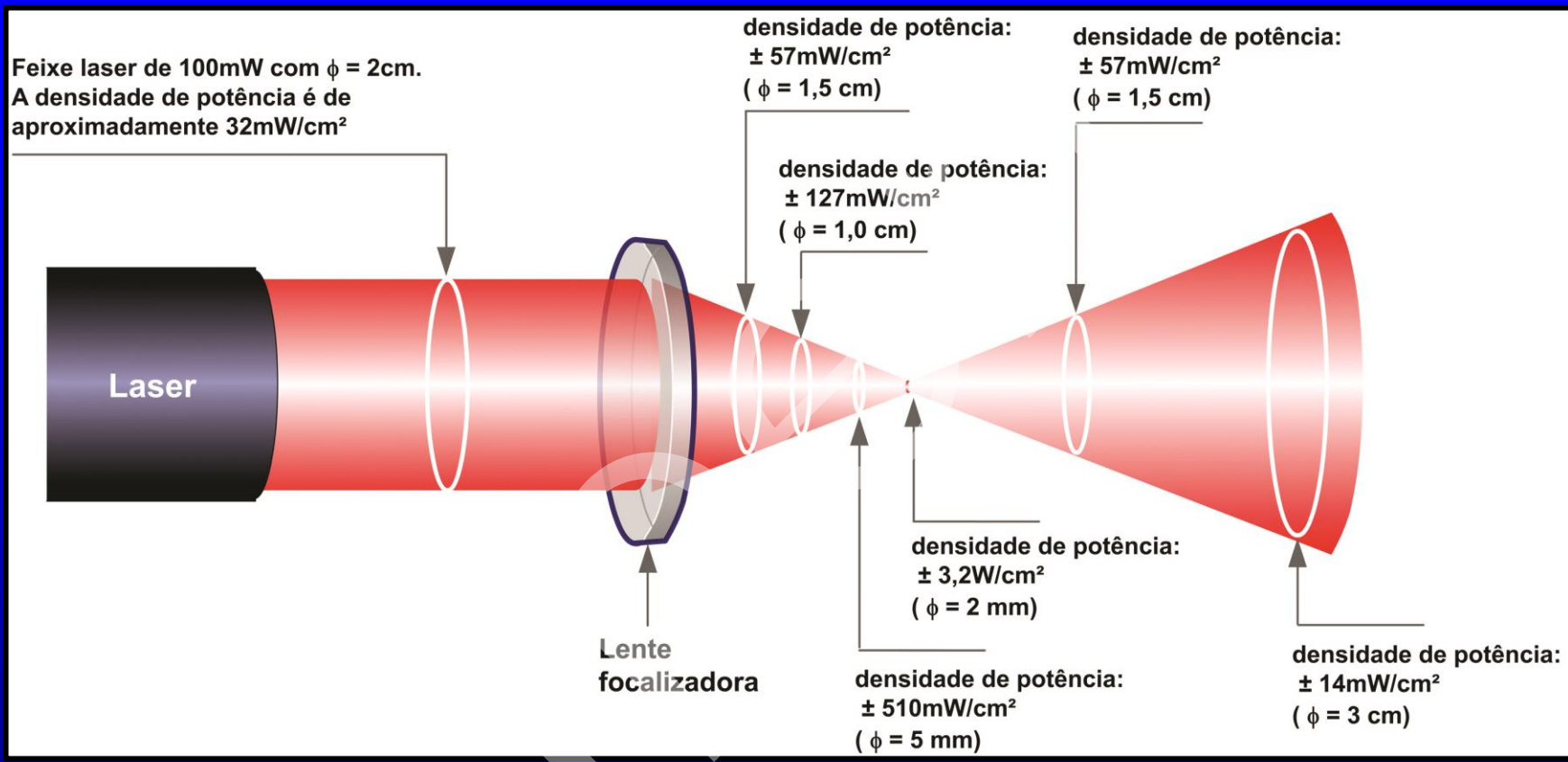
(Sliney, 2007)

Densidade de Potência (Irradiância / Taxa de Fluência)

(potência de saída da luz, por unidade de
área)

**Grandeza física que avalia a
possibilidade de dano microtérmico**

$$I \text{ (W/cm}^2\text{)} = \frac{P \text{ (W)}}{A \text{ (cm}^2\text{)}}$$





Desenho esquemático de um feixe paralelo que incide sobre o olho. O feixe é focalizado na retina. A densidade de potência torna-se tão alta, que pode ocorrer dano

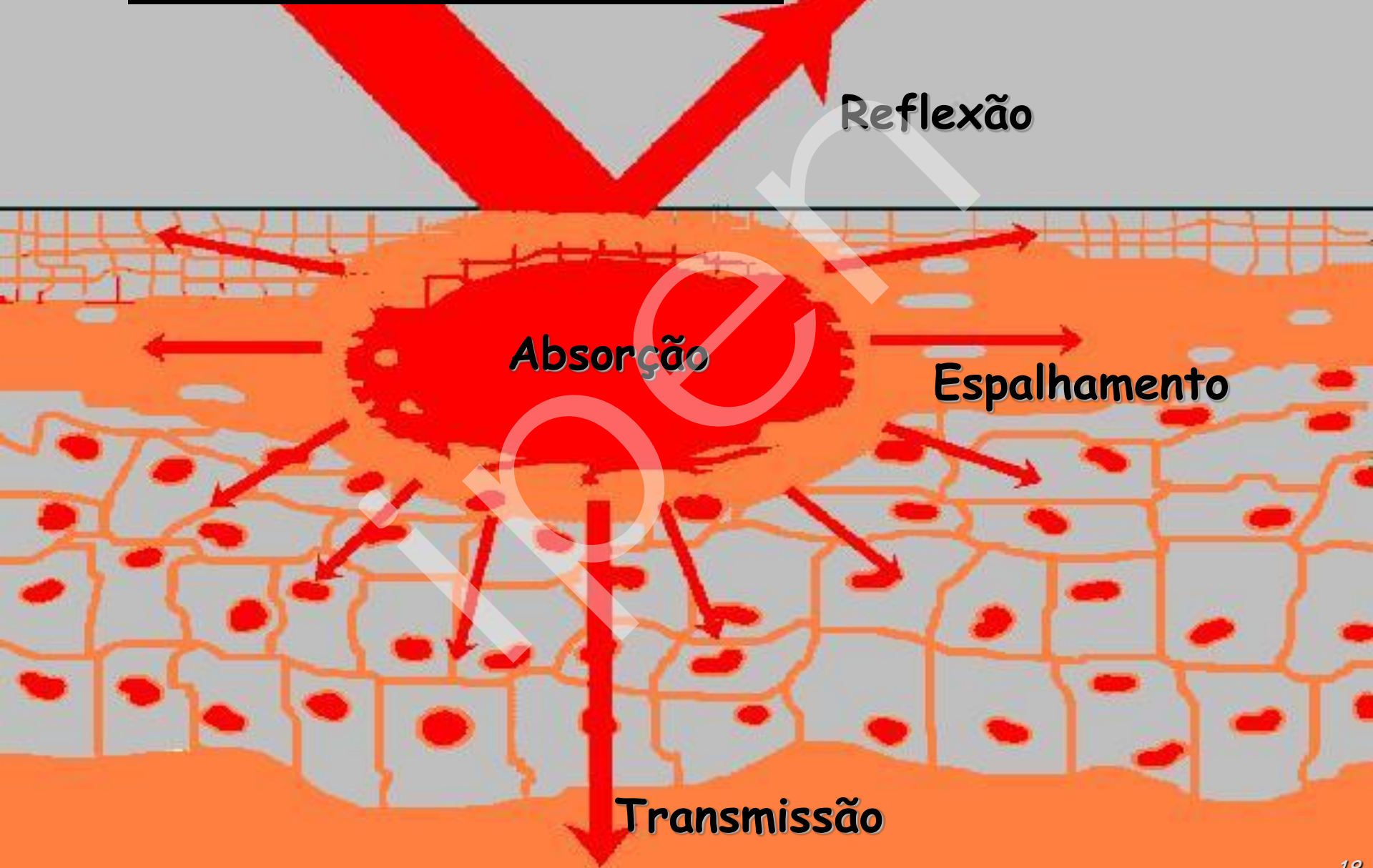
Densidade de Energia (Exposição Radiante / Fluênciа)

(quantidade de energia, por unidade de área, transferida à matéria)

$$DE \text{ (J/cm}^2\text{)} = \frac{E \text{ (J)}}{A \text{ (cm}^2\text{)}}$$

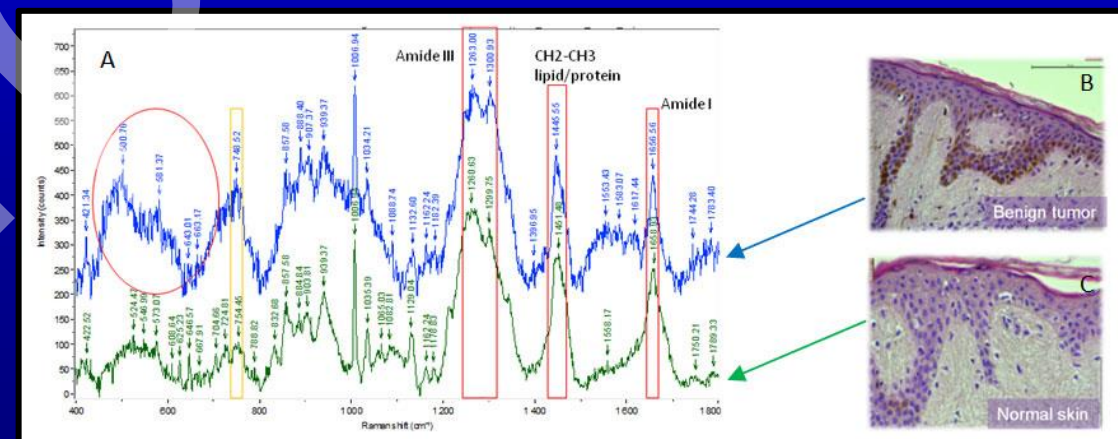
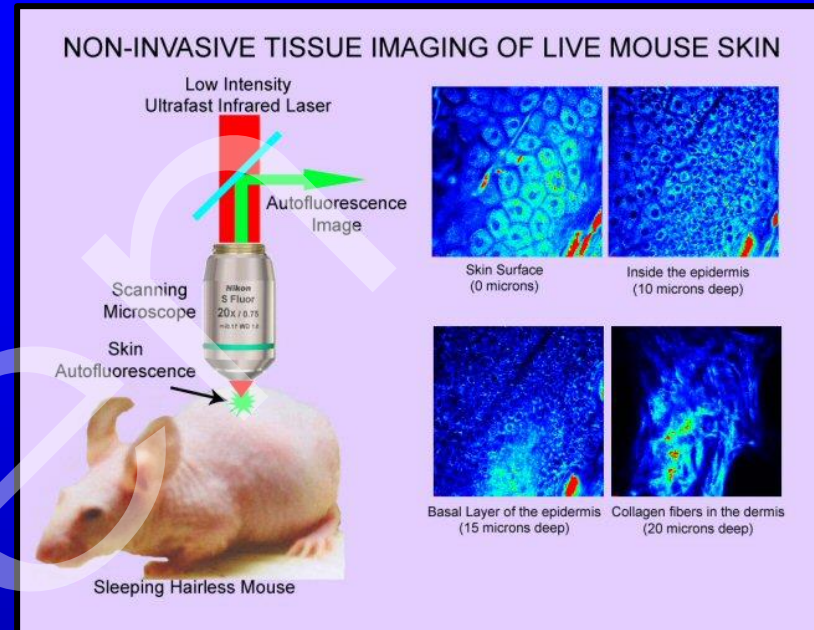
$$E \text{ (J)} = P \text{ (W)} \times t \text{ (s)}$$

INTERAÇÃO DA LUZ COM O TECIDO



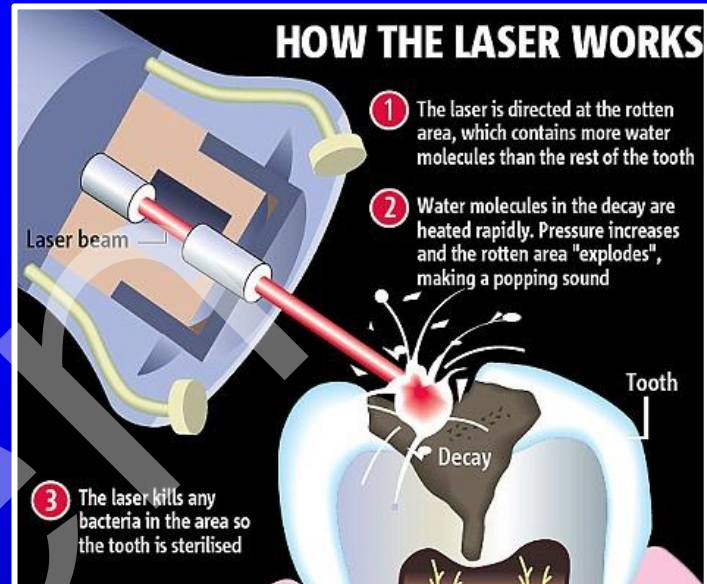
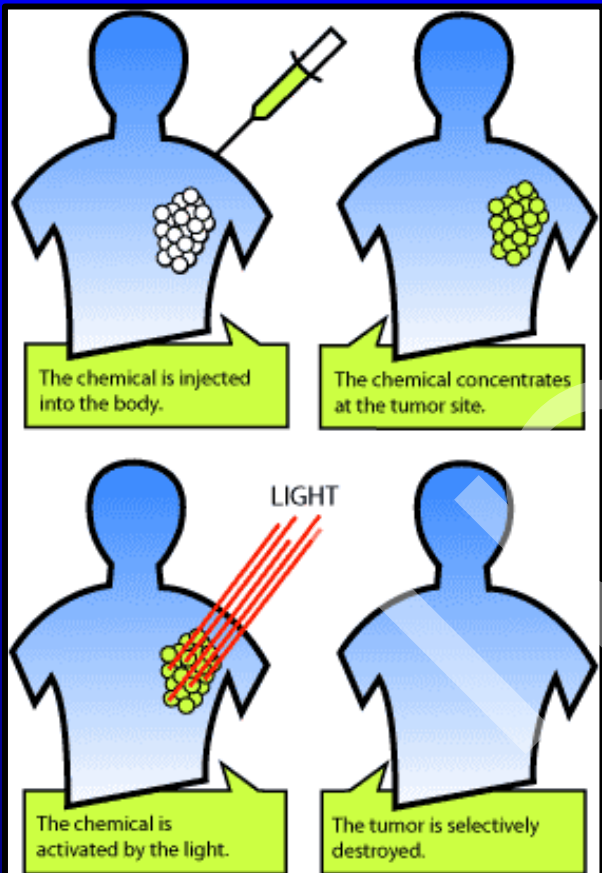
Onde o tecido afeta a luz ?

técnicas diagnósticas: imagem, espectroscopia, sensores



Onde a luz afeta o tecido?

técnicas terapêuticas: incisão cirúrgica, ablação, PDT



Refractive index = speed of light in air

speed of light in substance

Refraction

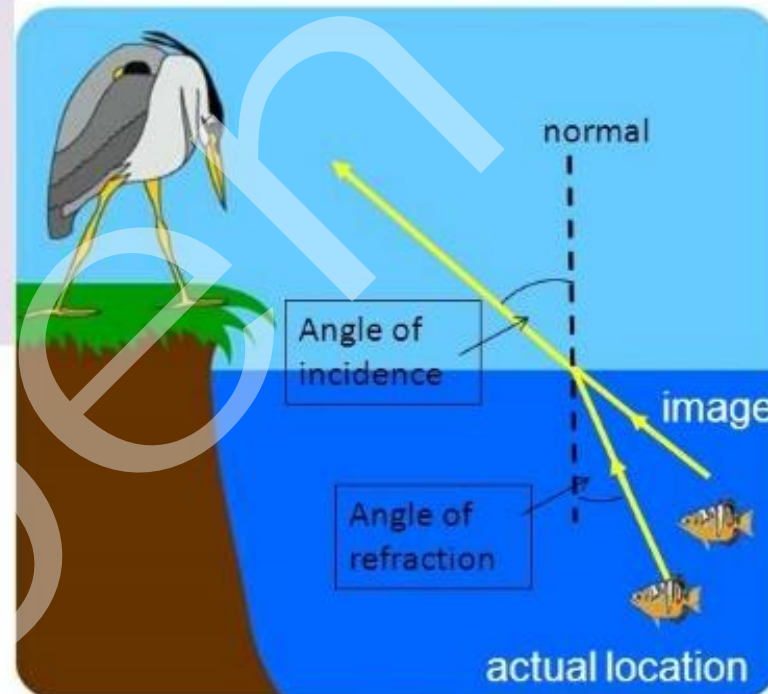
- In a **denser** medium the waves travels **slower**
- Wave changes direction = **refraction**
- If **slowed** down – refract **towards** the normal
- If travelling **faster** = refract **away** from normal

Snell's Law

- Links the angles of **incidence** and **refraction** when waves travel from one medium to another.
- The **constant** is related to the refractive index (n) of each material

$$\frac{\sin i}{\sin r} = \frac{n_r}{n_i}$$

n_r - refractive index of medium ray is travelling into
 n_i - refractive index of medium ray is travelling from



Tissue / Cell Component	Refractive Index
water	1.33
collagen hydrated	1.43
collagen dehydrated	1.53
melanin	1.7
stratum corneum	1.55
adipose tissue	1.46
extracellular fluid	1.35
cytoplasm	1.37
nucleus	1.39
mitochondria	1.42

Absorção

- A absorção é devido à conversão parcial de energia luminosa em outra forma de energia (química, térmica, mecânica,...) no material absorvedor.
- As propriedades de transparência ou opacidade dependem do comprimento de onda da radiação incidente e do tecido.

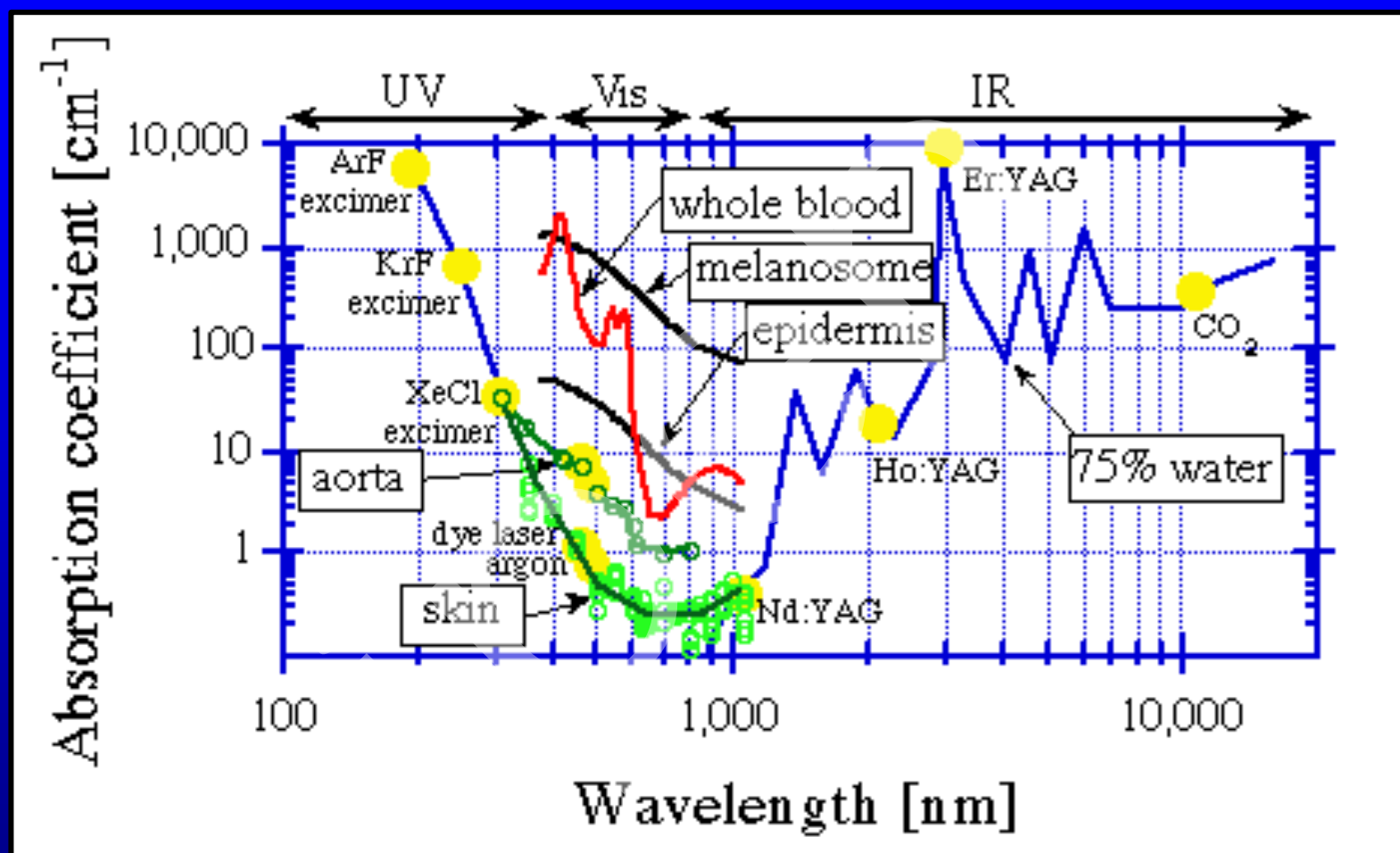
Ex. A córnea é transparente no visível e absorvedora no UV

Lei de Lambert-Beer

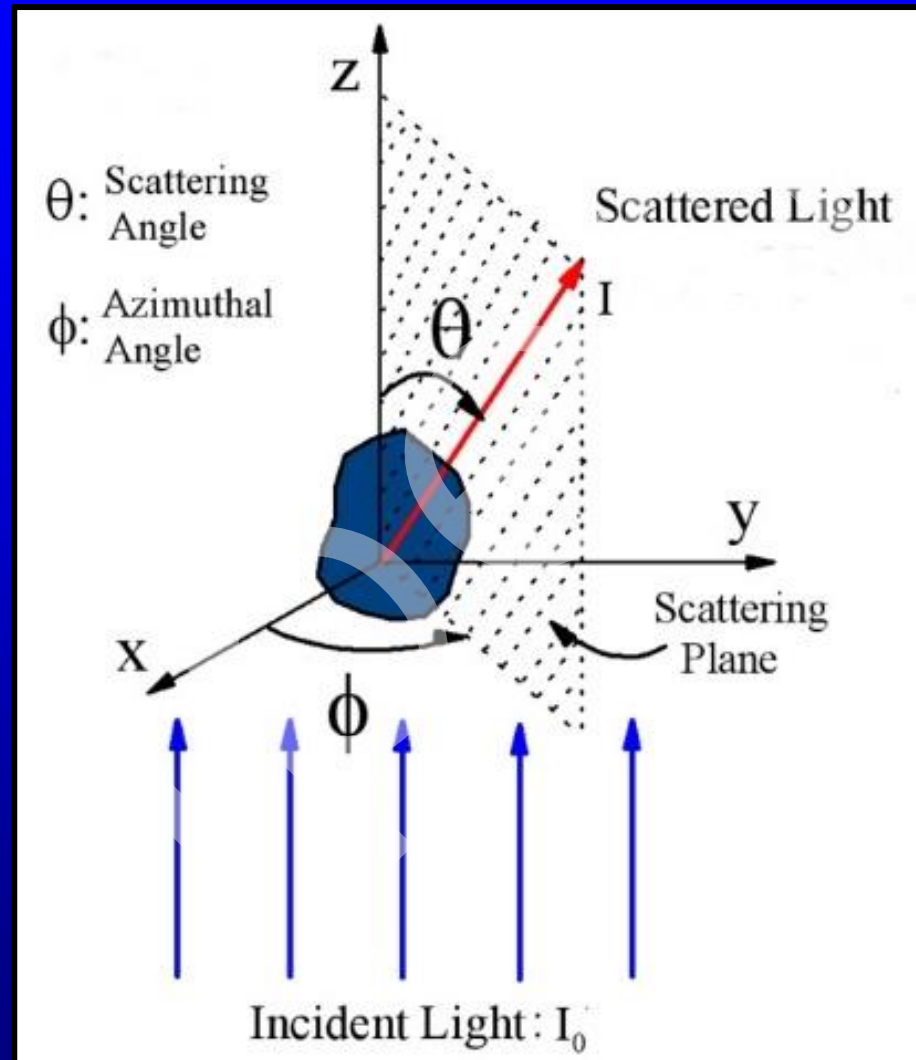
$$I(x) = I_0 e^{-\mu_a x}$$

Absorção predomina sobre o espalhamento

Comprimento de absorção (L_a) é $1/\mu_a$ e corresponde à distância x na qual a intensidade cai para $1/e$ (~ 37%) do seu valor de incidência I_0 .

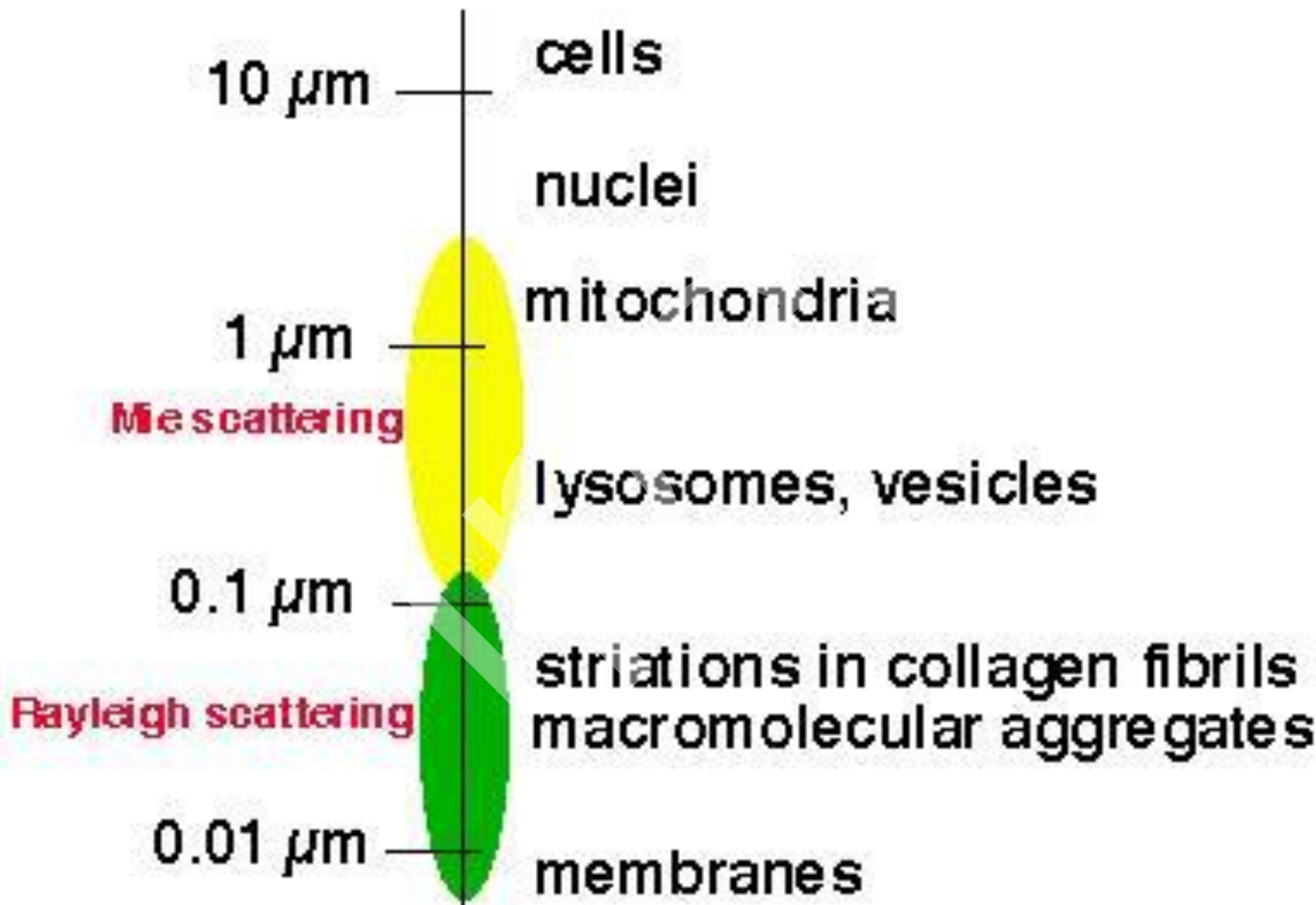


Espalhamento



- A luz espalhada pelo tecido interagiu com a ultraestrutura do tecido. A ultraestrutura vai de membrana, organelas celulares, células, fibras.
- Espalhamento da luz por estruturas da ordem de λ é descrito pelo espalhamento Mie.
- Espalhamento da luz por estruturas muito menores que λ é descrito pelo espalhamento Rayleigh.

Hierarchy of ultrastructure



Espalhamento elástico (fóton incidente e espalhado têm a mesma frequência)

Tipo Rayleigh

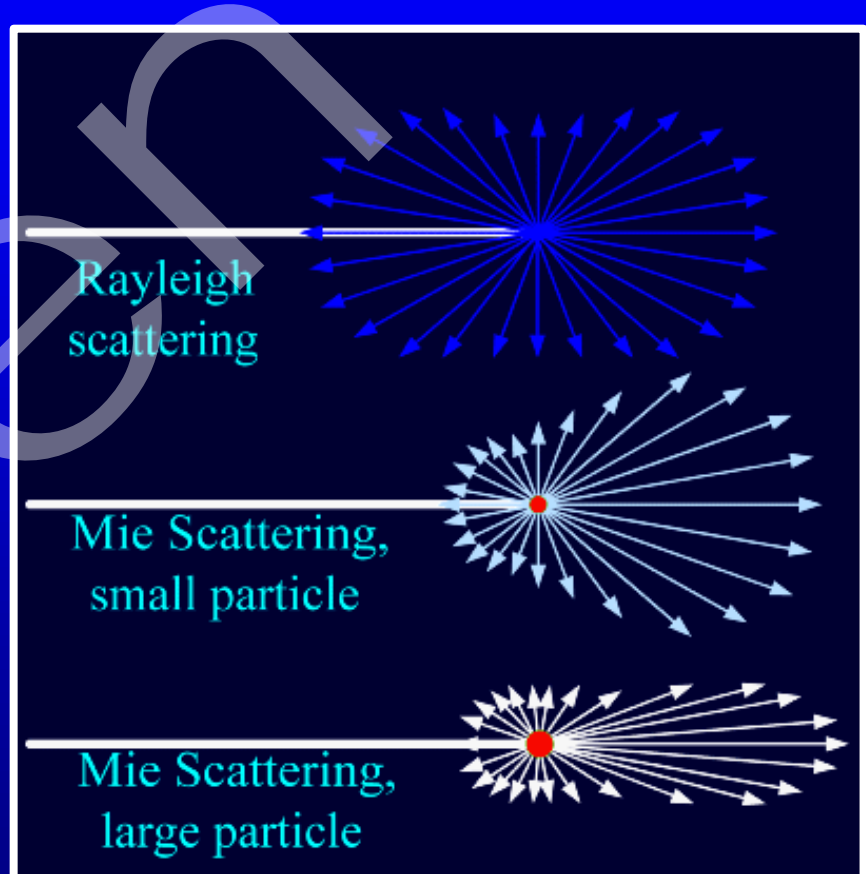
Partícula $\ll \lambda$
difuso, isotrópico

$$\mu_s \propto 1/\lambda^4$$

Tipo Mie

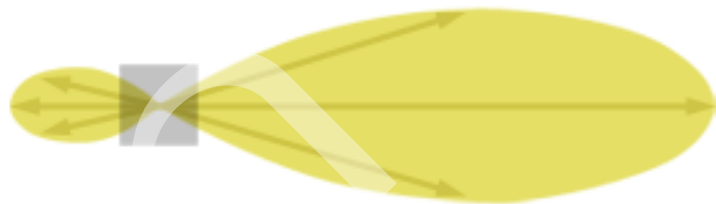
Partícula $\approx \lambda$
dirigido, anisotrópico

$$\mu_s \propto 1/\lambda^{1/4}$$

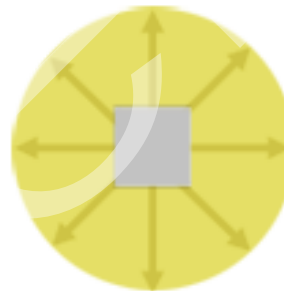




Forward scattering



Isotropic scattering



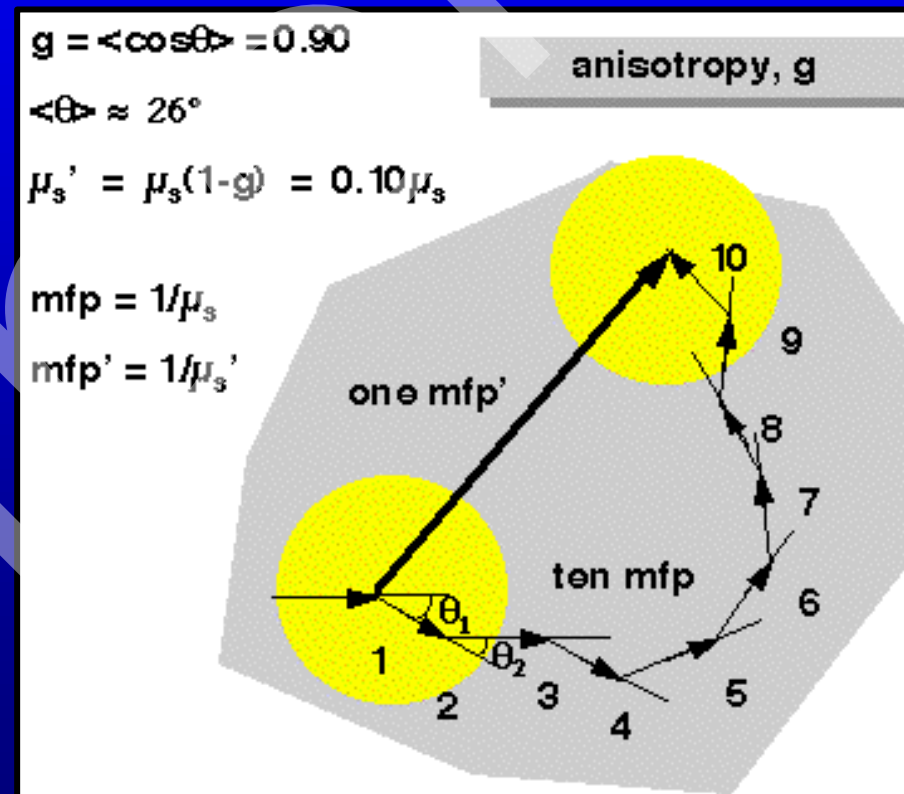
Backward scattering

Espalhamento reduzido

$$\mu_s' = \mu_s(1 - g) [\text{cm}^{-1}]$$

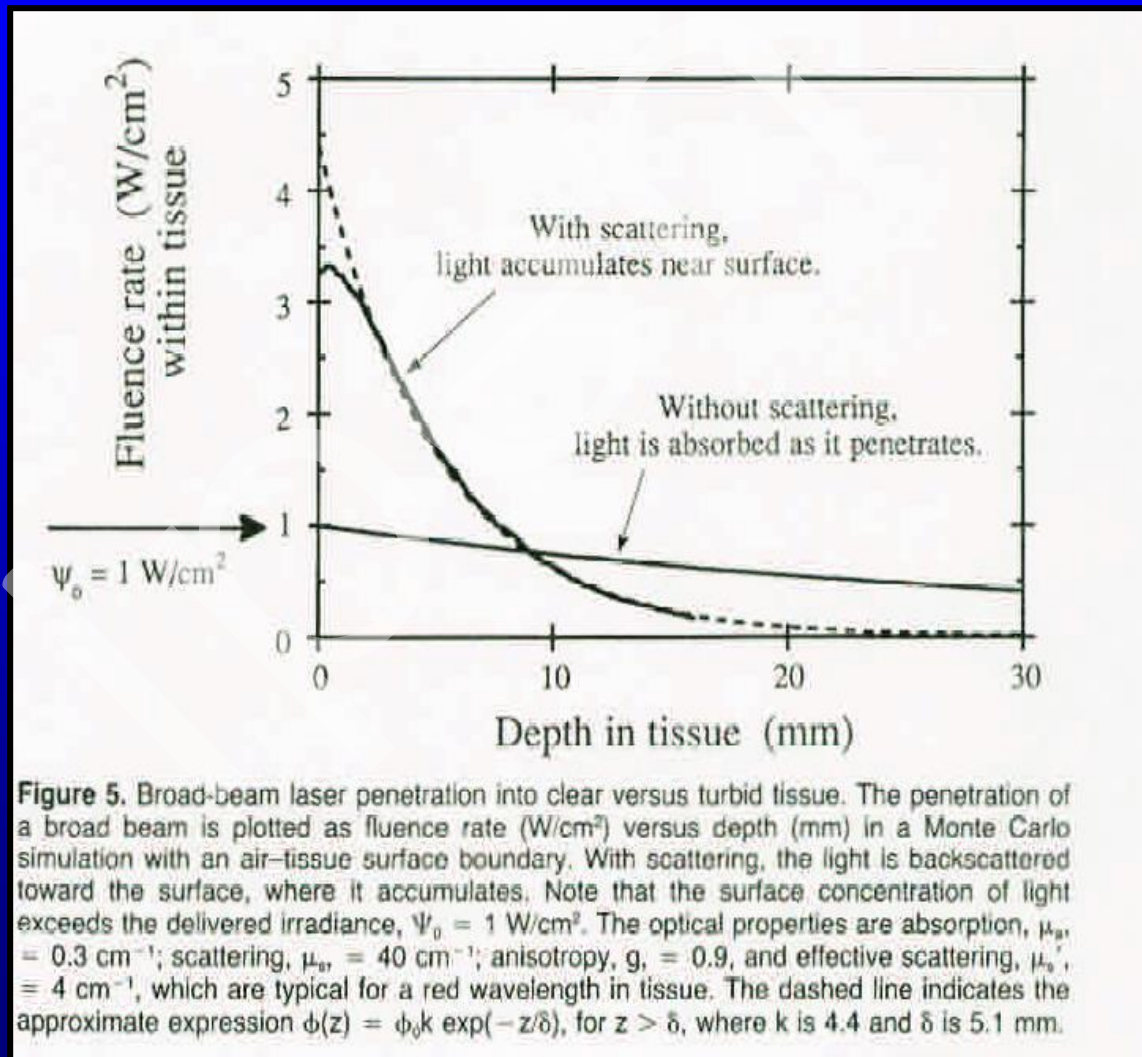
g : coeficiente de anisotropia

O valor de g varia no intervalo de 0 a 1: $g=0$, corresponde ao espalhamento isotrópico e $g=1$ corresponde ao espalhamento completamente dirigido.

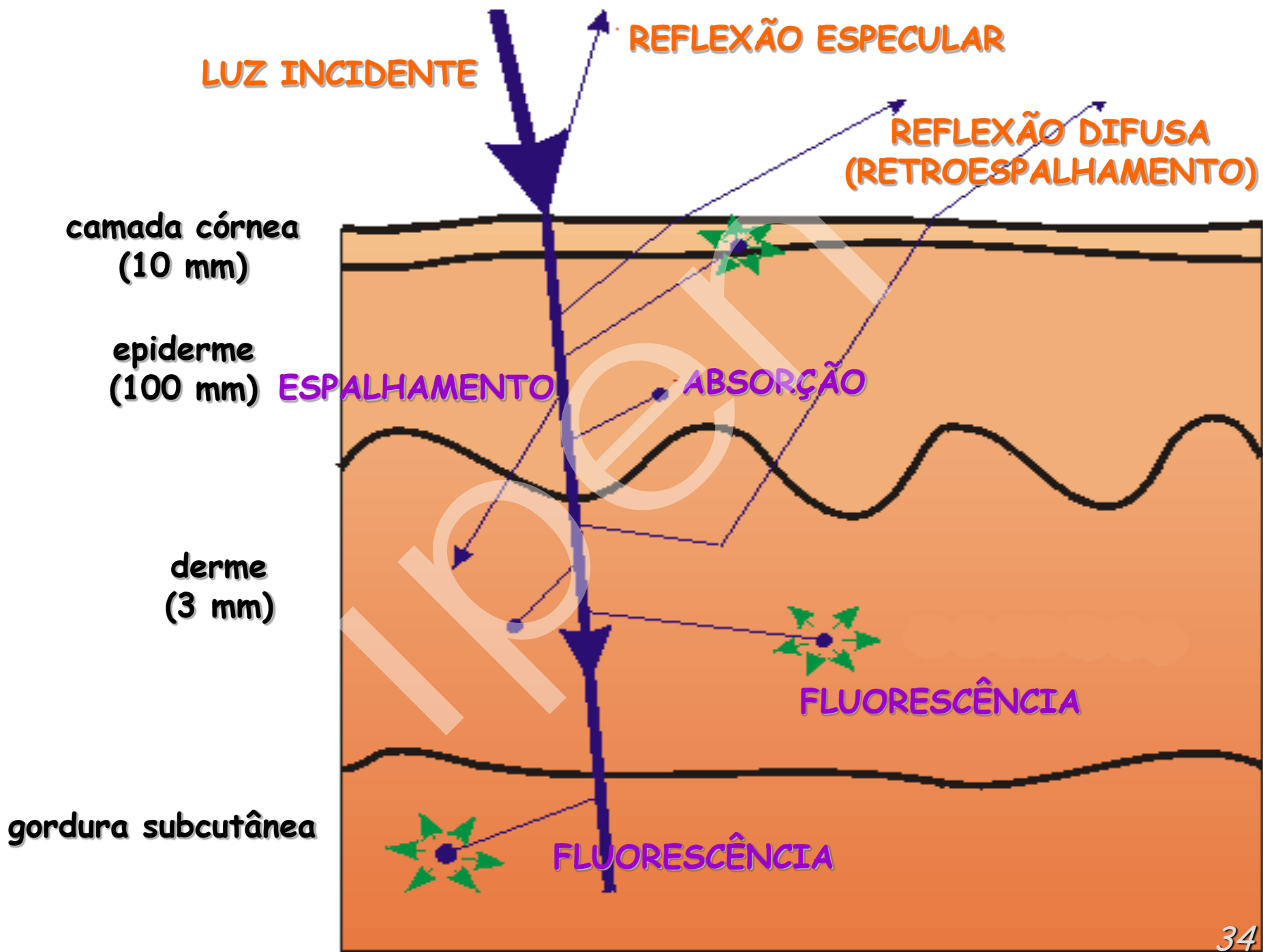


Atenuação

$$\mu_t = \mu_a + \mu_s(1 - g) \text{ [cm}^{-1}\text{]}$$



- Tecidos biológicos são meios absorvedores opticamente inhomogêneos
- Na interface ar-biotecido parte da radiação é refletida e parte penetra o biotecido
 - A luz é expandida e atenuada devido a múltiplos espalhamentos e absorção
 - Por causa do espalhamento, parte da radiação laser se propaga na direção oposta (retroespalhamento)



UV e IR ($\lambda \geq 2$ mm)

- absorção predomina e a influência do espalhamento é relativamente pequena:
 - a onda de luz não penetra profundamente no biotecido.

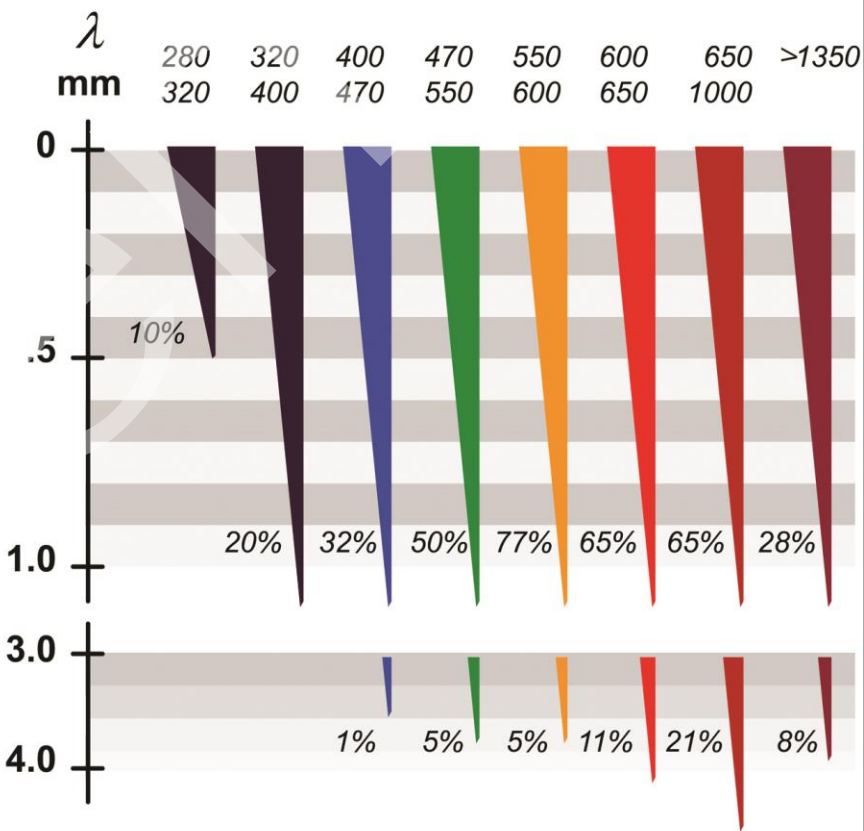
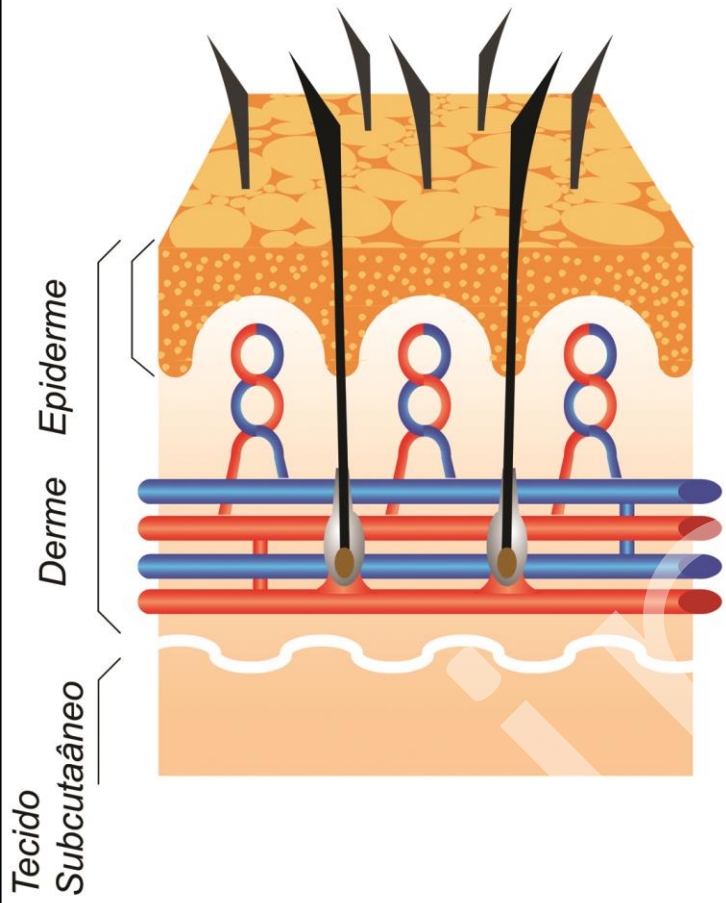
Região do visível com menores λ

- há absorção e espalhamento;
- a profundidade de penetração varia de 0.5 a 2.5 mm.

$$\lambda = 0.6 \text{ } \mu\text{m} \text{ a } 1 \text{ } \mu\text{m}$$

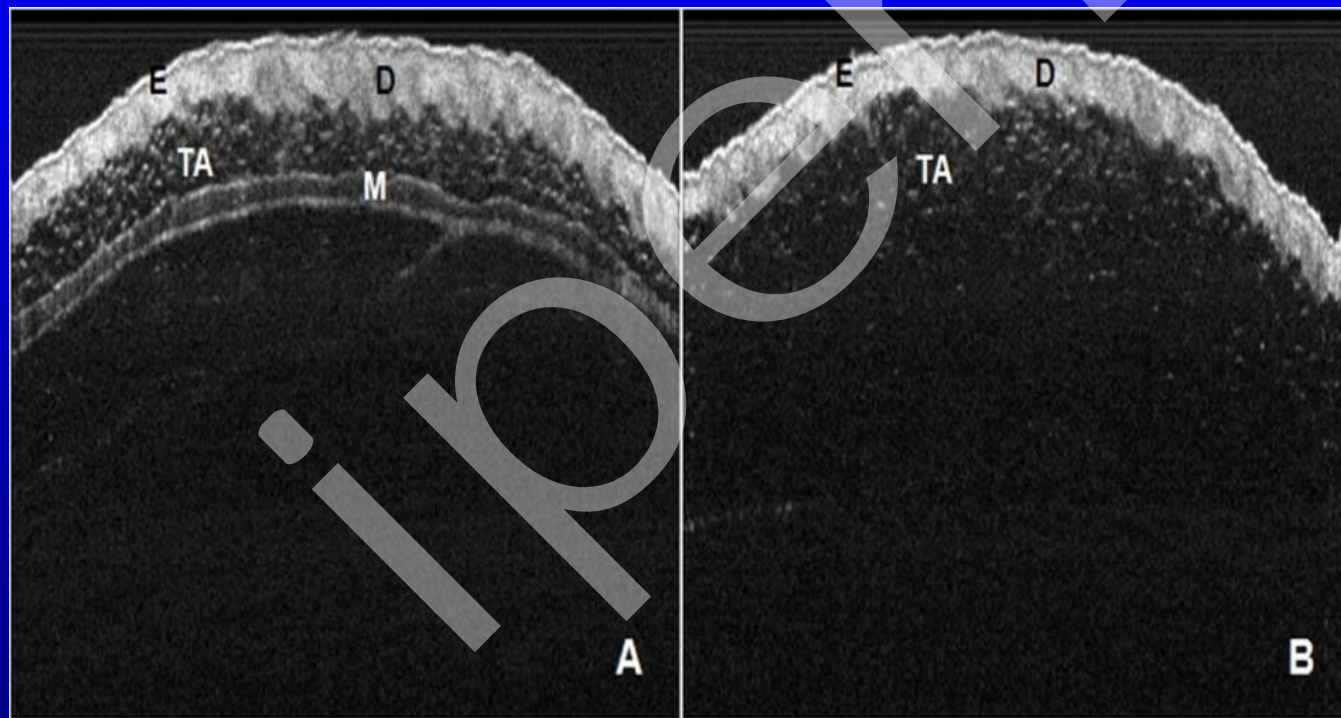
- **espalhamento predomina em relação à absorção;**
 - profundidade de penetração aumenta até 8-10 mm.

(Tuchin, 1995)

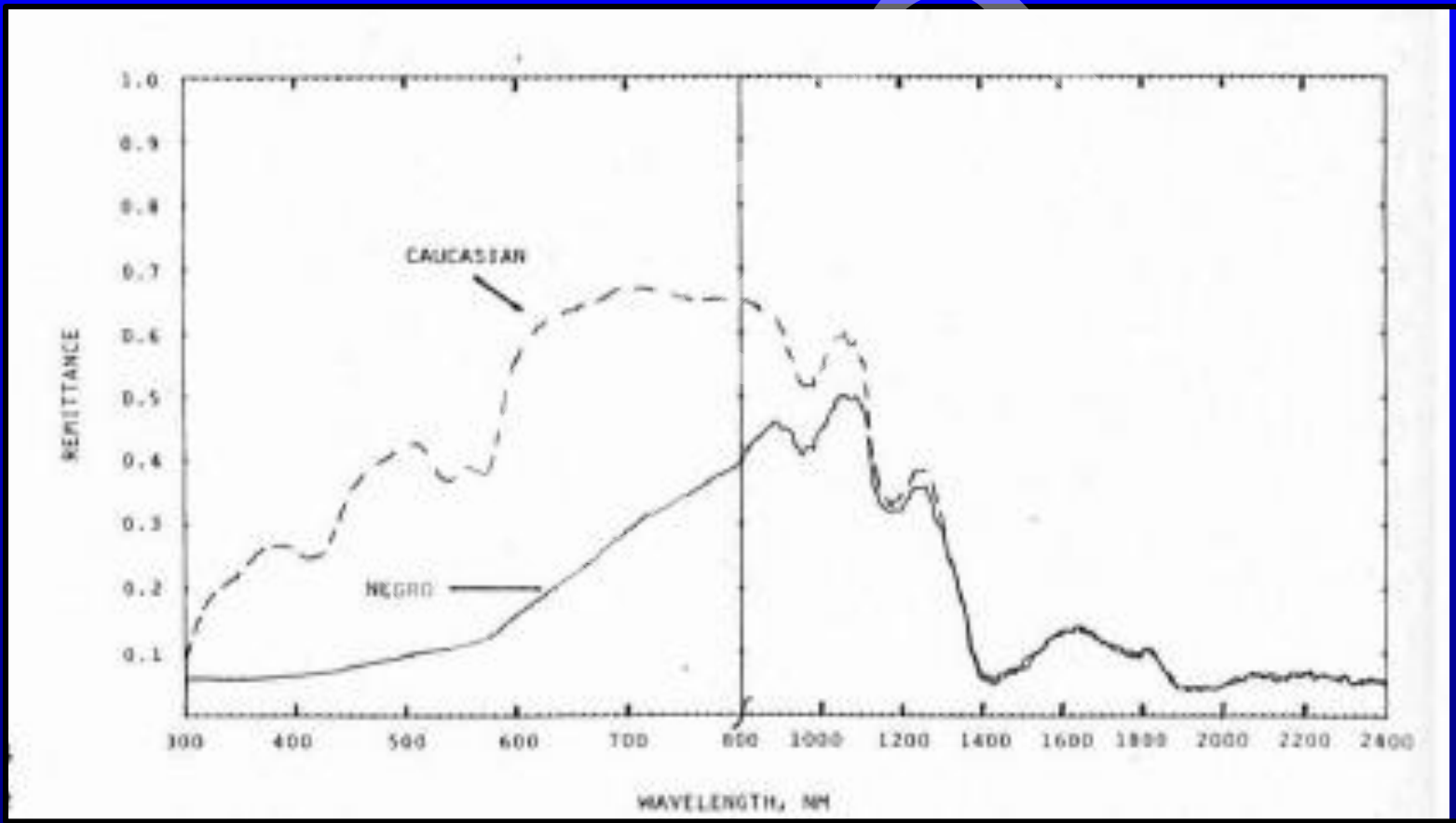


Parâmetros importantes

Massa corpórea



Cor da pele

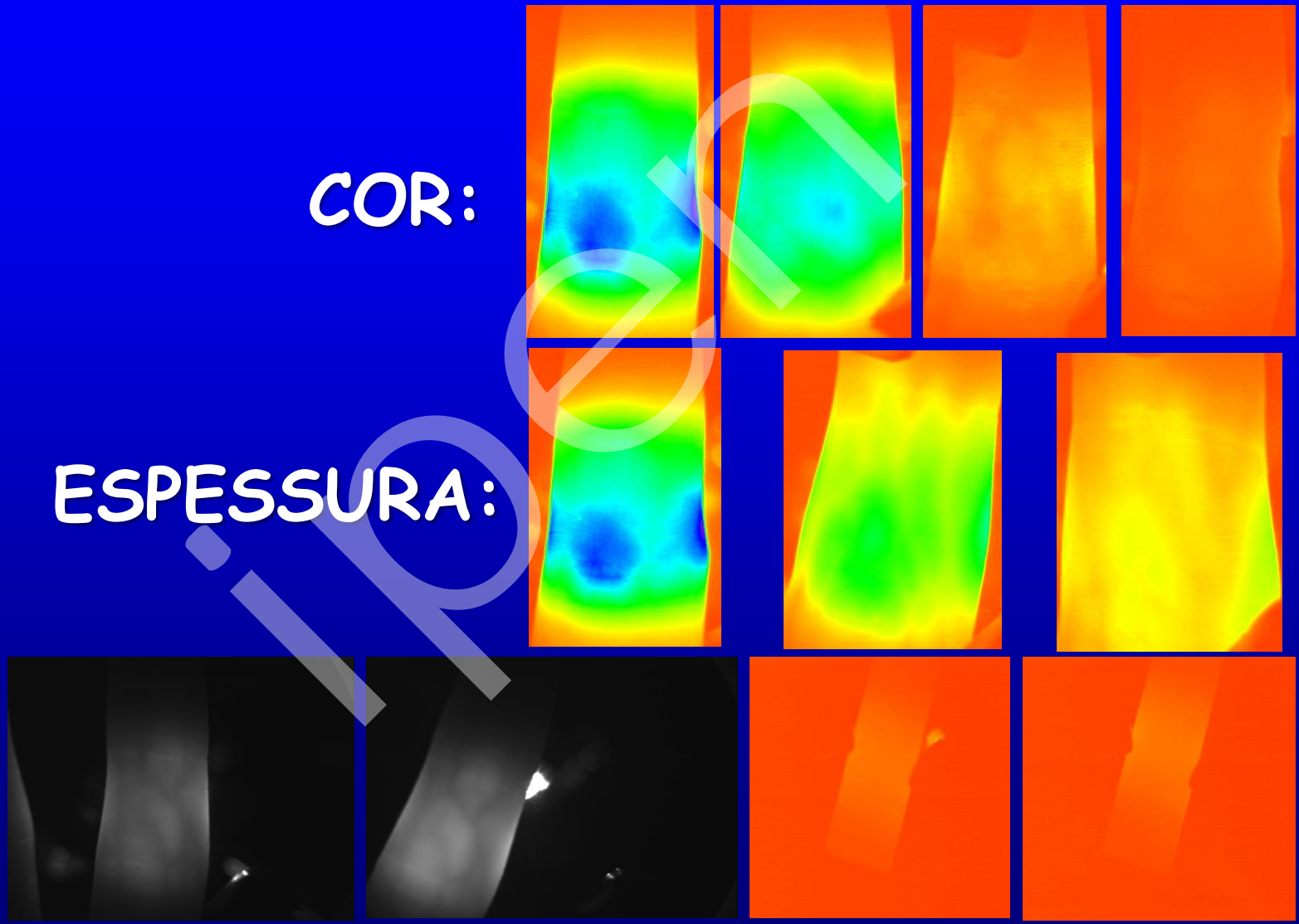


Transmitancia

COR:

ESPESSURA:

λ :



(633 nm)

(820 nm)

**Ring finger inflamed from a jam.
Red & Infrared from a halogen light can't
make it through the inflamed tissue as well.**

Light attenuation in rat skin following low level laser therapy on burn healing process

Daniela Fátima Teixeira Silva^a; Martha Simões Ribeiro^b

Nove de Julho University, São Paulo, Brazil^a
Center for Lasers and Applications, IPEN-CNEN/SP, Brazil^b

ABSTRACT

Low-level laser therapy (LLLT) is commonly used to accelerate wound healing. Besides, the technique of imaging the light distribution inside biological tissues permits us to understand several effects about light-tissue interaction. The purpose of this study was to determine the relative attenuation coefficient of the light intensity in healthy and burned skin rats during cutaneous repair following LLLT or not. Two burns about 6mm in diameter were cryogenerated using liquid N₂ on the back of 15 rats. Lesion L was irradiated by a He-Ne laser ($\lambda = 632.8\text{nm}$) and fluence 1.0J/cm^2 ; Lesion C was control and received sham irradiation. A healthy skin area (H) was also analyzed. The lesions were irradiated at days 3, 7, 10 and 14 post-burning. The animals were euthanized at days 3, 10 and 31 and skin samples were carefully removed and placed between two microscope slides, spaced by $z=1\text{mm}$. A laser beam irradiated the sandwiched tissue from epidermis to dermis. A CCD camera was placed orthogonal to the beam path and it photographed the distribution of the scattered light. The light decay occurred according to the Beer's Law. Significance was accepted at $p < 0.01$ by using t-Student test. Our results show that the light decay along any direction was close to an exponential. Burned skin samples presented decay significantly faster than healthy skin samples. Besides, attenuation coefficient changed during burning healing comparing treated and control lesions. These findings suggest that the relative attenuation coefficient is a suitable parameter to optimize LLLT during wound healing.

Key words: absorption; attenuation coefficient; laser therapy; polarized light; red laser; scattering; skin repair

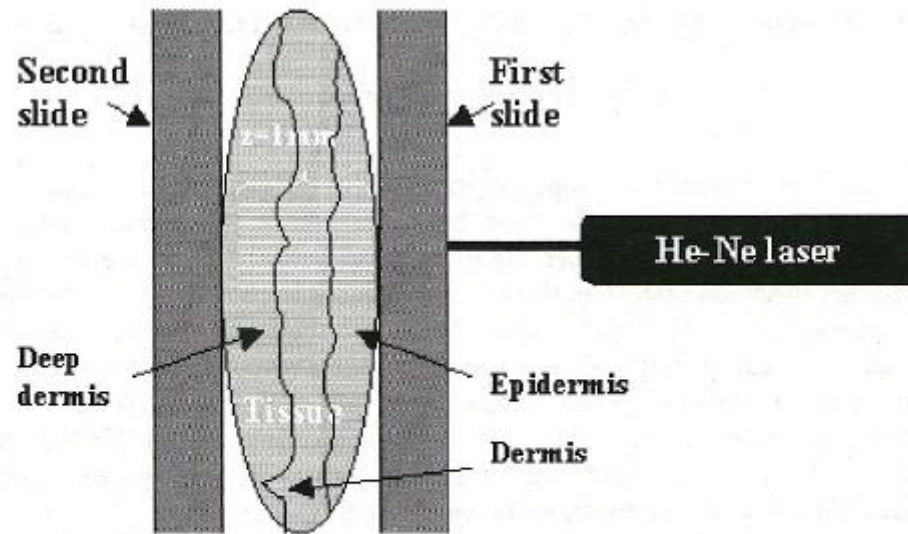


Figure 1: Measurement scheme of the attenuation coefficient.

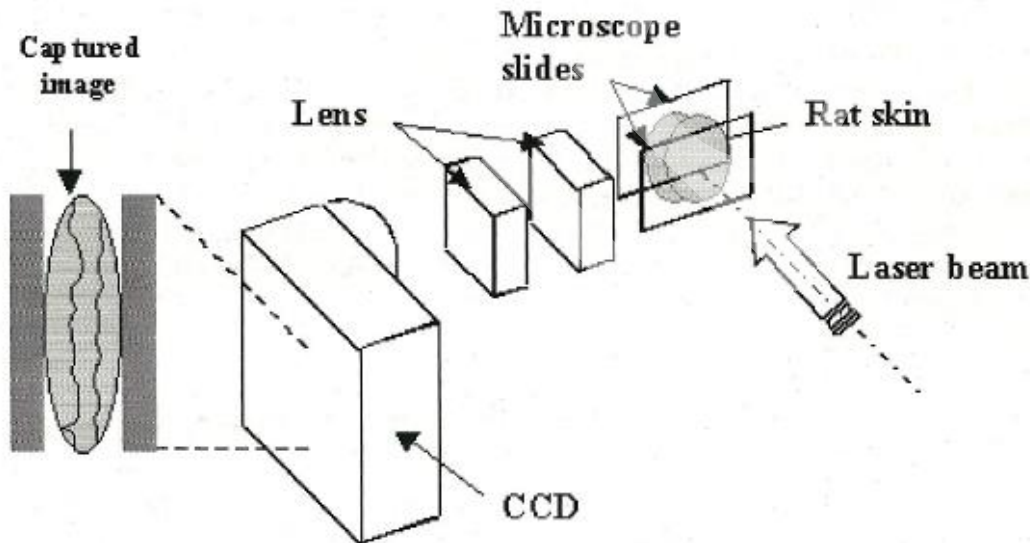


Figure 2: Experimental setup to capture scattered light from the skin sample.

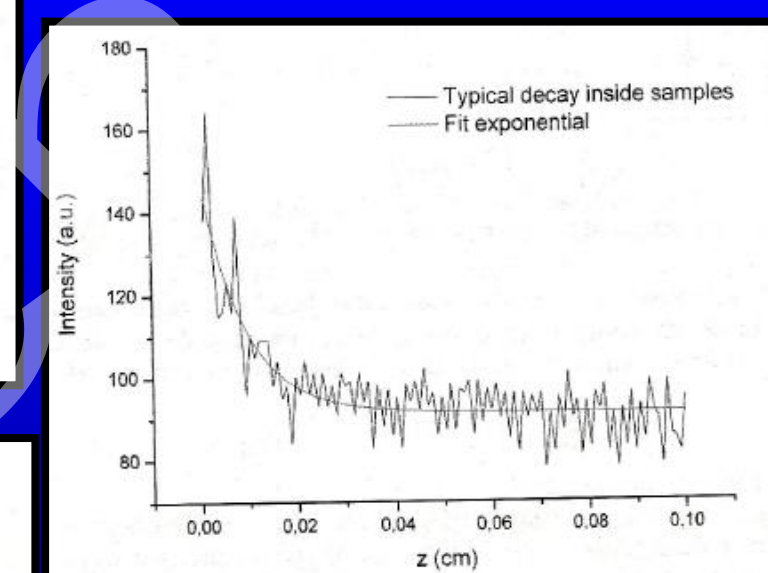
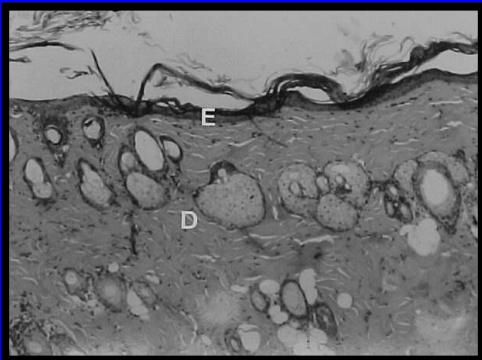


Figure 3: Exponential decay of the light inside biological tissue.



healthy skin of rat. E- epidermis; D- dermis

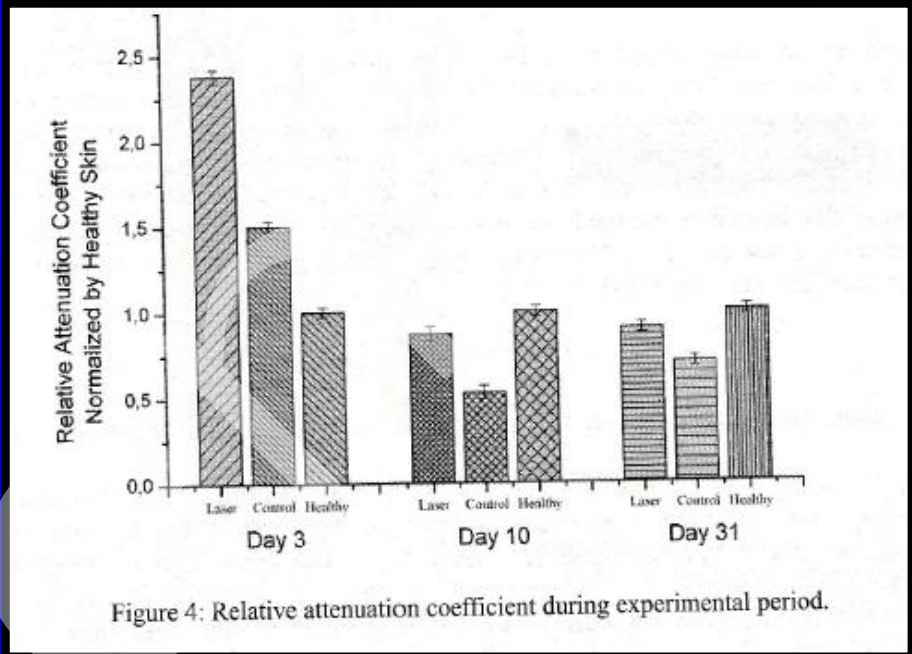
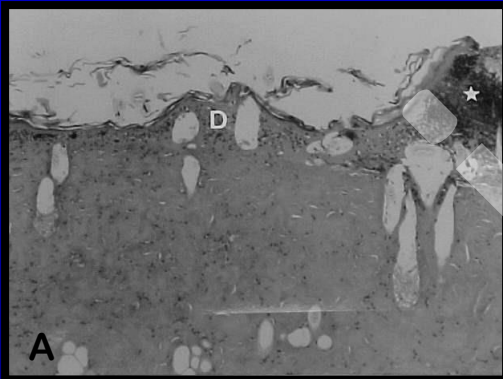


Figure 4: Relative attenuation coefficient during experimental period.



During spontaneous burn healing. A- 3 days after injury; B- 17 days after injury. Note the necrotic area (*) and cell debris (arrow).

Red laser attenuation in biological tissues: study of the inflammatory process and pigmentation influence

Caetano P. Sabino; Daiane T. Meneguzzo; Endi Benetti, Ilka T. Kato; Renato A. Prates; Martha S. Ribeiro

Centro de Lasers e Aplicações, IPEN-CNEN/SP, Brazil

ABSTRACT

Several studies indicate that low level laser therapy (LLLT) accelerates the healing process, however, for a determined pathology, dosimetry remains difficult to be established. To understand the tissue optical properties under different conditions is extremely relevant since the dose delivered to the target tissue is known to be critical. The skin pigmentation influence on the laser attenuation is not yet well established on different mice lineages or human ethnical groups, making the dose problematic. Along the same line, inflammatory processes may cause similar problems since the tissues in this condition change their optical properties due to inflammatory cell accumulation. This work evaluated the attenuation pattern of a HeNe laser ($\lambda=632.8$ nm) using *ex vivo* skin samples from Balb/C and C57BL/6 mice under inflammatory stages induced in their paw by local carrageenan inoculation. The samples were placed between two microscope slides, and a CCD camera was placed orthogonal to the beam path. The intensity distribution of the scattered light was photographed in grayscale and analyzed by ImageJ software. Our findings suggest that even slight differences of the epithelial pigmentation could result in a relevant dose loss delivered to the deeper tissues. The increase of the inflammatory cell density in the connective tissue indicated a highly scattering area also resulting in a dose loss for the deeper tissues when compared to control group.

Keywords: light attenuation; red laser; inflammation; oedema; skin pigmentation

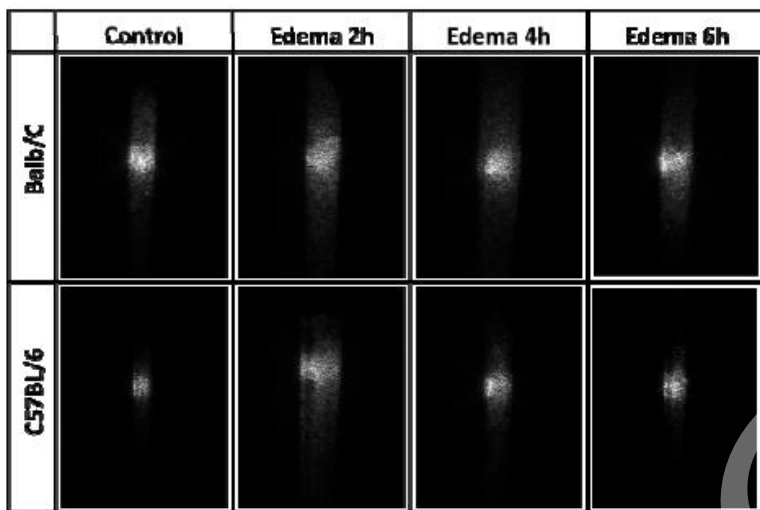


Figure 2. Images obtained by CCD. Beam pathway from left to right.

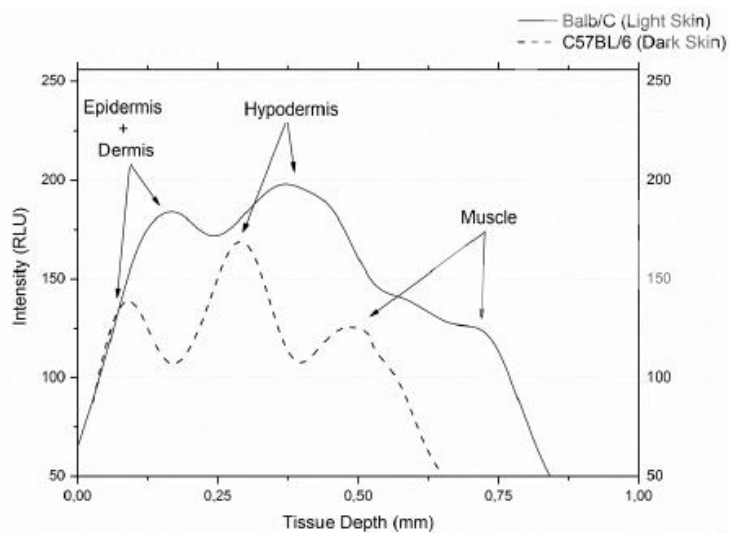
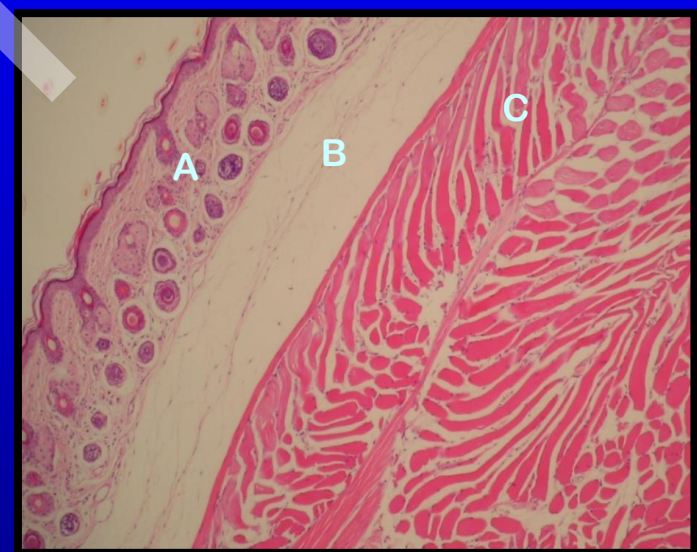


Figure 3. Light intensity (RLU) in function of depth (mm).



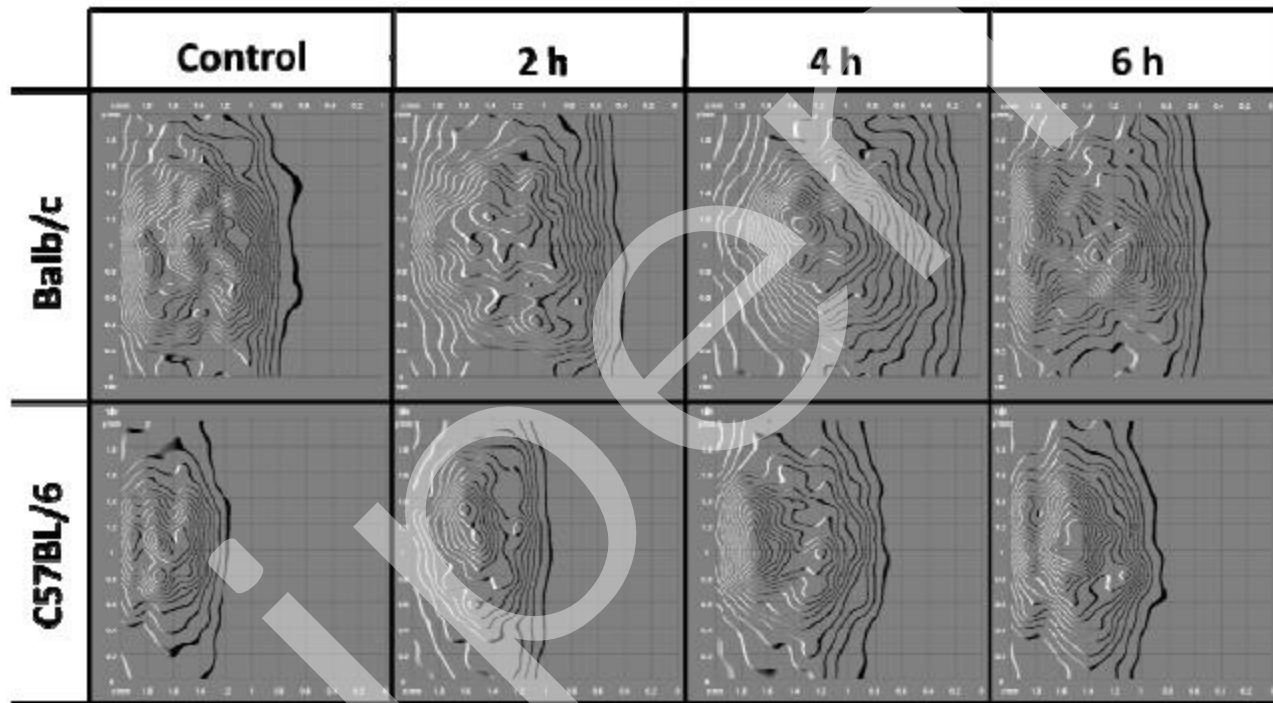
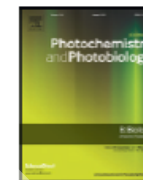


Figure 5. Three-dimensional plots in isolines of light distribution along the samples under inflammatory processes. Space scale (x,y) in millimeters and light intensity (z) in RLU.



The optical properties of mouse skin in the visible and near infrared spectral regions



Caetano P. Sabino ^{a,b,c}, Alessandro M. Deana ^d, Tania M. Yoshimura ^a, Daniela F.T. da Silva ^d, Cristiane M. França ^d, Michael R. Hamblin ^{e,f,g}, Martha S. Ribeiro ^{a,*}

^a Center for Lasers and Applications, Nuclear and Energy Research Institute, IPEN-CNEN/SP, São Paulo, SP, Brazil

^b Institute for Biomedical Sciences, University of São Paulo, São Paulo, SP, Brazil

^c School of Pharmaceutical Sciences, University of São Paulo, São Paulo, SP, Brazil

^d Biophotonics Post-Graduation Program, Universidade de Nove de Julho, São Paulo, SP, Brazil

^e Wellman Center for Photomedicine, Massachusetts General Hospital, Boston, MA, USA

^f Department of Dermatology, Harvard Medical School, Boston, MA, USA

^g Harvard-MIT Division of Health Sciences and Technology, Cambridge, MA, USA

ARTICLE INFO

Article history:

Received 19 August 2015

Received in revised form 7 March 2016

Accepted 24 March 2016

Available online 3 April 2016

Keywords:

Biophotonics

Tissue spectroscopy

Skin optics

Photodiagnosis

Phototherapy

Radiative transfer

ABSTRACT

Visible and near-infrared radiation is now widely employed in health science and technology. Pre-clinical trials are still essential to allow appropriate translation of optical methods into clinical practice. Our results stress the importance of considering the mouse strain and gender when planning pre-clinical experiments that depend on light-skin interactions. Here, we evaluated the optical properties of depilated albino and pigmented mouse skin using reproducible methods to determine parameters that have wide applicability in biomedical optics. Light penetration depth (δ), absorption (μ_a), reduced scattering (μ'_s) and reduced attenuation (μ'_t) coefficients were calculated using the Kubelka-Munk model of photon transport and spectrophotometric measurements. Within a broad wavelength coverage (400–1400 nm), the main optical tissue interactions of visible and near infrared radiation could be inferred. Histological analysis was performed to correlate the findings with tissue composition and structure. Disperse melanin granules present in depilated pigmented mouse skin were shown to be irrelevant for light absorption. Gender mostly affected optical properties in the visible range due to variations in blood and abundance of dense connective tissue. On the other hand, mouse strains could produce more variations in the hydration level of skin, leading to changes in absorption in the infrared spectral region. A spectral region of minimal light attenuation, commonly referred as the "optical window", was observed between 600 and 1350 nm.

© 2016 Elsevier B.V. All rights reserved.

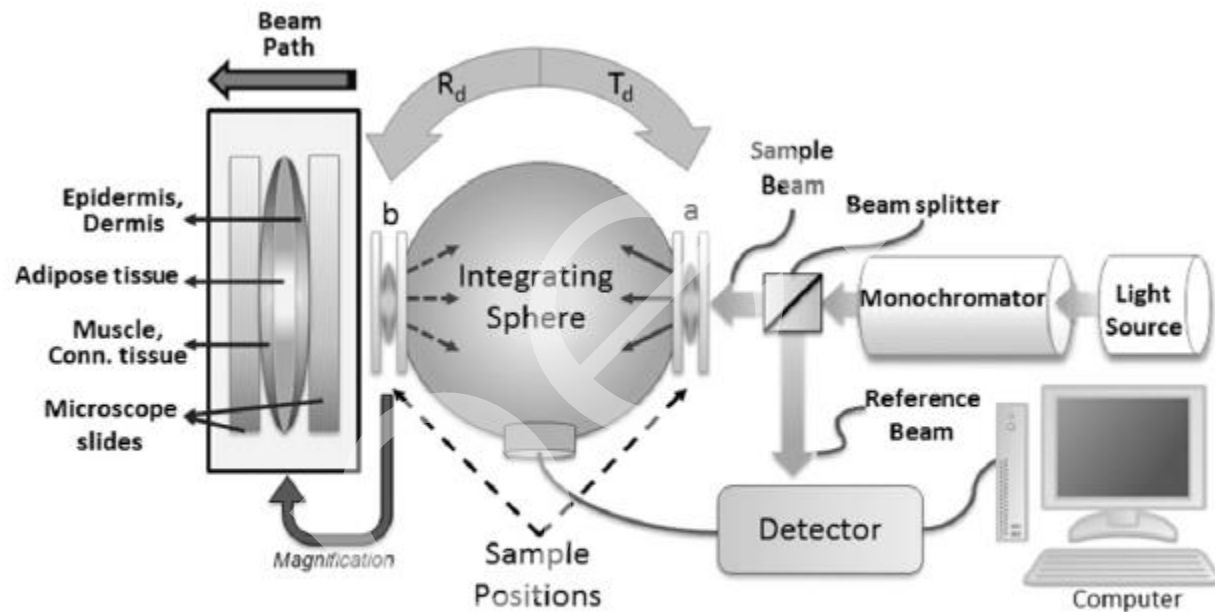
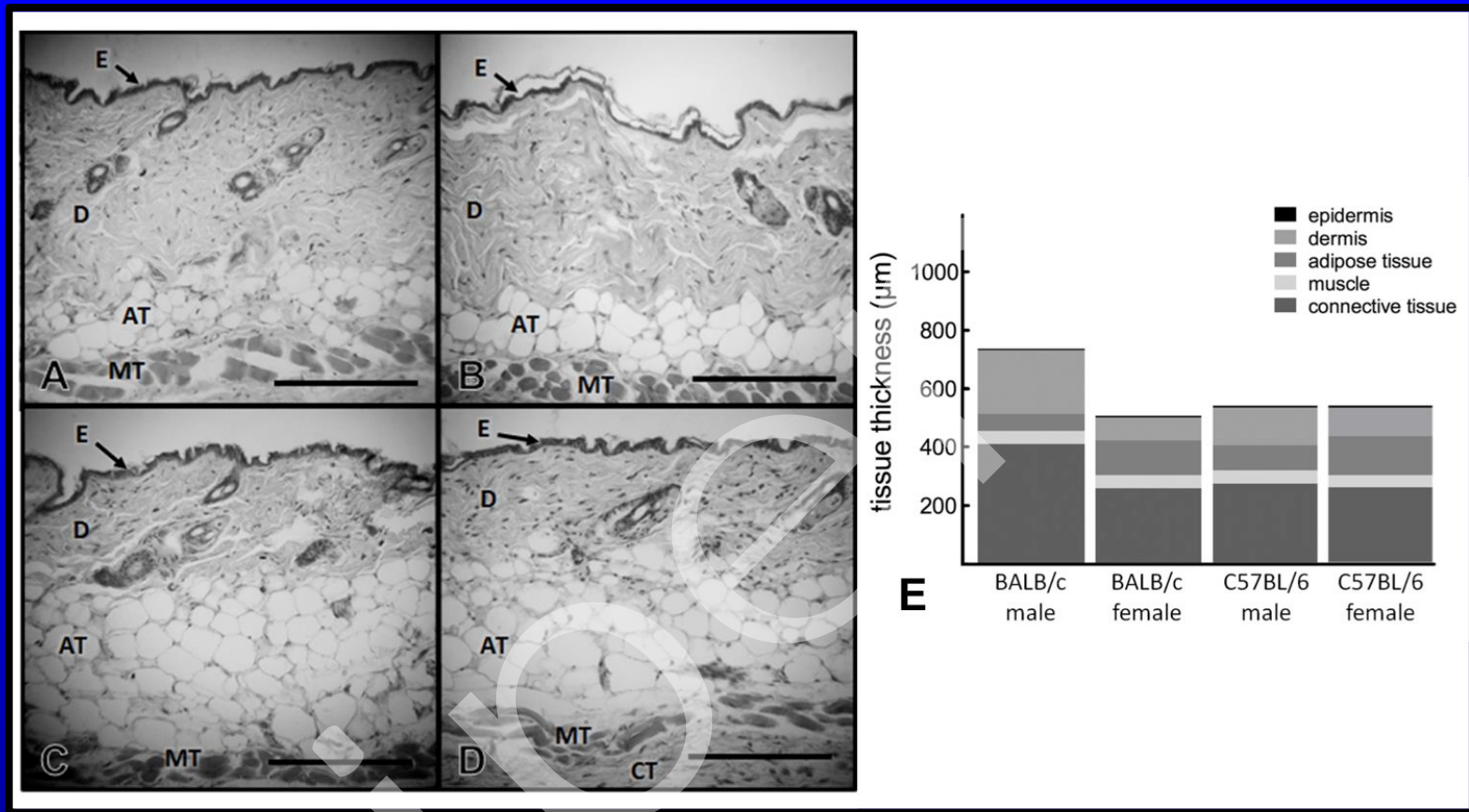


Fig. 1. Schematic diagram of the commercial spectrometer system coupled to a single integrating sphere. To provide mechanical support, each sample was placed in between two glass microscopy slides. The transmittance spectra were obtained by placing the sample at position "a" with port "b" closed, and reflectance spectra were acquired shifting the sample to position "b". For all measurements, the sample beam was directed in the epidermis-dermis direction.



Fotomicrografias de pele de camundongos. (A e B) Pele de um macho albino e *black*, respectivamente, mostrando epiderme (E), derme espessa (D), tecido adiposo (AT) e muscular (MT). **(C e D)** Pele de uma fêmea albina e *black*, respectivamente, mostrando as mesmas camadas, mas com derme mais fina e mais tecido adiposo.

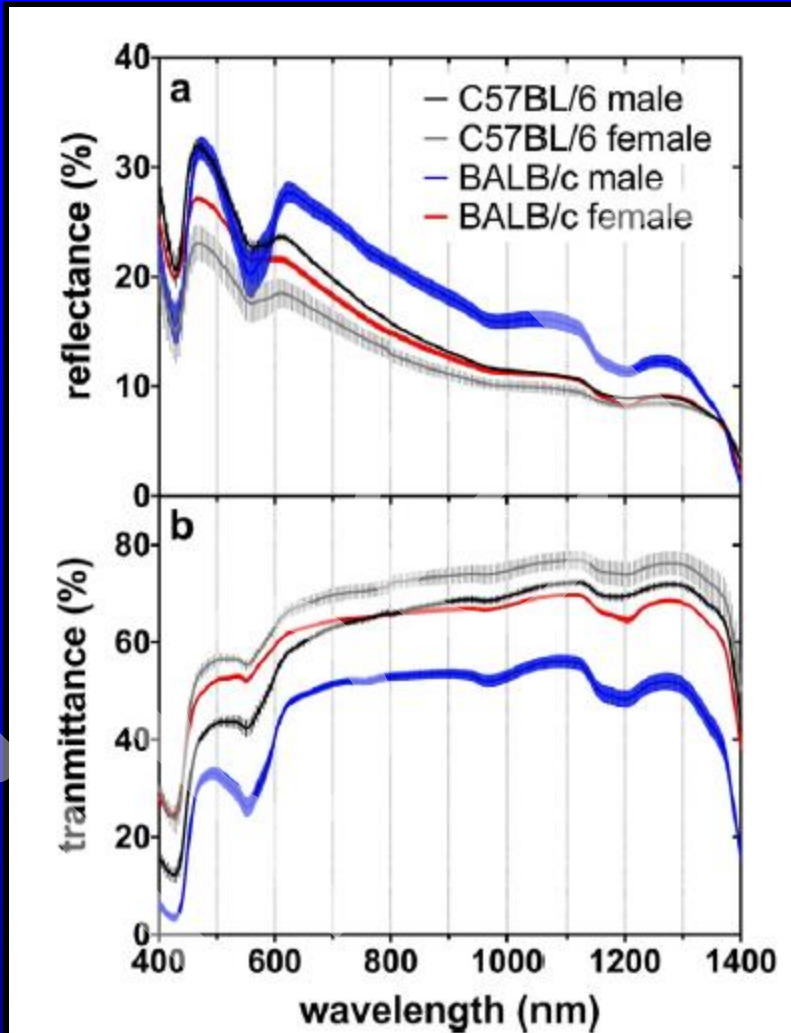


Fig. 2. Average and SEM of (a) diffuse reflectance and (b) diffuse transmittance versus wavelength

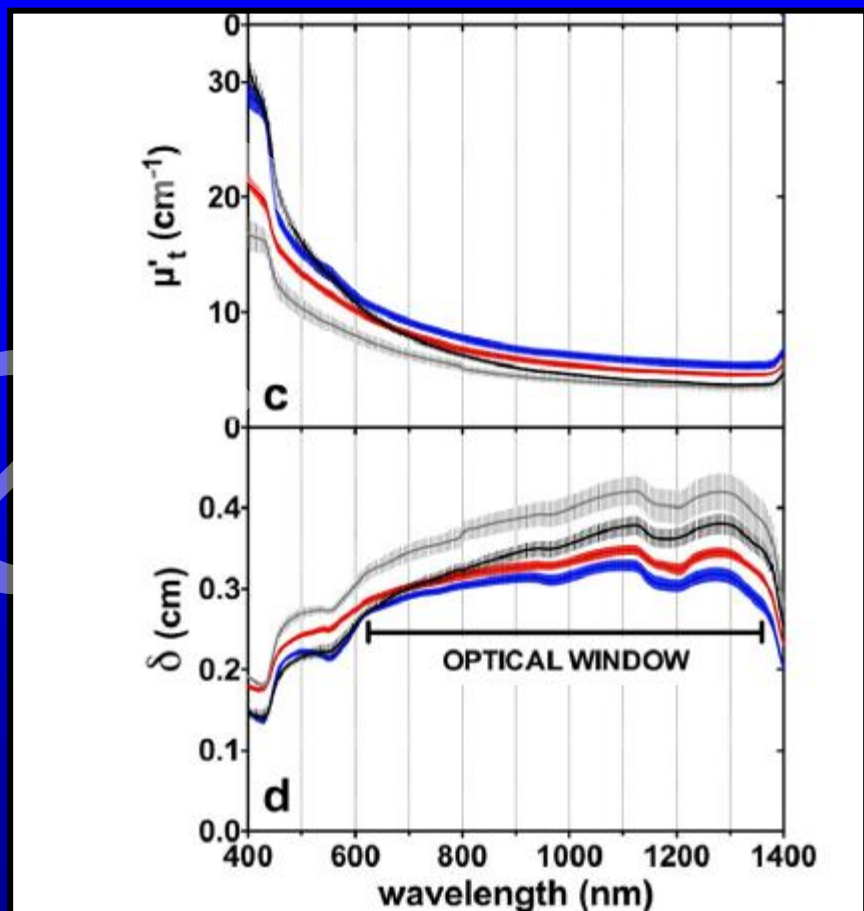
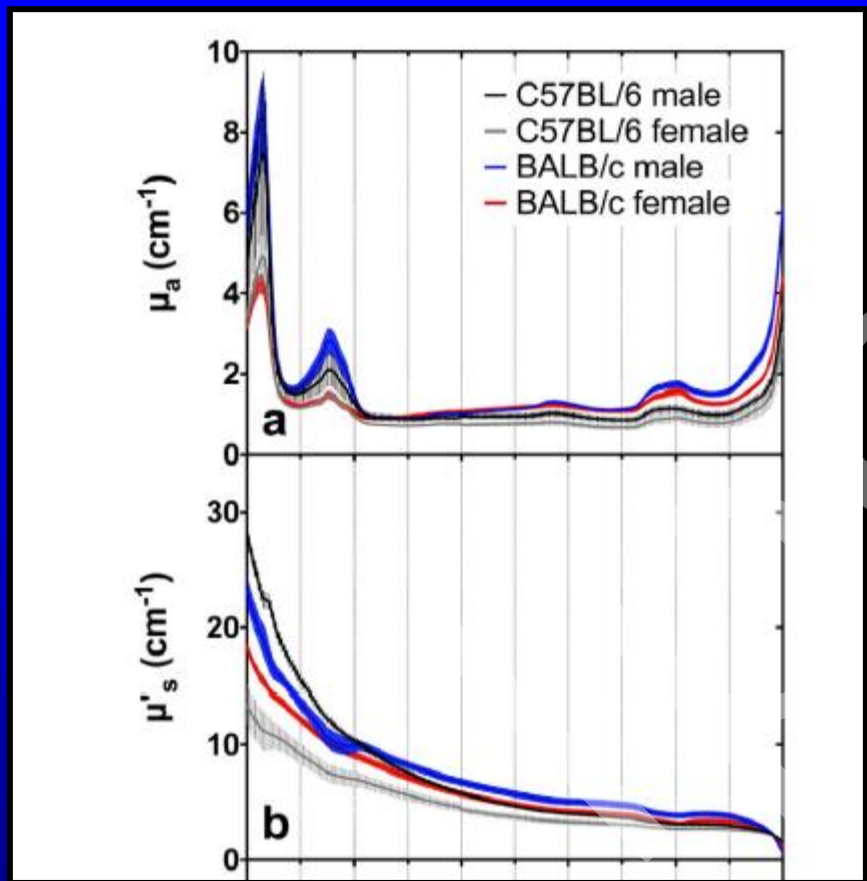
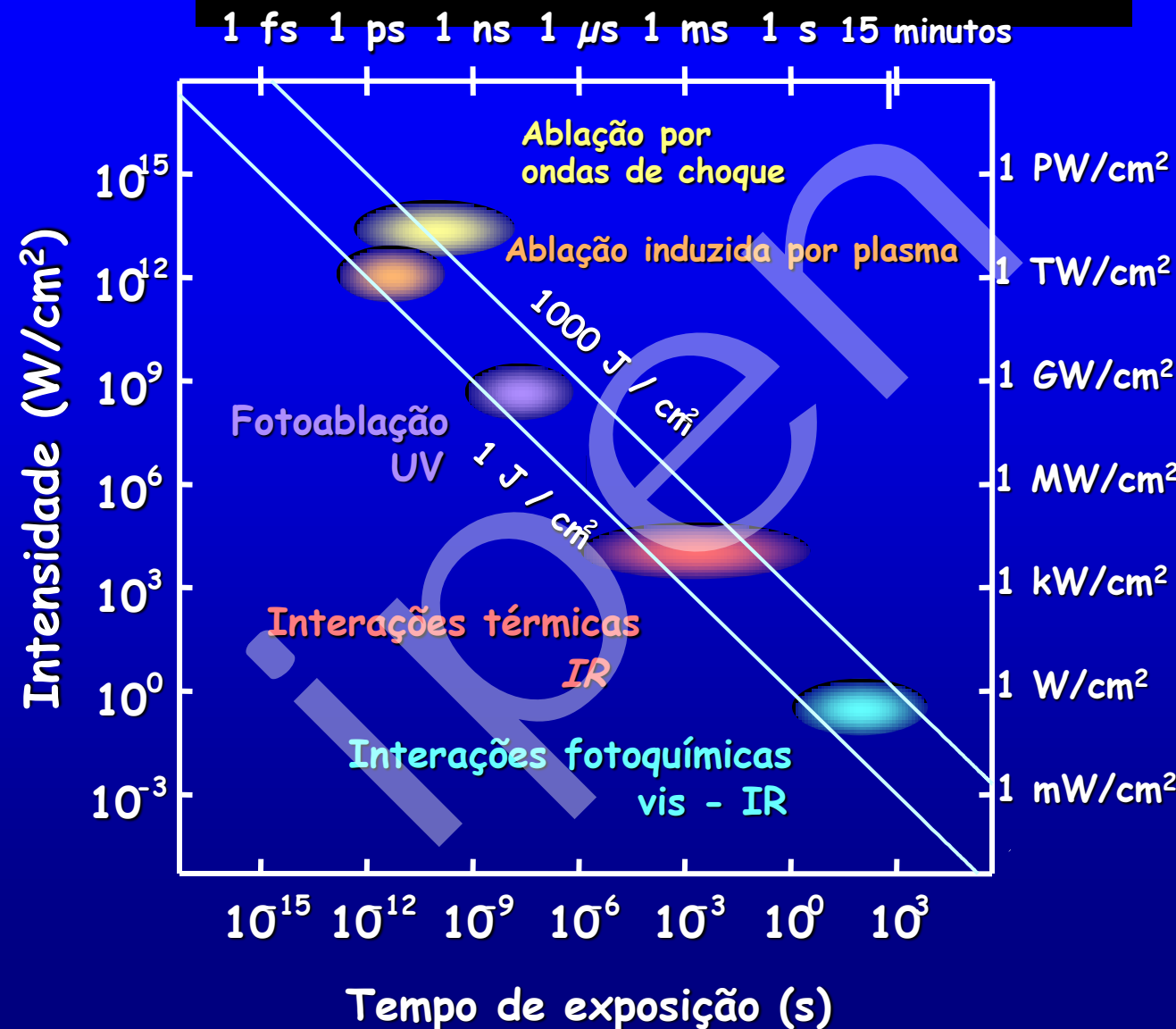
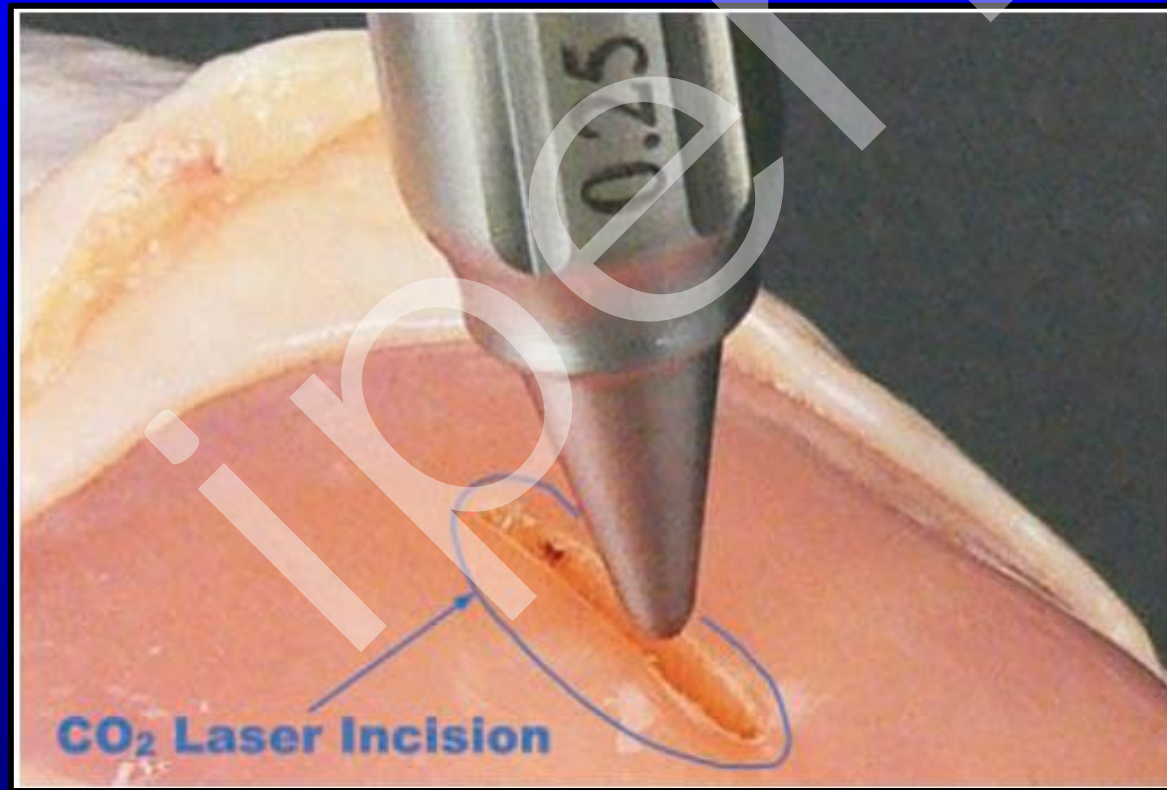


Fig. 3. Average and SEM of (a) Absorption, (b) reduced scattering, (c) reduced attenuation coefficients and (d) penetration depth versus wavelength. The maxima penetration depth at (d) represents the "optical window" for light penetration into depilated mice skin.

Interação Luz-Tecido

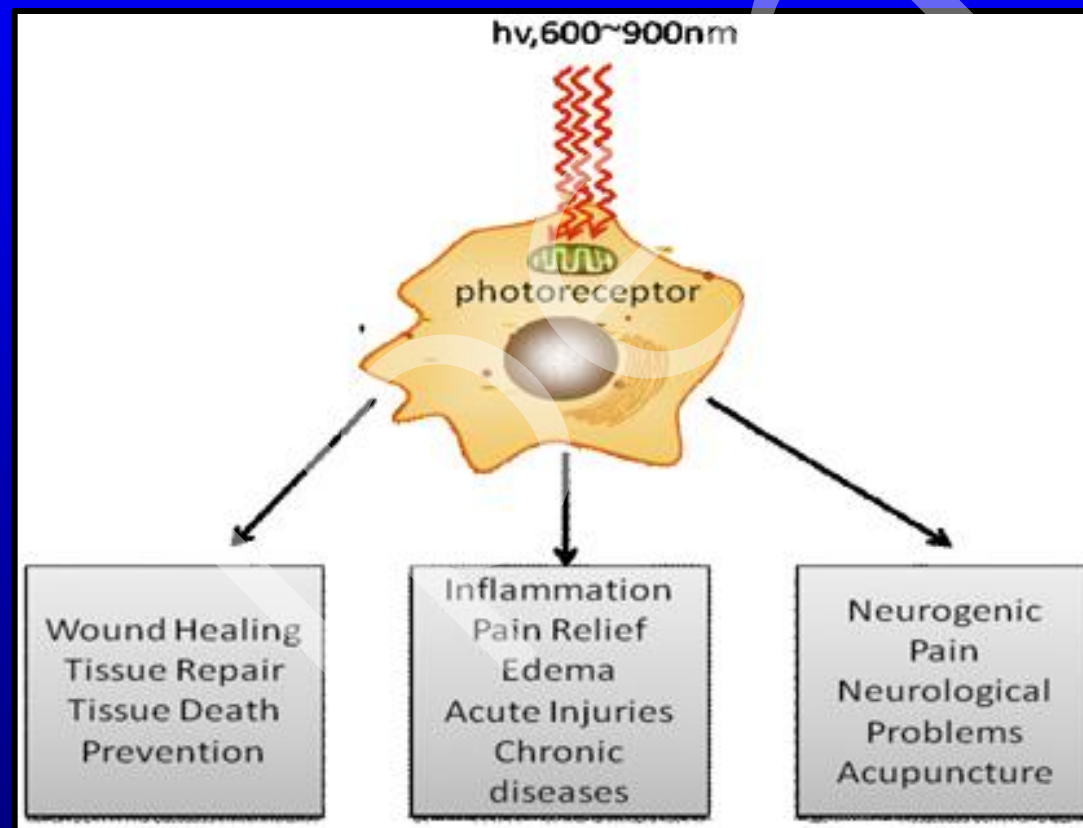


EFEITOS TÉRMICOS (altas densidades de potência)





EFEITOS NÃO-TÉRMICOS (baixas densidades de potência)



TERAPIA COM LUZ

- Helioterapia



Mais de 100 anos de reconhecimento

The screenshot shows the Nobelprize.org homepage with a search bar and navigation links for Nobel Prizes, Alfred Nobel, Educational, Video Player, and Nobel Organizations. A blue arrow points from the text on the right to the search bar. Below the header, a breadcrumb trail leads to the specific prize page. The main content area displays the title "The Nobel Prize in Physiology or Medicine 1903" and the laureate's name, Niels Ryberg Finsen. It includes a portrait of him and a detailed description of his contribution: "in recognition of his contribution to the treatment of diseases, especially lupus vulgaris, with concentrated light radiation, whereby he has opened a new avenue for medical science".

Nobelprize.org
The Official Web Site of the Nobel Prize

Nobel Prizes Alfred Nobel Educational Video Player Nobel Organizations

Home / Nobel Prizes / Nobel Prize in Physiology or Medicine / The Nobel Prize in Physiology or Medicine 1903

About the Nobel Prizes Facts and Lists Nobel Prize in Physics Nobel Prize in Chemistry Nobel Prize in Physiology or Medicine

All Nobel Prizes in Physiology or Medicine Facts on the Nobel Prize in Physiology or Medicine Prize Awardee for the Nobel Prize in Physiology or Medicine Nomination and Selection of Medicine Laureates Nobel Medal for Medicine Nobel Prizes and the Immune System Nobel Prizes in Nerve Signaling Video Interviews Video Nobel Lectures Articles in Medicine

Printer Friendly Share Tell a Friend Comments

1901 2012 1903 Sort and list Nobel Prizes and Nobel Laur Prize category: Medicine

The Nobel Prize in Physiology or Medicine 1903
Niels Ryberg Finsen

The Nobel Prize in Physiology or Medicine 1903
Niels Ryberg Finsen



Niels Ryberg Finsen

O Premio Nobel em Fisiologia ou Medicina (1903) foi dado a Niels Ryberg Finsen "*in recognition of his contribution to the treatment of diseases, especially lupus vulgaris, with concentrated light radiation, whereby he has opened a new avenue for medical science*".



PHOTOTHERAPY

- (1) THE CHEMICAL RAYS OF LIGHT AND SMALL-POX.
- (2) LIGHT AS A STIMULANT.
- (3) THE TREATMENT OF LUPUS VULGARIS BY CONCENTRATED CHEMICAL RAYS.

BY
PROFESSOR NIELS R. FINSEN
COPENHAGEN

TRANSLATED FROM THE GERMAN EDITION AND WITH
AN APPENDIX ON

The Light Treatment of Lupus

BY
JAMES H. SEQUEIRA, M.D., LOND., M.R.C.P.
DERMATOLOGICAL ASSISTANT AND MEDICAL OFFICER IN CHARGE OF THE LIGHT DEPARTMENT
AT THE LONDON HOSPITAL
PHYSICIAN TO THE NORTH EASTERN HOSPITAL FOR CHILDREN

LONDON
EDWARD ARNOLD
37 BEDFORD STREET, STRAND, W.C.
1901

Tratamento de tuberculose cutânea com luz solar "filtrada e concentrada"

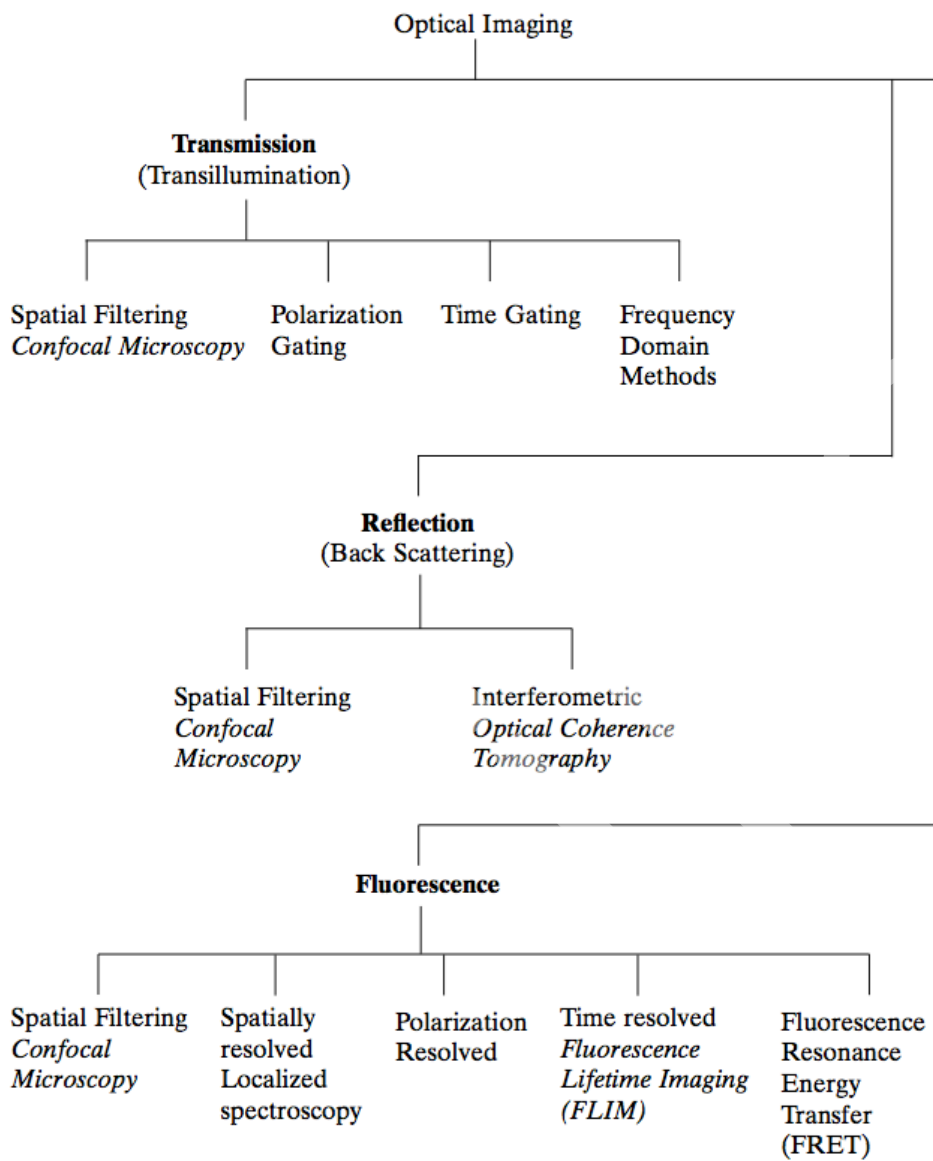
“Radioisótopos e Luz em Saúde: Integrando competências e inovações”

Princípios de óptica do tecido para diagnóstico e terapia

Anderson Zanardi de Freitas

Martha Simões Ribeiro

Overview of Optical Imaging



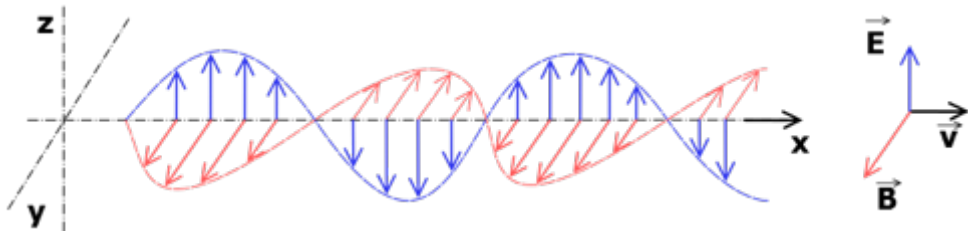
Spatial Filtering. It is one of the simplest methods and relies on the fact that diffuse photons, undergoing multiple scattering, are more spread out and off-axis. Therefore, applying spatial filtering by using a transmitted light collection using an aperture provides rejection of a substantial amount of off-axis diffuse light.

Polarization Gating. Here one utilizes a linearly polarized light. The transmitted ballistic and snake photons still retain much of the initial polarization, while the multiply scattered diffuse light are depolarized.

Time Gating. This method utilizes a short laser pulse as the illumination source. The transmitted light is passed through an optical gate that opens and closes to allow transmission only of the ballistic and/or snake photons. Synchronization can be achieved by using a reference optical pulse that controls the opening and closing of the optical gate.

Frequency-Domain Methods. In this method the time gating is transformed to intensity modulation in frequency domain. In this mode, the specimen is illuminated with an intensity-modulated beam from a CW laser, and the AC modulation amplitude and the phase shift of the transmitted signal are measured using methods such as heterodyning. One often uses the diffuse photon density wave description to analyze the transport of the modulated beam. The advantage of this method is that less expensive CW laser sources can be utilized.

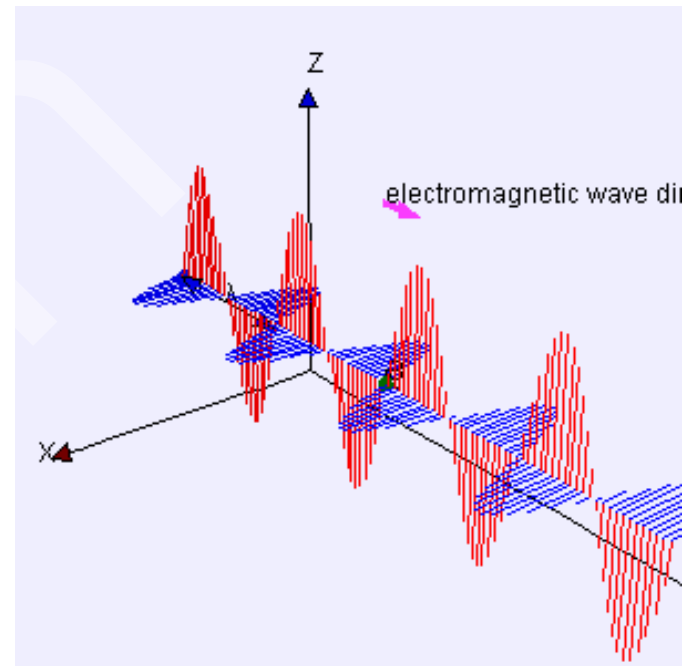
O que é um fóton?



Wave model

Electromagnetic radiation is a [transverse wave](#), meaning that its oscillations are perpendicular to the direction of energy transfer and travel. The electric and magnetic parts of the field stand in a fixed ratio of strengths in order to satisfy the two [Maxwell equations](#) that specify how one is produced from the other. These **E** and **B** fields are also in phase, with both reaching maxima and minima at the same points in space (see illustrations)

$$\nu = \frac{c}{\lambda}$$



Point Form	Integral Form
$\nabla \times \mathbf{H} = \mathbf{J}_c + \frac{\partial \mathbf{D}}{\partial t}$	$\oint \mathbf{H} \cdot d\mathbf{l} = \int_S \left(\mathbf{J}_c + \frac{\partial \mathbf{D}}{\partial t} \right) \cdot d\mathbf{S} \quad (\text{Ampère's law})$
$\nabla \times \mathbf{E} = - \frac{\partial \mathbf{B}}{\partial t}$	$\oint \mathbf{E} \cdot d\mathbf{l} = \int_S \left(- \frac{\partial \mathbf{B}}{\partial t} \right) \cdot d\mathbf{S} \quad (\text{Faraday's law; } S \text{ fixed})$
$\nabla \cdot \mathbf{D} = \rho$	$\oint \mathbf{D} \cdot d\mathbf{S} = \int_V \rho \, dv \quad (\text{Gauss' law})$
$\nabla \cdot \mathbf{B} = 0$	$\oint \mathbf{B} \cdot d\mathbf{S} = 0 \quad (\text{nonexistence of monopole})$

O que é um fóton?

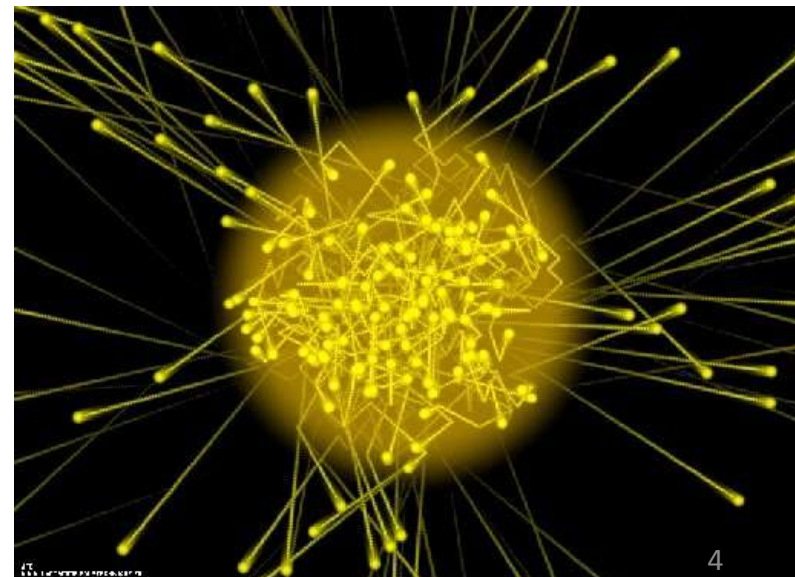
Particle model and quantum theory

An anomaly arose in the late 19th century involving a contradiction between the wave theory of light and measurements of the electromagnetic spectra that were being emitted by thermal radiators known as black bodies. Physicists struggled with this problem, which later became known as the ultraviolet catastrophe, unsuccessfully for many years. In 1900, Max Planck developed a new theory of black-body radiation that explained the observed spectrum. Planck's theory was based on the idea that black bodies emit light (and other electromagnetic radiation) only as discrete bundles or packets of energy. These packets were called quanta. Later, Albert Einstein proposed that light quanta be regarded as real particles. Later the particle of light was given the name photon, to correspond with other particles being described around this time, such as the electron and proton. A photon has an energy, E, proportional to its frequency, f, by

$$E = h\nu = \frac{hc}{\lambda}$$

where h is Planck's constant, λ is the wavelength and c is the speed of light. This is sometimes known as the Planck–Einstein equation.

In quantum theory (see first quantization) the energy of the photons is thus directly proportional to the frequency of the EMR wave.



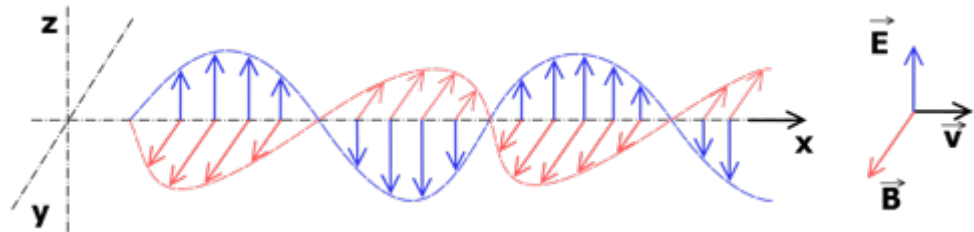
O que é um fóton?

Wave-particle duality

The modern theory that explains the nature of light includes the notion of wave-particle duality. More generally, the theory states that everything has both a particle nature and a wave nature, and various experiments can be done to bring out one or the other. The particle nature is more easily discerned using an object with a large mass. A bold proposition by Louis de Broglie in 1924 led the scientific community to realize that electrons also exhibited wave-particle duality.



Campo Elétrico

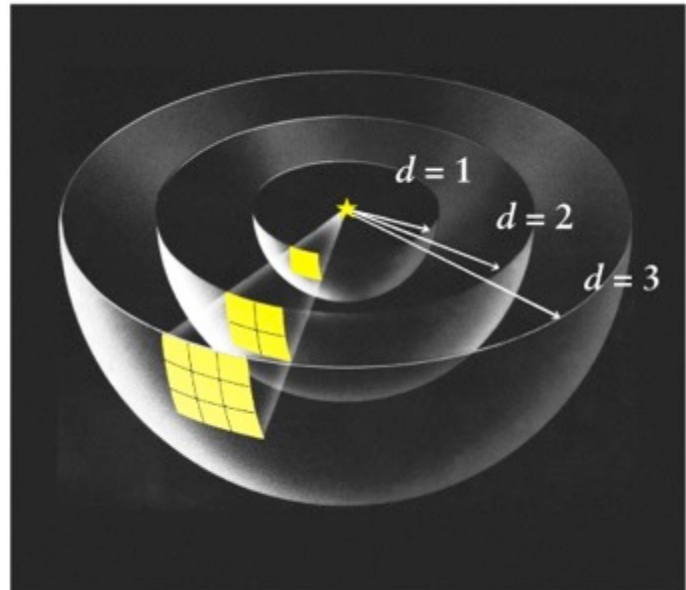
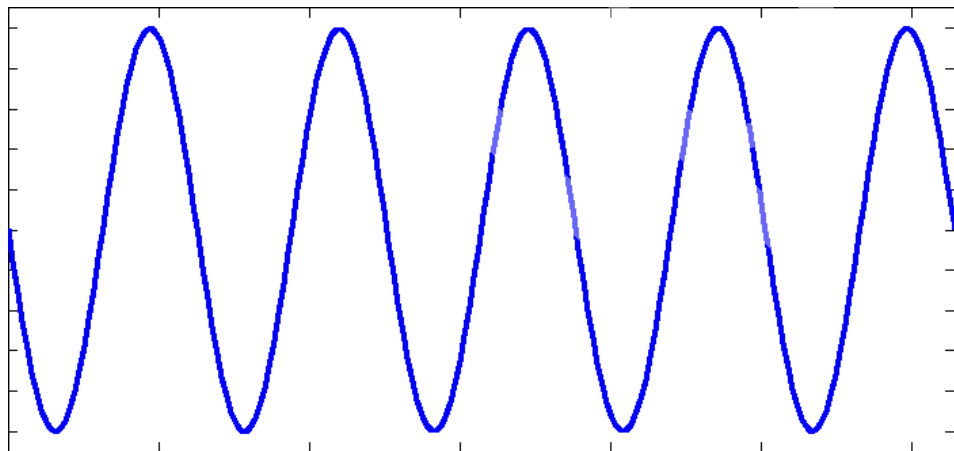


Fundamentals of Optics- Jenkins and White

Parte 2 - Capítulo 11

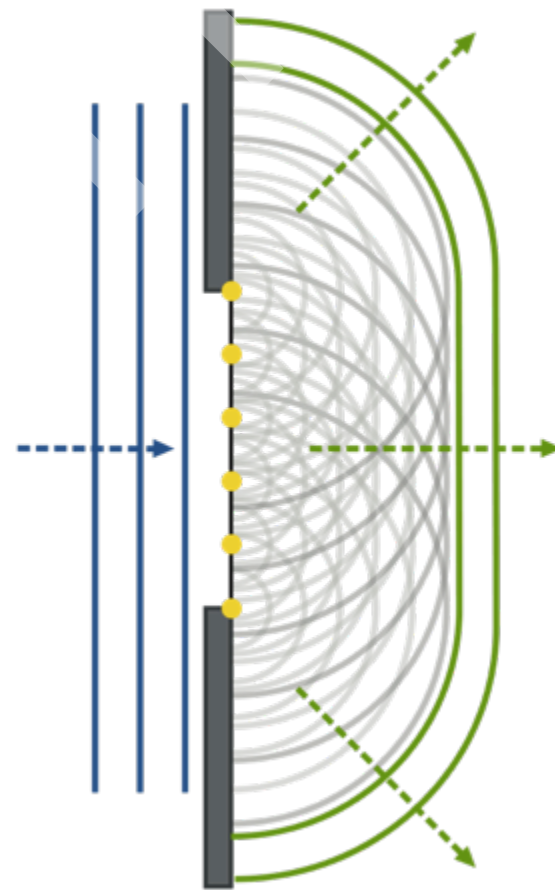
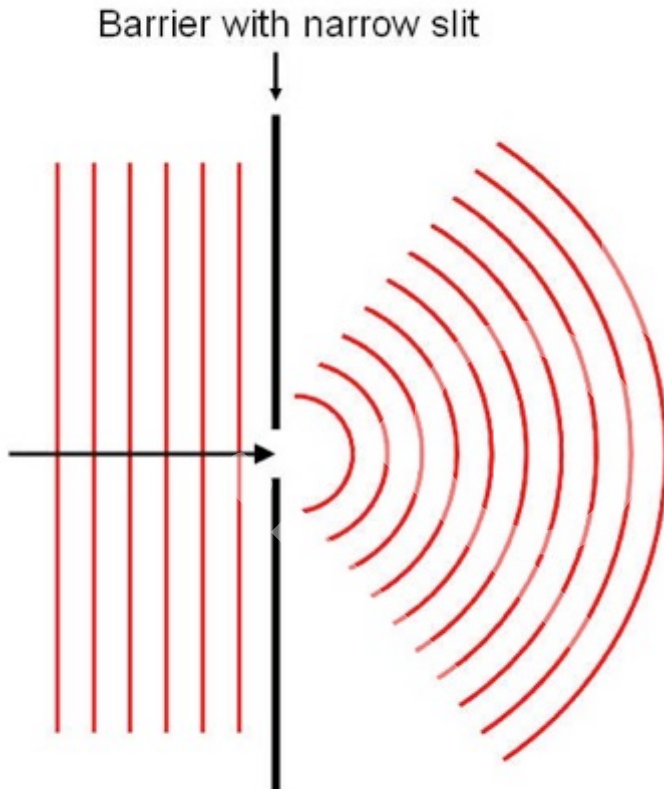
$$\vec{E}(r, t) = \vec{E}_0 \cos(\omega t - \vec{k} \cdot \vec{r})$$

$$\vec{E}(r, t) = \vec{E}_0 e^{-i(\omega t - \vec{k} \cdot \vec{r})}$$



Principio de Huygens

Single Slit Diffraction



[http://www.acoustics.salford.ac.uk/feschools/
waves/diffract3.php](http://www.acoustics.salford.ac.uk/feschools/waves/diffract3.php)

Difração

Cap 15

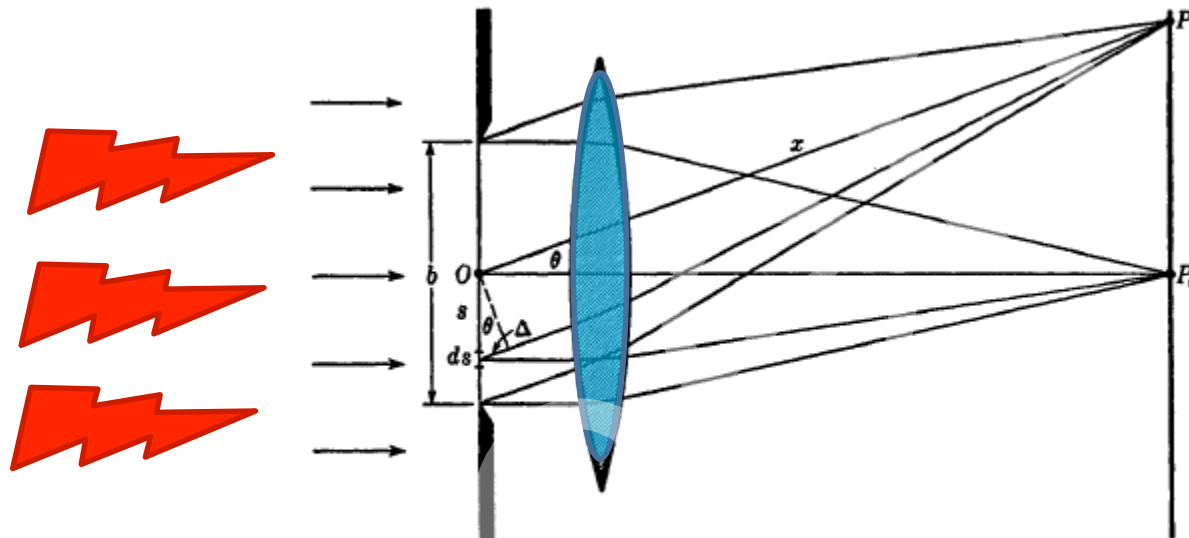


FIGURE 15C
Geometrical construction for investigating the intensity in the single-slit diffraction pattern.

$$I = \frac{A_0^2 \sin^2(\beta)}{\beta} \quad \beta = \pi b / \lambda \sin \theta$$

<https://www.youtube.com/watch?v=-mNQW5OShMA>

Difração

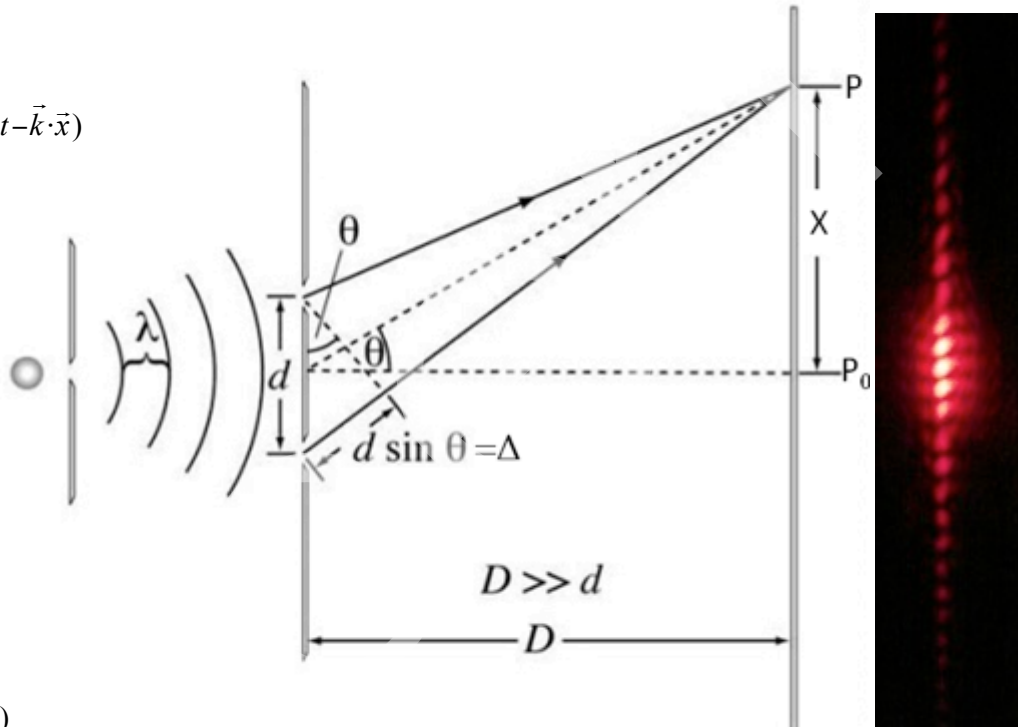
Cap. 13

$$\vec{E}(x,t) = \vec{A} e^{i(\omega t - \vec{k} \cdot \vec{x})}$$

Fonte coerente

$$E_1(x_1, t) = A_1 e^{i(\omega t - k \cdot x_1)}$$

$$E_2(x_2, t) = A_2 e^{i(\omega t - k \cdot x_2)}$$



Campo elétrico resultante

$$\vec{E} = \vec{E}_1 + \vec{E}_2$$

Intensidade

$$I = |\vec{E}|^2$$

$$I = 4A^2 \cos^2 \frac{\delta}{2}$$

Máximos

$$x_n = n \frac{\lambda}{d} D \quad n = 0, 1, 2, 3, \dots$$

Mínimos

$$x_m = (2m+1) \frac{\lambda}{2d} D \quad m = 0, 1, 2, 3, \dots$$

$$\delta = \vec{k} \cdot (\vec{x}_2 - \vec{x}_1)$$

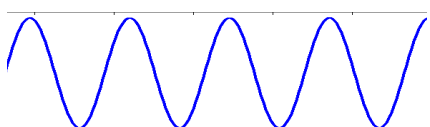
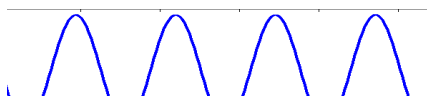
Superposição de ondas

$$\vec{E}_1(r, t) = \vec{E}_0 \cos(\omega t - \vec{k} \cdot \vec{r}_1)$$

$$\vec{E}_2(r, t) = \vec{E}_0 \cos(\omega t - \vec{k} \cdot \vec{r}_2)$$

Fundamentals of Optics- Jenkins and White

Parte 2 - Capítulo 13



Interferência destrutiva

Superposição de ondas

$$\vec{E}_1(r, t) = \vec{E}_0 \cos(\omega t - \vec{k} \cdot \vec{r}_1)$$

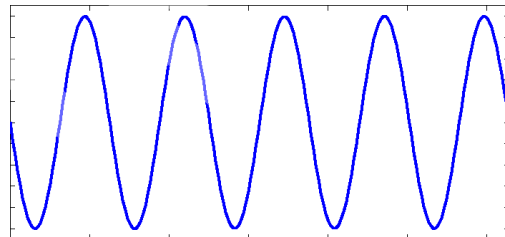
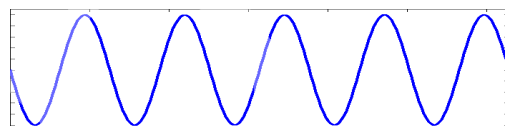
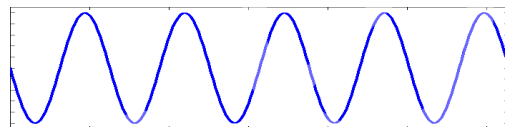
$$\vec{E}_2(r, t) = \vec{E}_0 \cos(\omega t - \vec{k} \cdot \vec{r}_2)$$

Fundamentals of Optics- Jenkins and White

Parte 2 - Capítulo 13

Campo resultante

$$\vec{E}_R(r, t) = \vec{E}_1 + \vec{E}_2$$



Interferência construtiva

Superposição de ondas

$$\vec{E}_1(r, t) = \vec{E}_0 \cos(\omega t - \vec{k} \cdot \vec{r}_1)$$

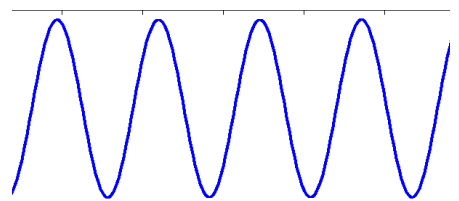
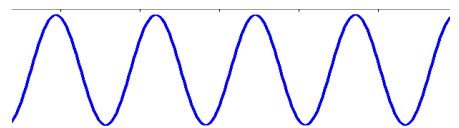
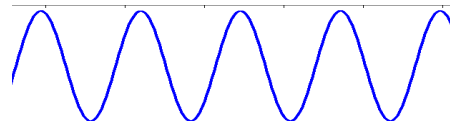
$$\vec{E}_2(r, t) = \vec{E}_0 \cos(\omega t - \vec{k} \cdot \vec{r}_2)$$

Campo resultante

$$\vec{E}_R(r, t) = \vec{E}_1 + \vec{E}_2$$

Fundamentals of Optics- Jenkins and White

Parte 2 - Capítulo 13



Interferência parcial

Superposição de ondas

$$\vec{E}_1(r, t) = \vec{E}_0 \cos(\omega t - \vec{k} \cdot \vec{r}_1)$$

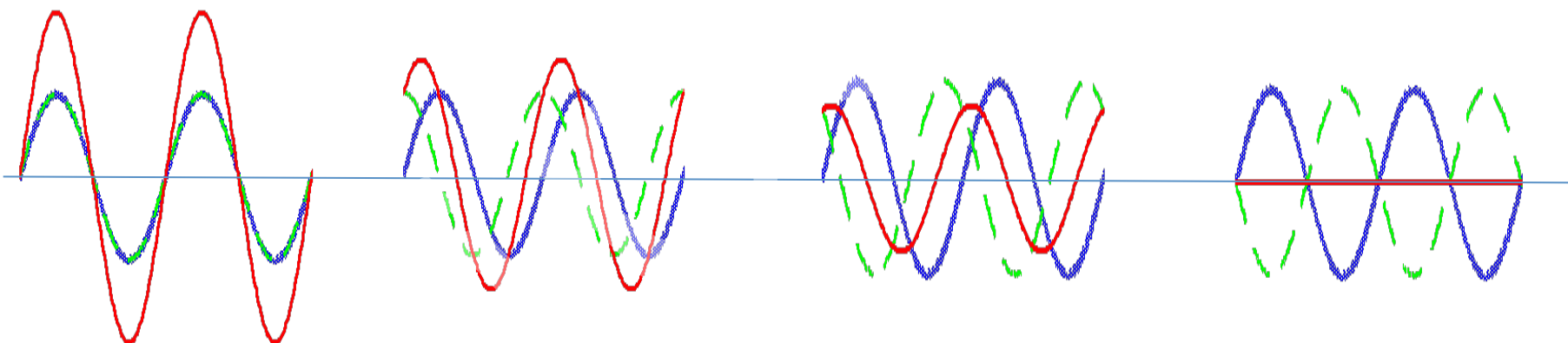
$$\vec{E}_2(r, t) = \vec{E}_0 \cos(\omega t - \vec{k} \cdot \vec{r}_2)$$

Fundamentals of Optics- Jenkins and White

Parte 2 - Capítulo 13

Campo resultante

$$\vec{E}_R(r, t) = \vec{E}_1 + \vec{E}_2$$



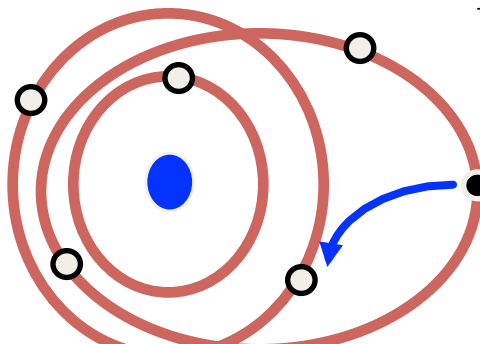
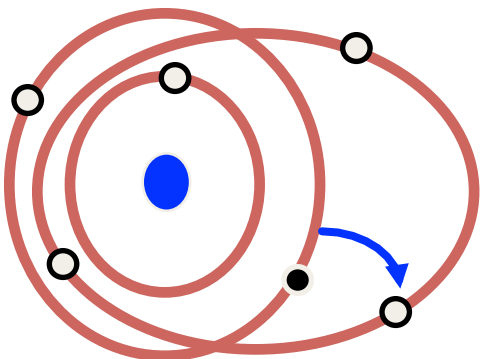
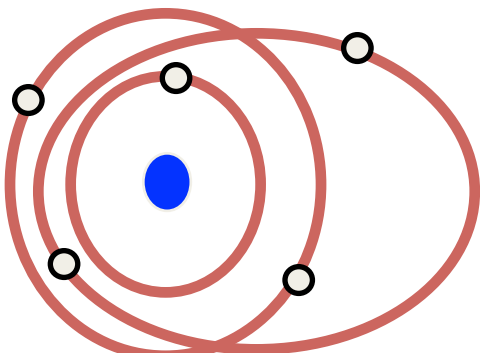
Interferência construtiva

Interferência parcial

Interferência destrutiva

LIGHT **AMPLIFICATION BY** **STIMULATED** **EMISSION OF** **RADIATION**

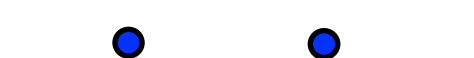
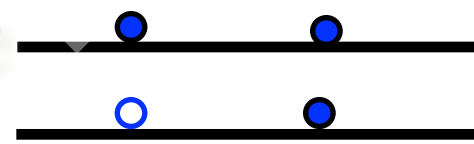
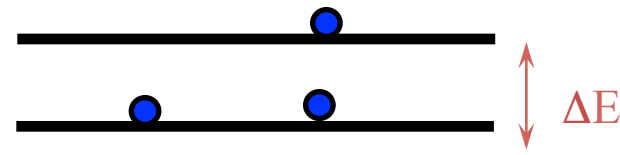
(Amplificação da Luz por Emissão Estimulada de Radiação)



**Absorção
Ressonante**

**Emissão
espontânea**

Fóton
 $\lambda \propto \Delta E$



ABSORÇÃO

$$E_2 - E_1 = h \cdot v = \Delta E$$

$$n_2 \sim 0$$

E_2



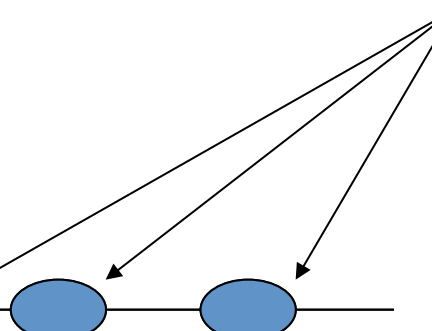
$$n_2 \ll n_1$$

elétrons

E_1



$$n_1$$

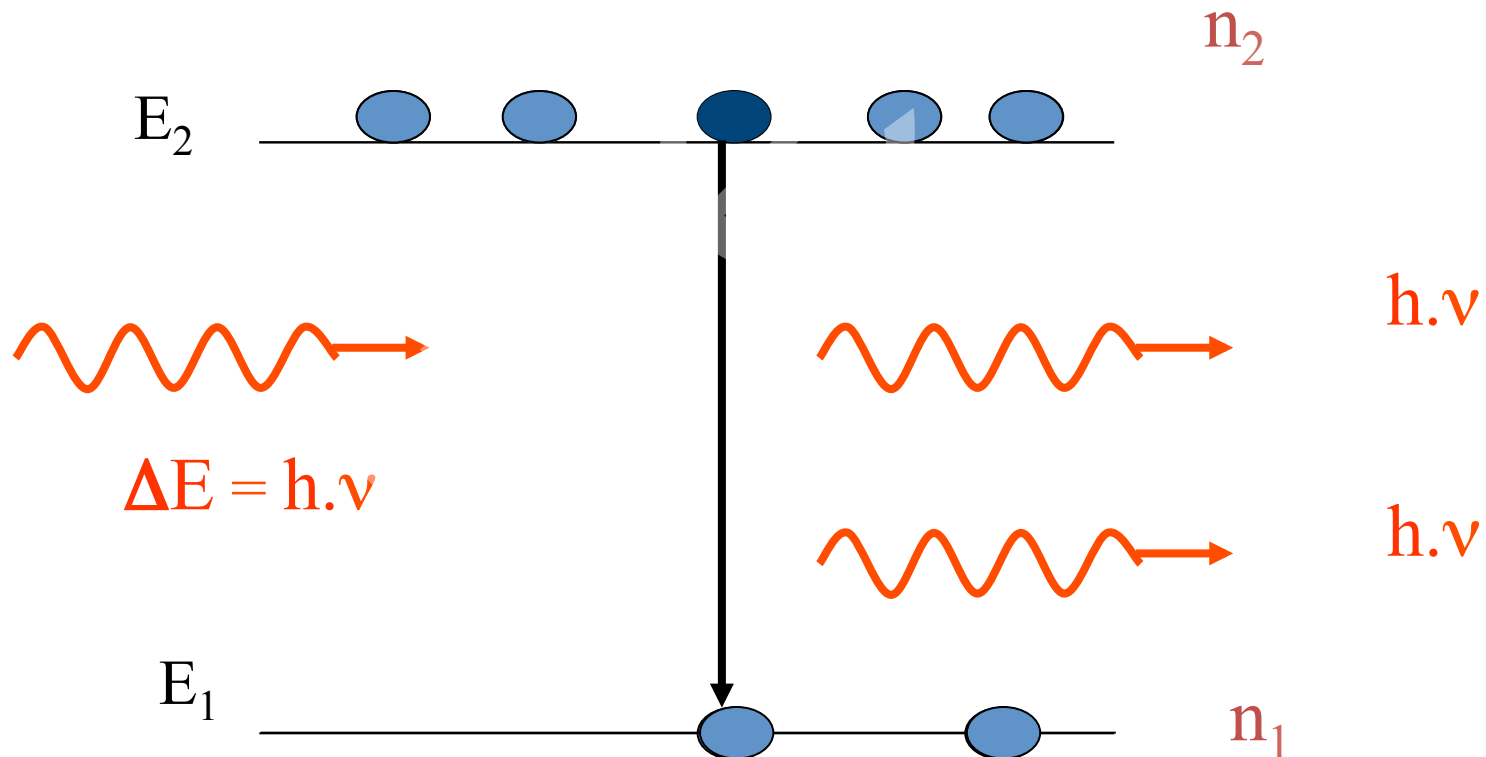


EMISSÃO ESTIMULADA

$$n_2 > n_1$$

$$E_2 - E_1 = h \cdot \nu = \Delta E$$

inversão de população

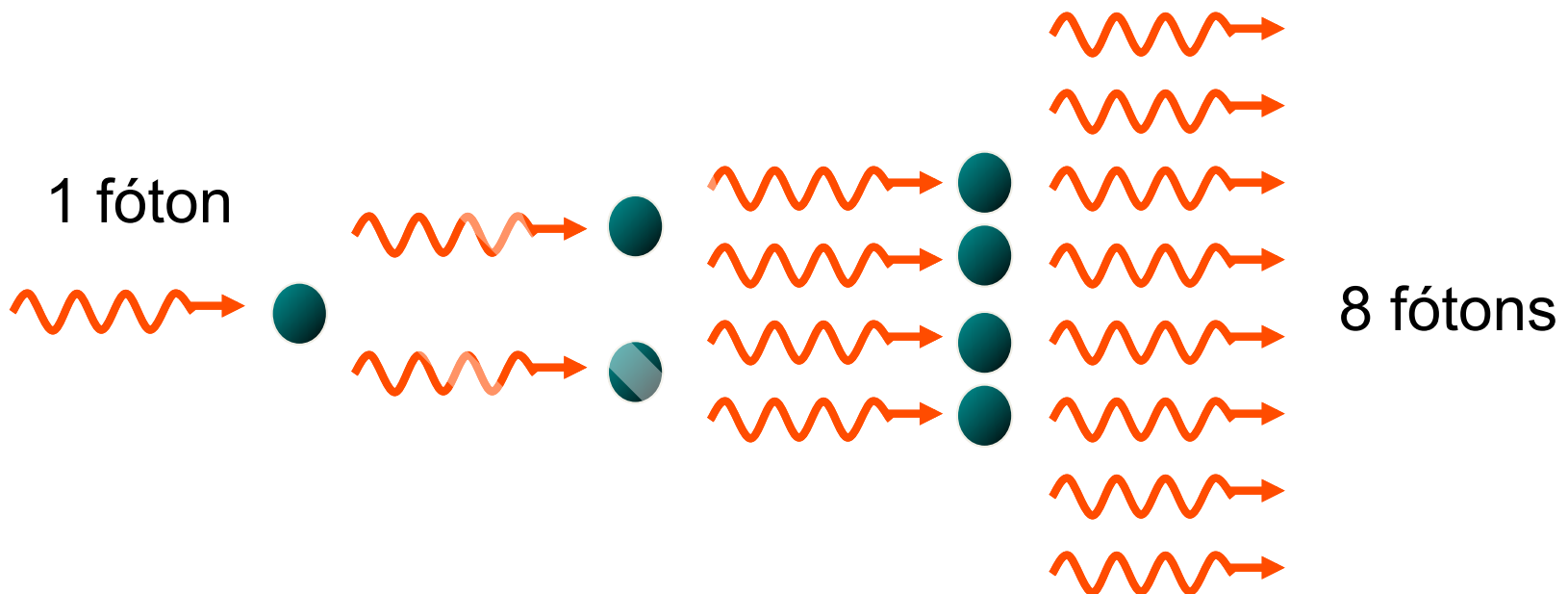


Einstein em 1917 de emissão estimulada pela radiação

EMISSÃO ESTIMULADA

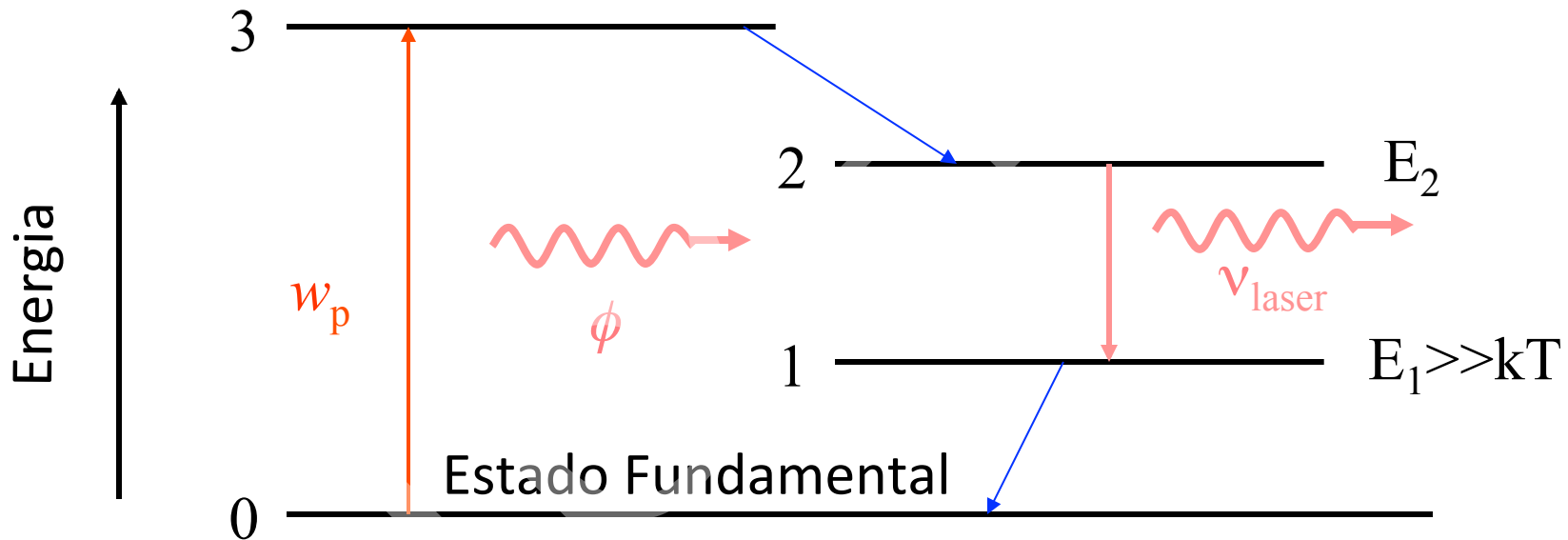
$I_{\text{trans.}} > I_{\text{inc}}$
e a radiação é amplificada.

Light
Amplification
by Stimulated
Emission of
Radiation



LASER

ciclo de bombeamento óptico de 4 níveis ideal



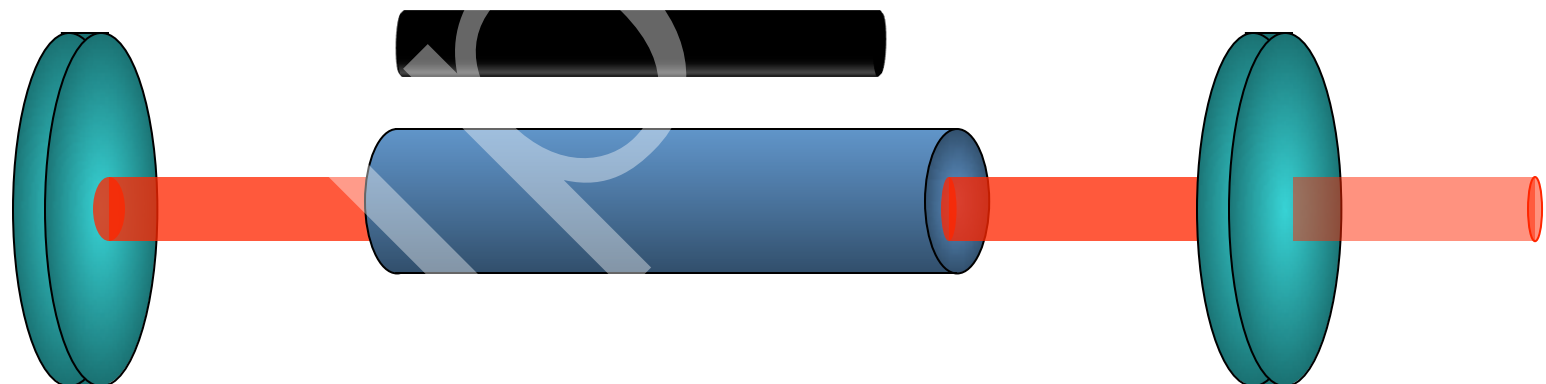
$$\frac{dn_2}{dt} = -n_2 \sigma_e \phi c - \frac{n_2}{\tau} + w_p n_0$$

LASER

Meio Ativo

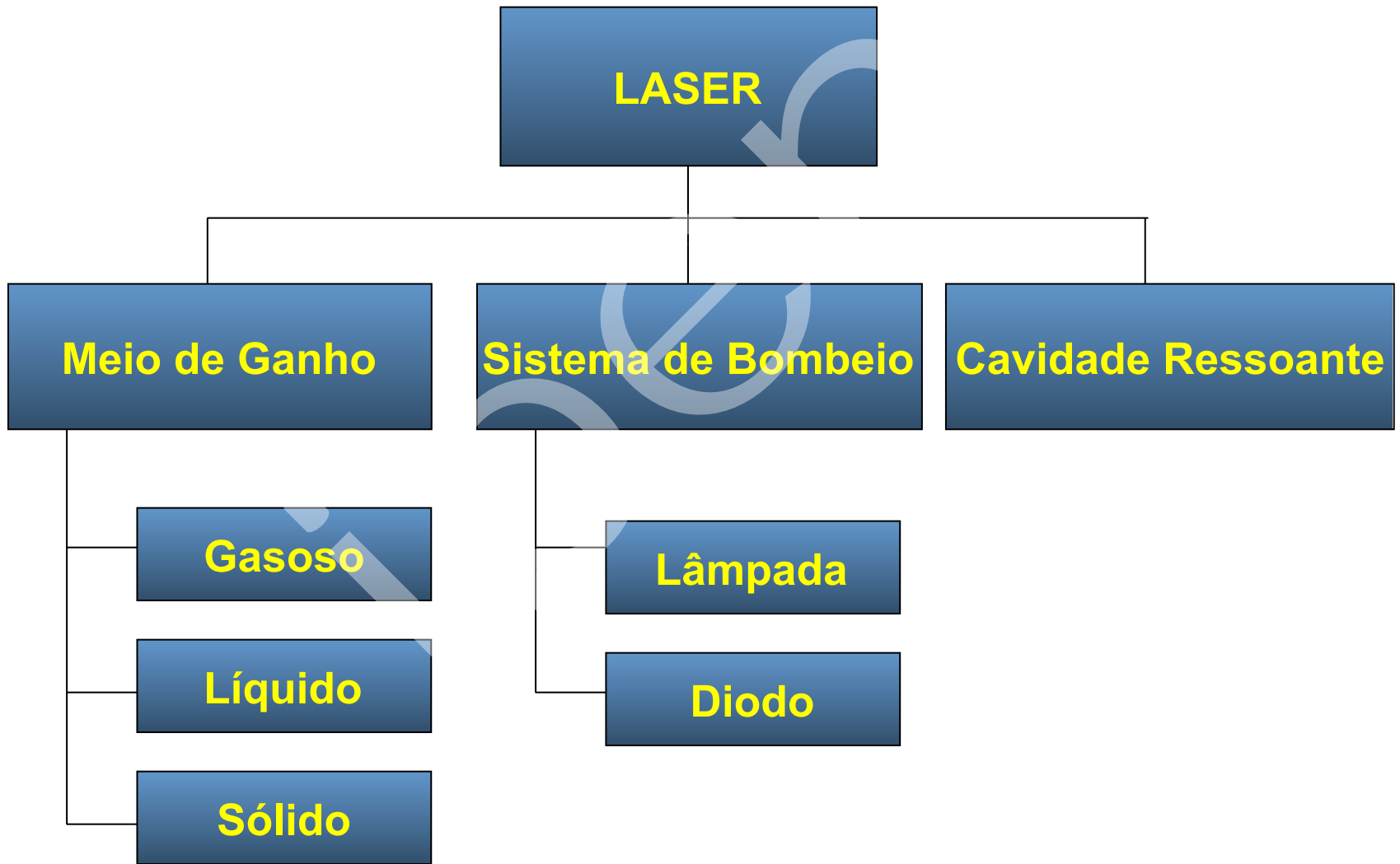
Sistema de Bombeio

Cavidade Ressonante



Radiação laser

Componentes de um Laser



FLUXÔMETRO LASER DOPPLER

VELOCIDADE SANGUÍNEA

VOLUME SANGUÍNEO

FLUXO SANGUÍNEO

NÃO INVASIVA

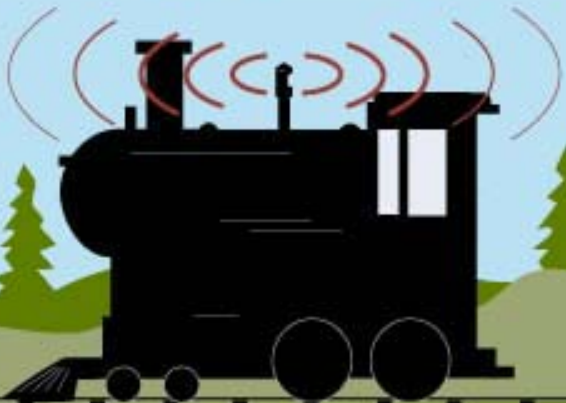
NÃO OFERECE RISCOS

PERMITE A MONITORAÇÃO CONTÍNUA DO FLUXO



CHRISTIAN DOPPLER FOI QUEM PELA PRIMEIRA VEZ, EM 1842, POSTULOU QUE A FREQUÊNCIA DE ONDAS ACÚSTICAS PODERIA MUDAR SE: OU A FONTE OU O OBSERVADOR ESTIVER EM MOVIMENTO.

mesma freqüência



Fonte estacionária

Freqüência
aumenta

Freqüência
diminui

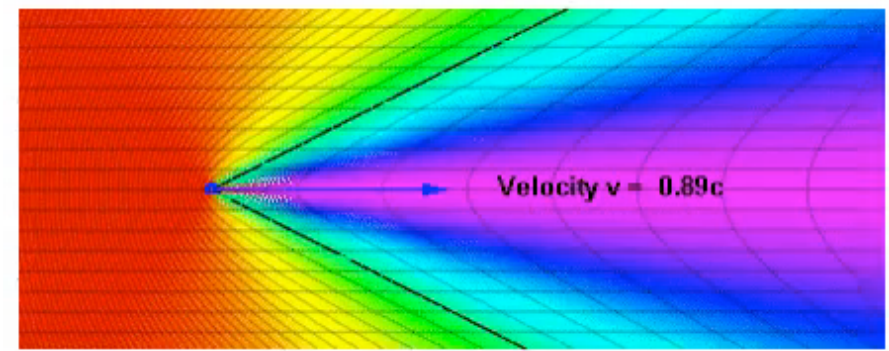


Fonte em movimento

O Efeito Doppler

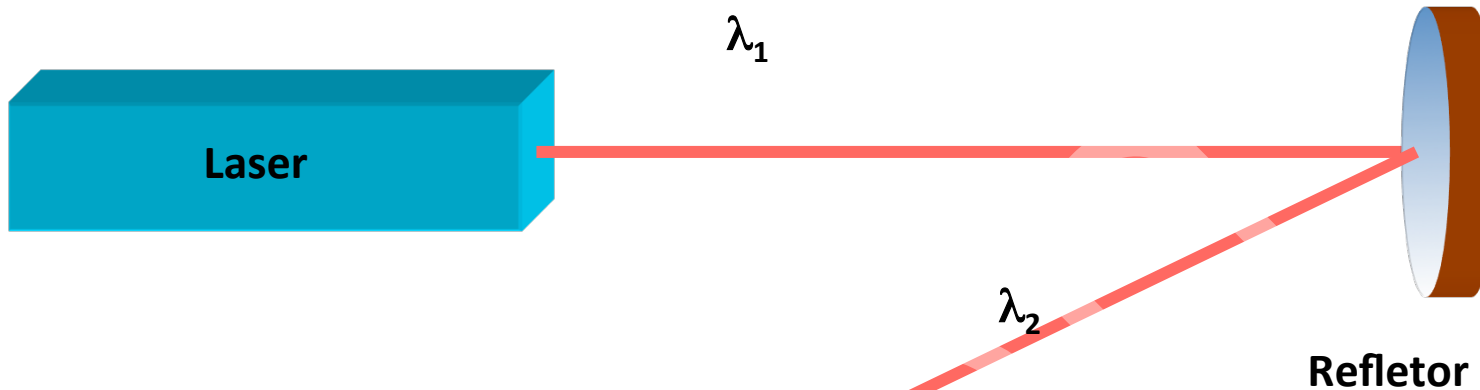
Existem muitos exemplos do efeito Doppler no cotidiano:

- Sirene de viatura
- Buzina de carro
- Apito de trem



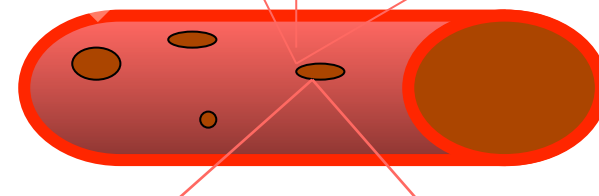
O Efeito Doppler

v
←

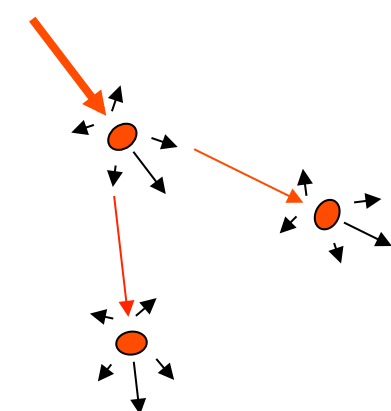


$$\lambda_2 - \lambda_1 \propto v$$

RADIAÇÃO LASER INCIDENTE

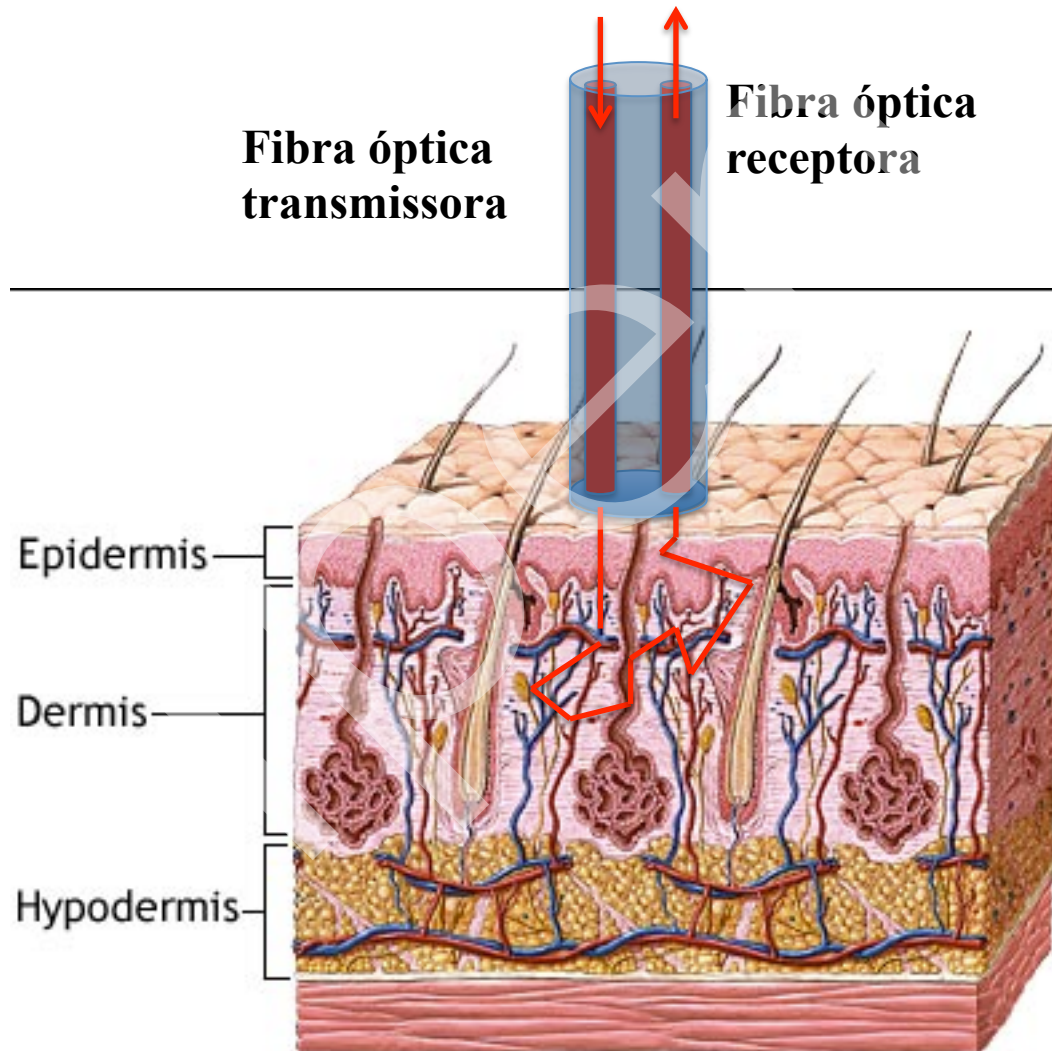


VASO SANGUÍNEO



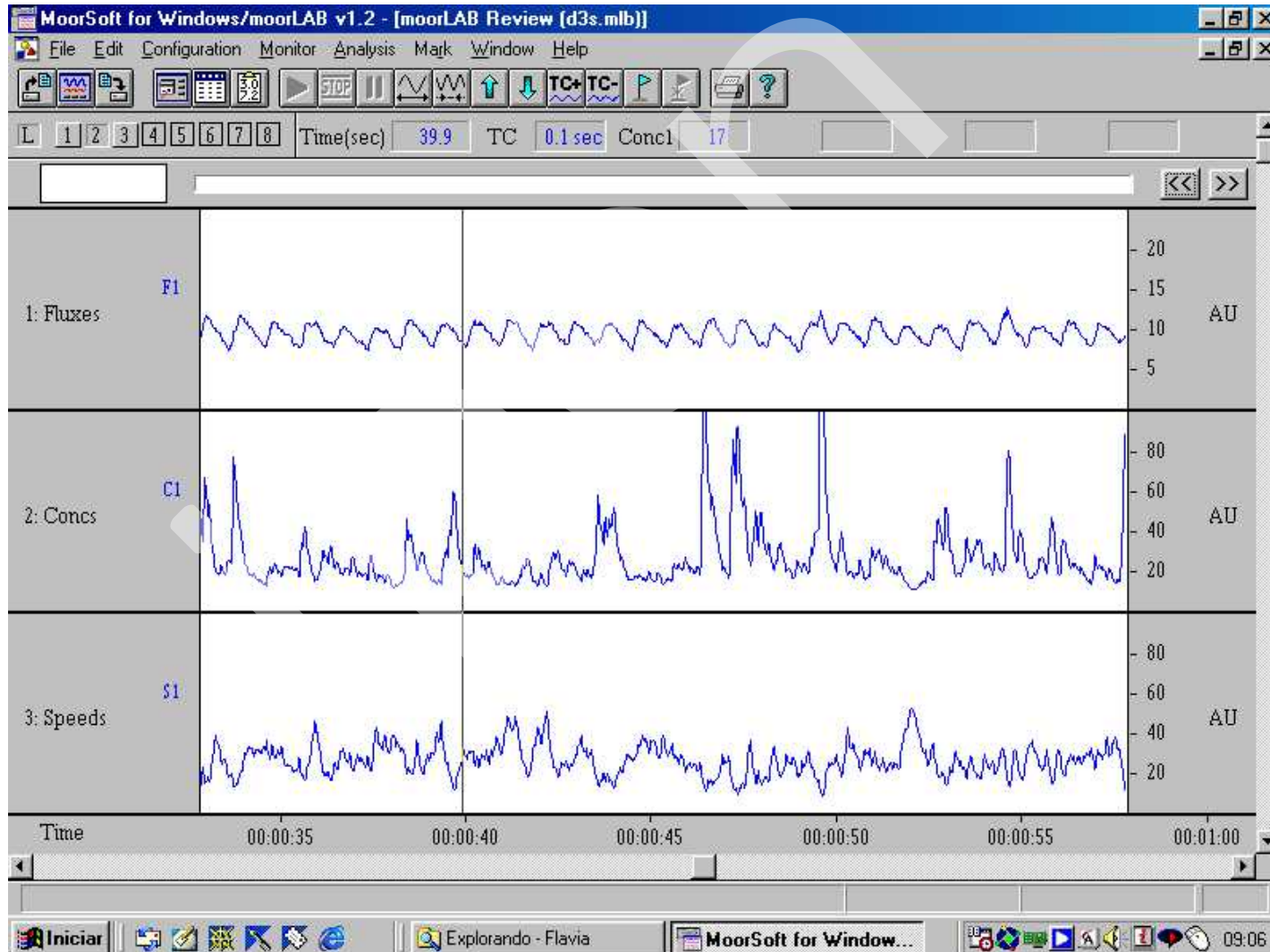
Fluxômetro Laser Doppler

ESTUDO DA MICROCIRCULAÇÃO



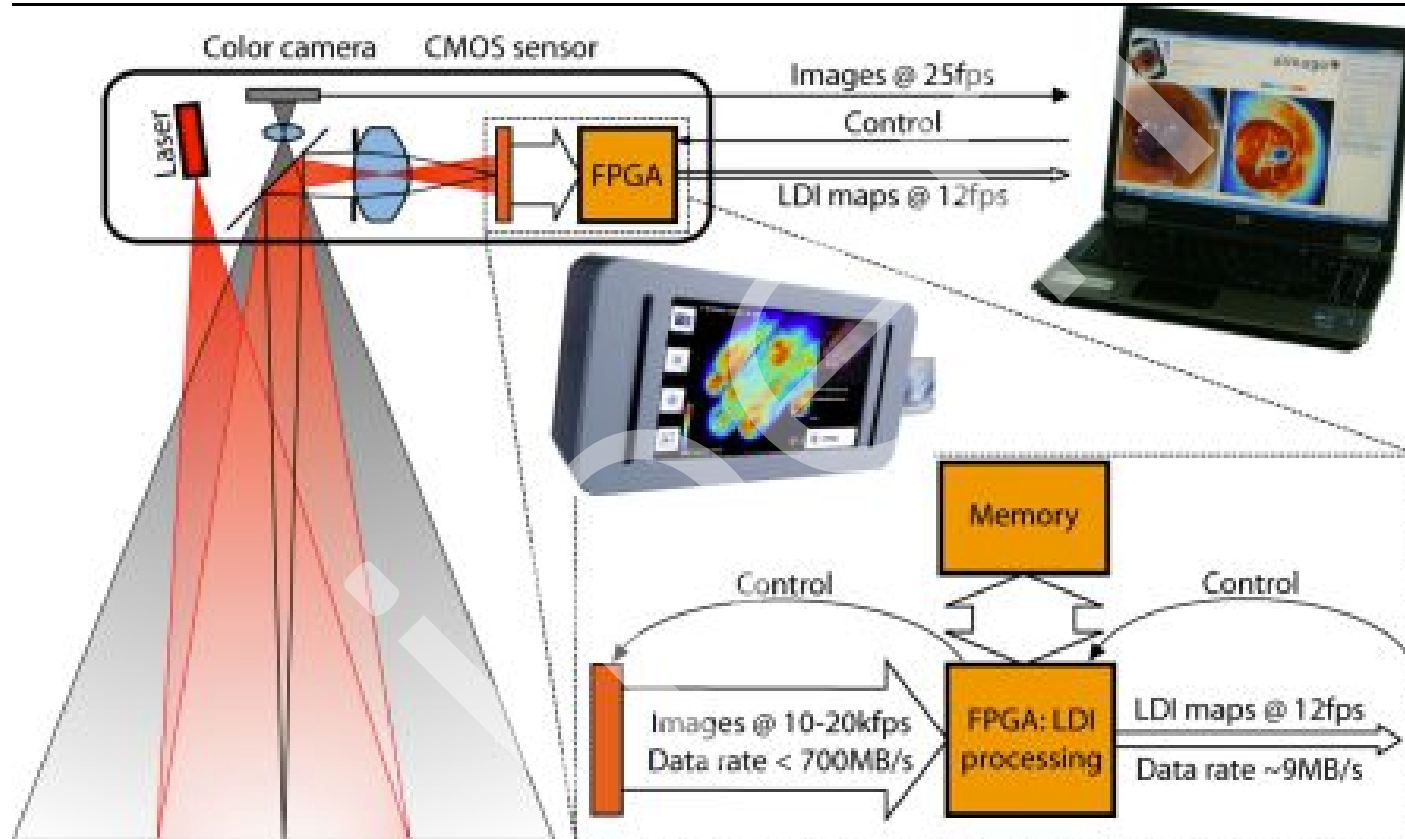
Fluxômetro Laser Doppler

APLICAÇÕES



IMAGENS VIA LASER DOPPLER

Visualização da Microvascularização



SISTEMA DE IMAGEM LASER DOPPLER

APLICAÇÕES

Reumatologia



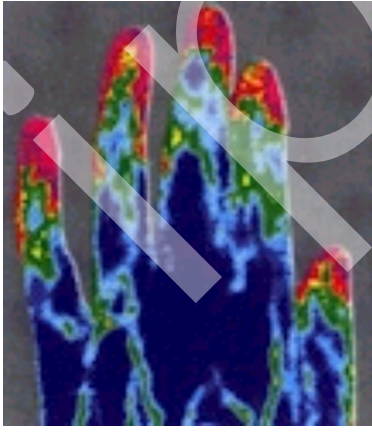
Controle



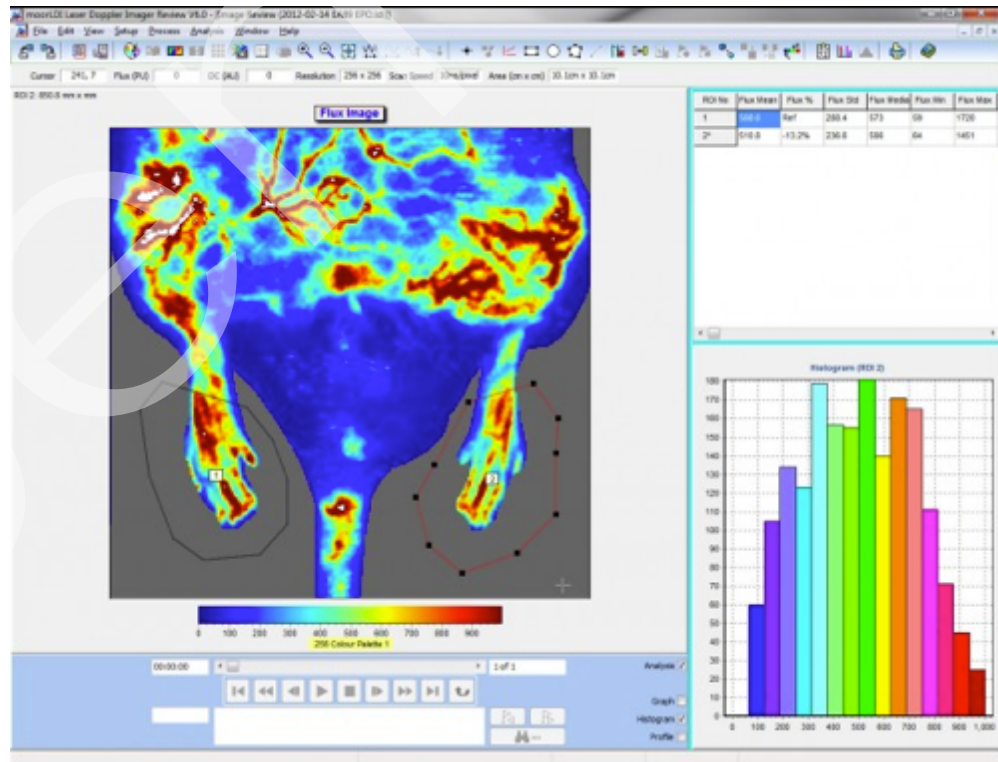
Após imersão
em água fria



Recuperação
após 7,5 min.



Recuperação
após 15 min.



Optical Spectroscopy

Optical Spectroscopy - Processes Monitored
 UV/ Fluorescence/ IR/ Raman/ Circular Dichroism

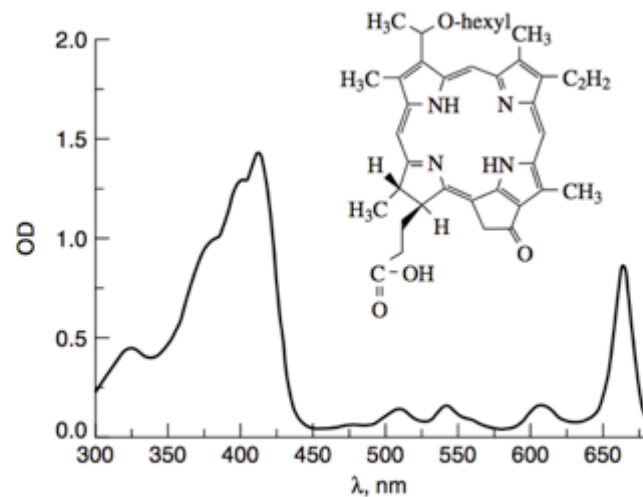
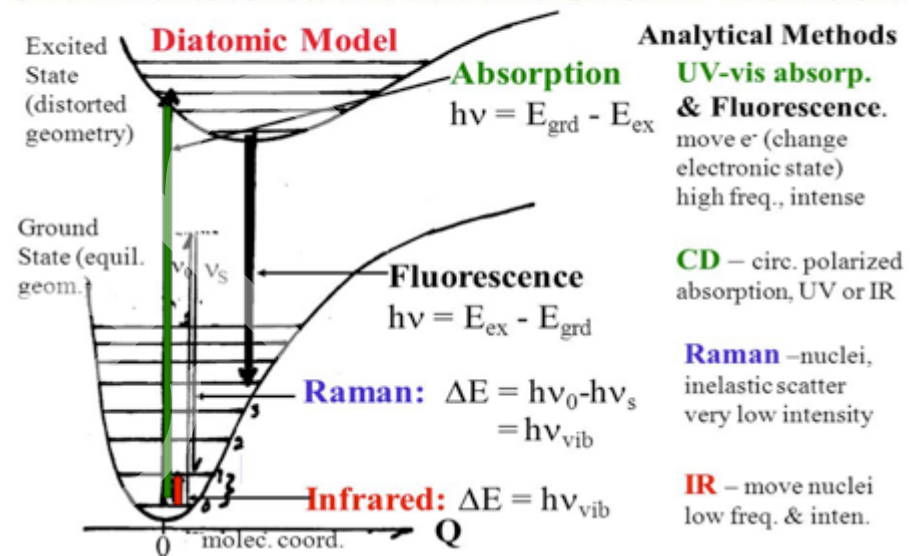
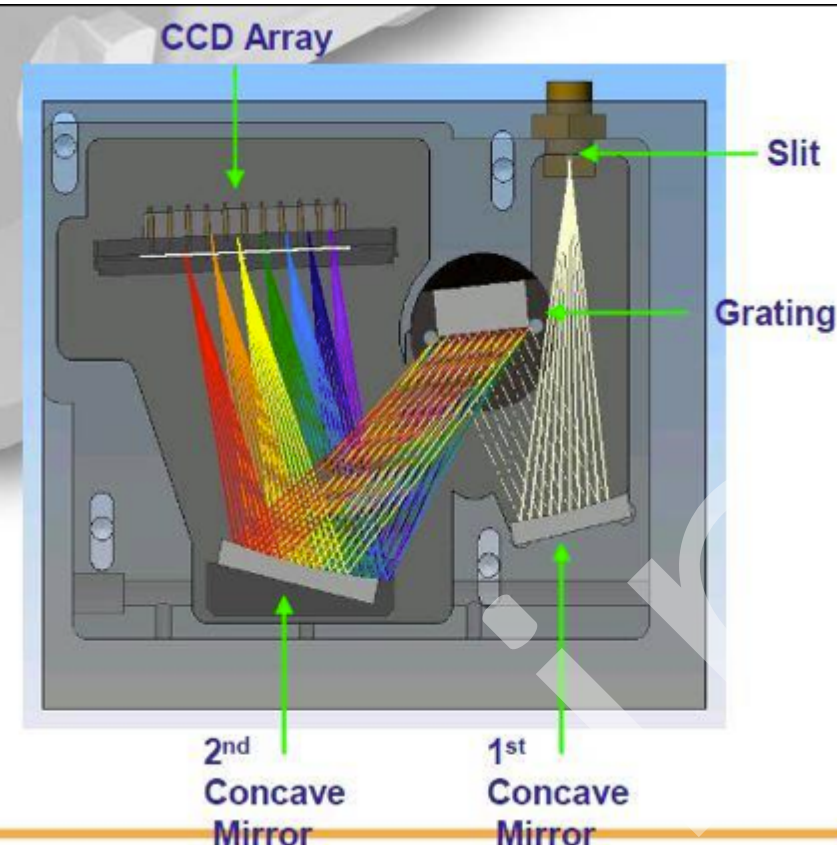
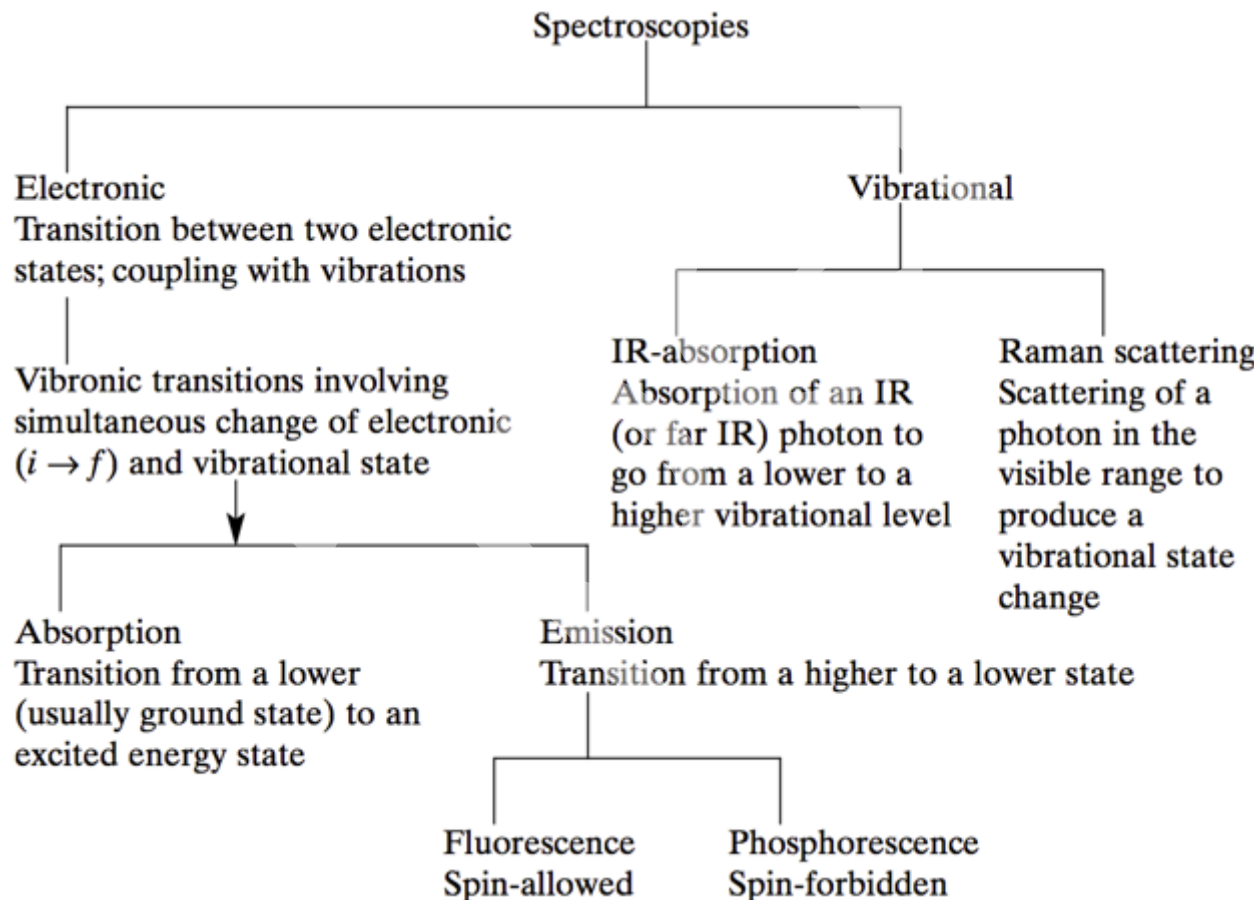


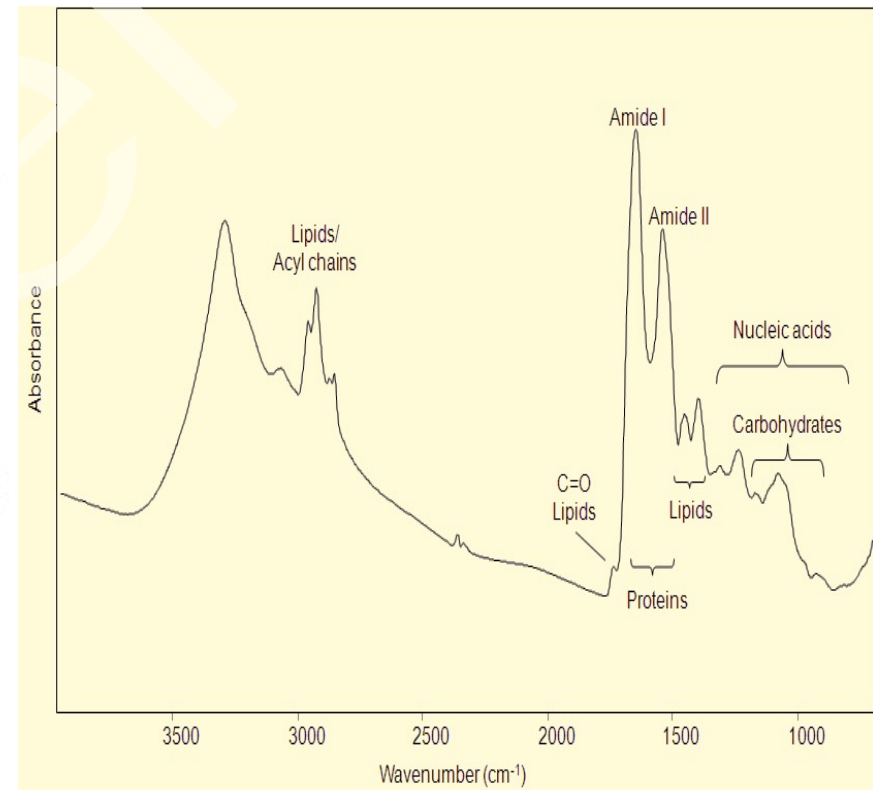
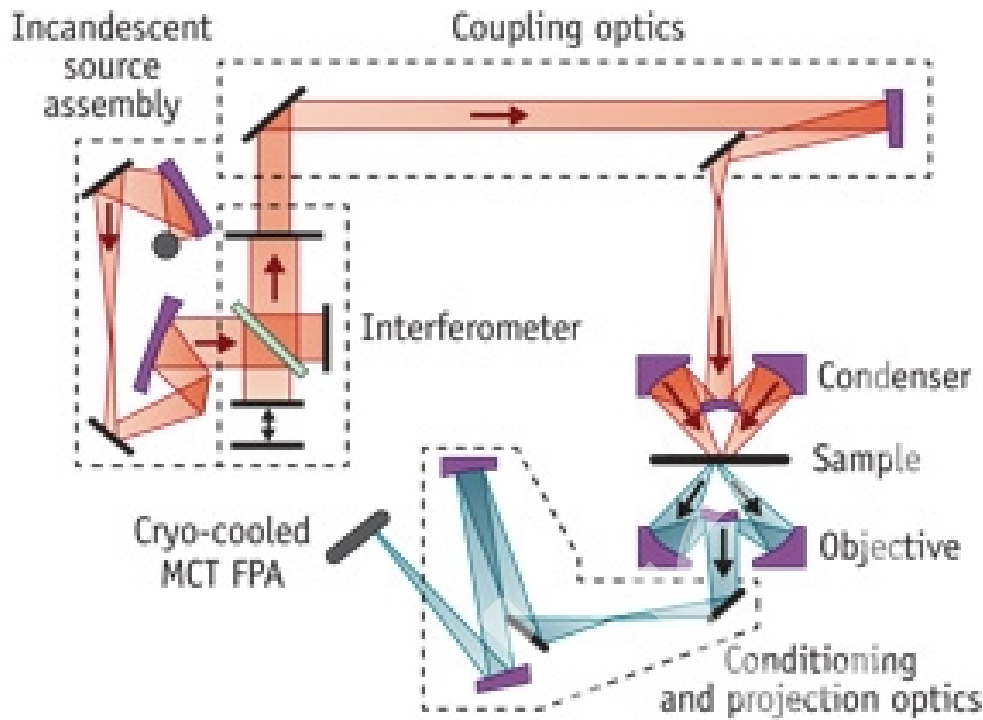
Figure 4.8. Absorption spectrum of HPPH (2-divinyl-2-(1-hexyloxyethyl)pyropheophorbide), a drug for photodynamic therapy. Water solution, $C = 22 \mu\text{M}$.

Various Spectroscopies Useful for Biophotonics

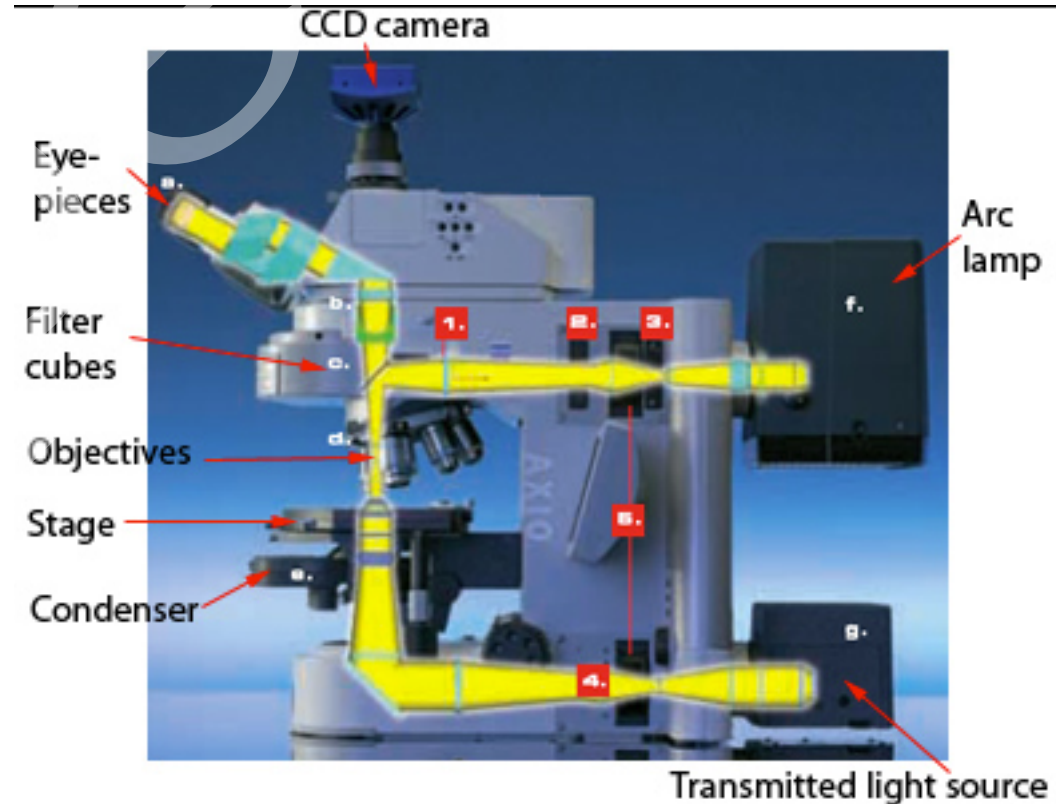
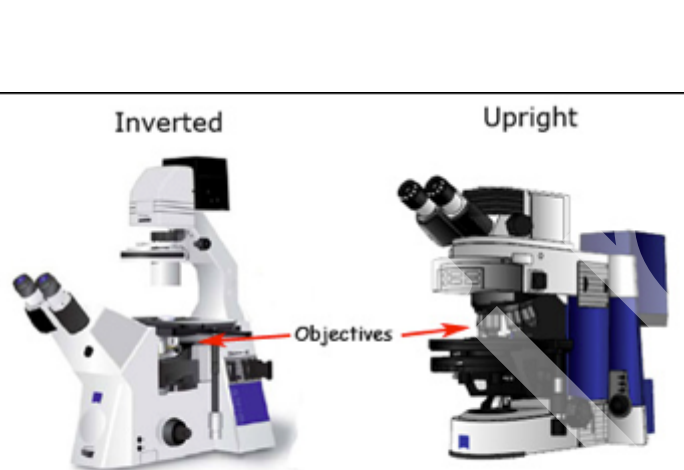
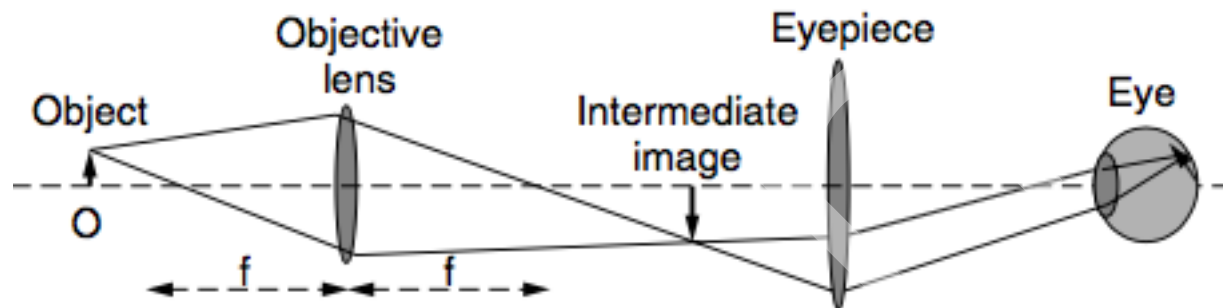


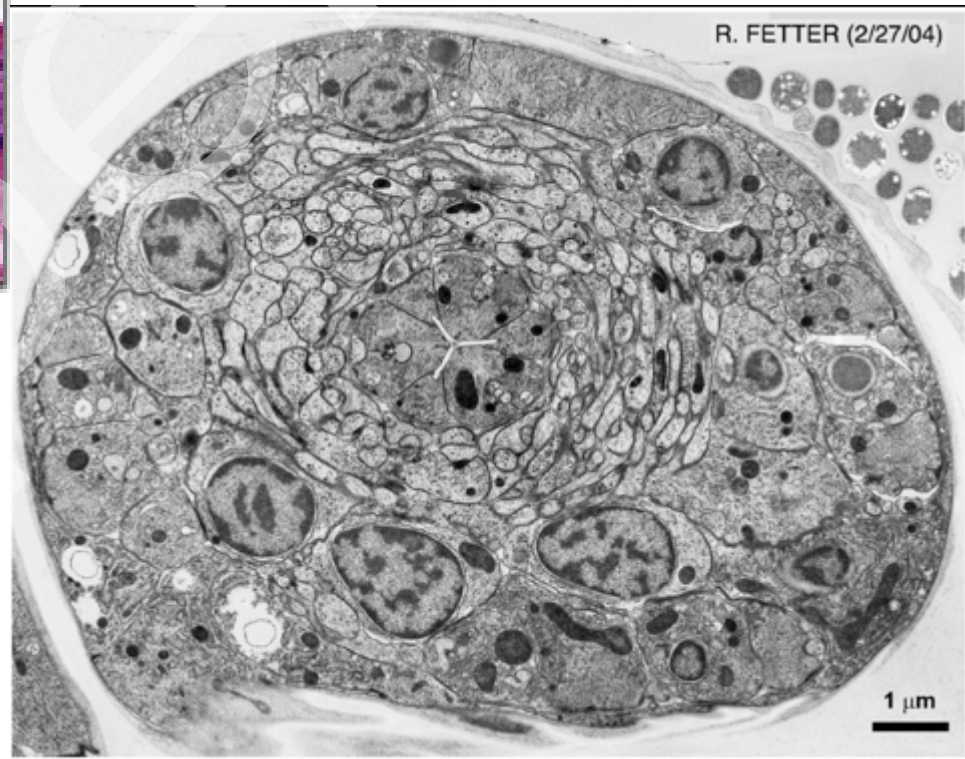
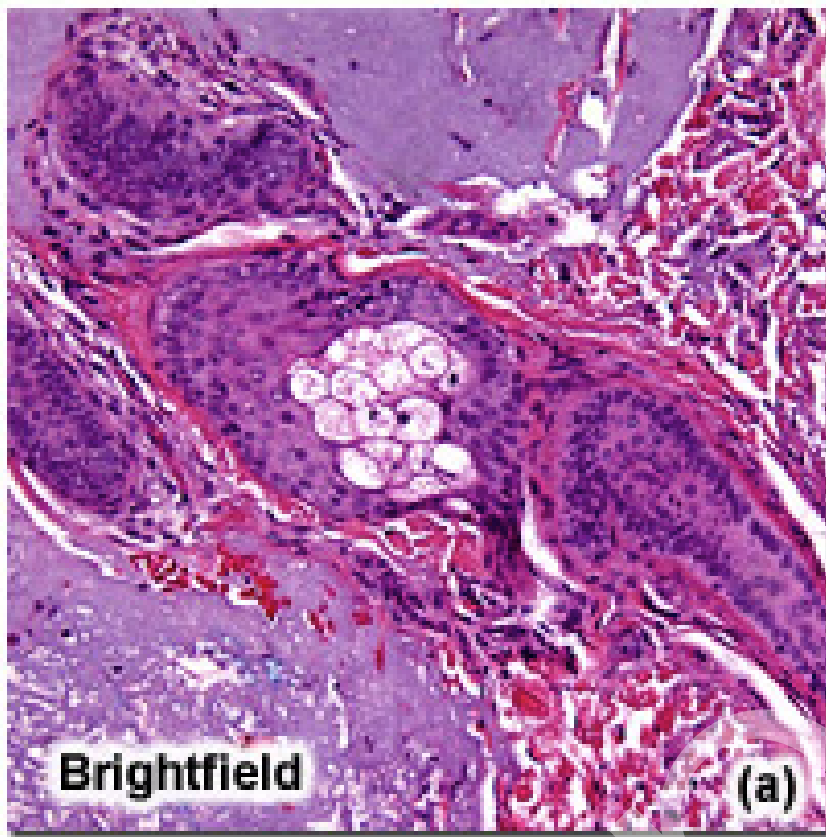
Fourier Transform Spectrometers FTIR

FTIR microscope



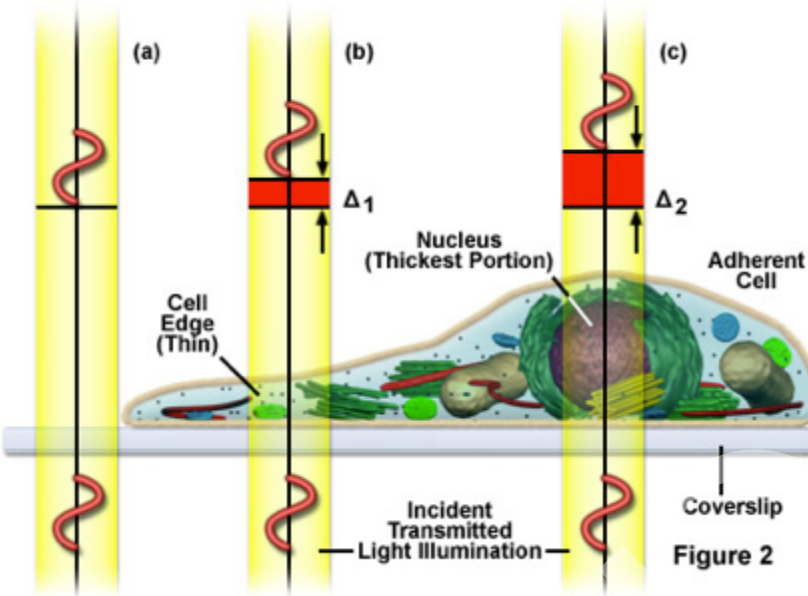
TRANSMISSION MICROSCOPY



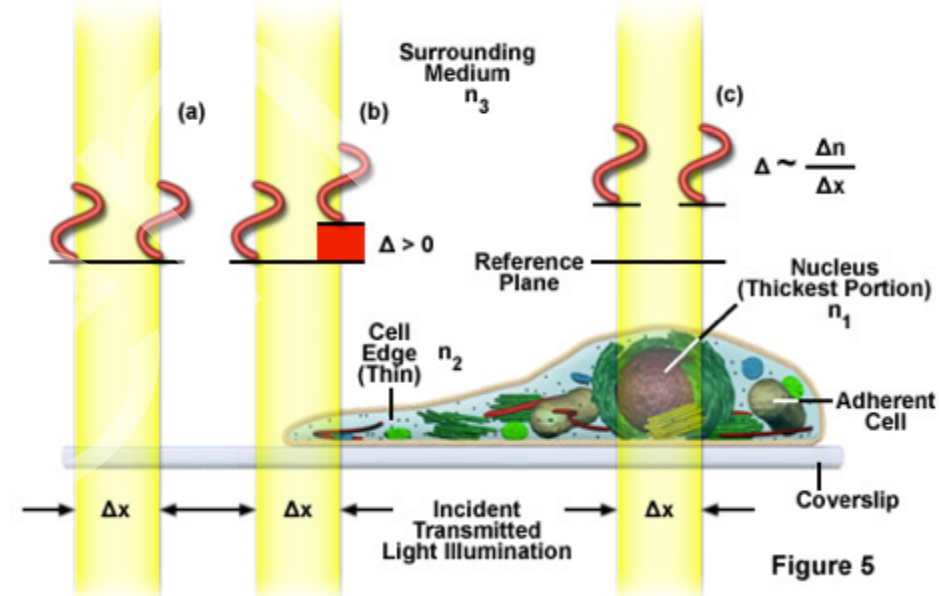


Differential Interference Contrast Microscopy (DIC)

Phase Contrast Imaging of Transparent Thin Specimens

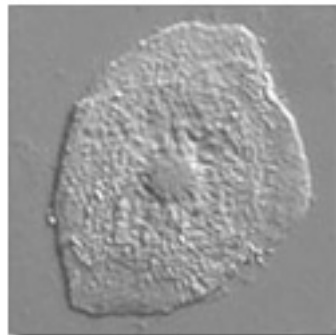
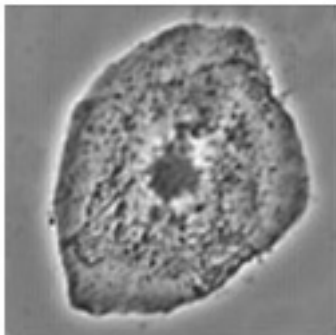
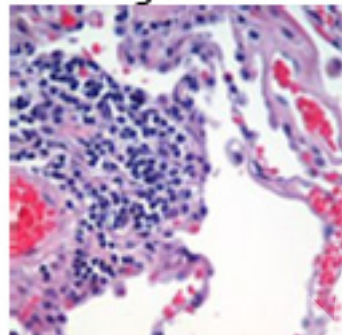


Differential Interference Contrast Imaging of Transparent Thin Specimens



- The split beams enter and pass through the specimen where their wave paths are altered in accordance with the specimen's varying thicknesses, slopes, and refractive indices. When the parallel beams enter the objective, they are focused above the rear focal plane where they enter a second modified Wollaston prism that combines the two beams at a defined distance outside of the prism itself.
- As a result of having traversed the specimen, the paths of the two beams are not of the same length (optical path difference) for different areas of the specimen.

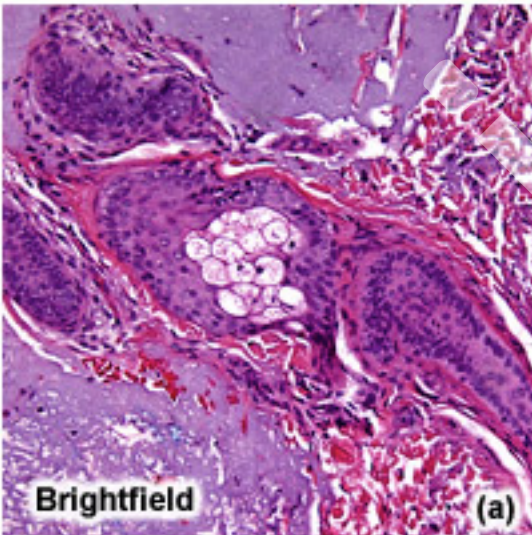
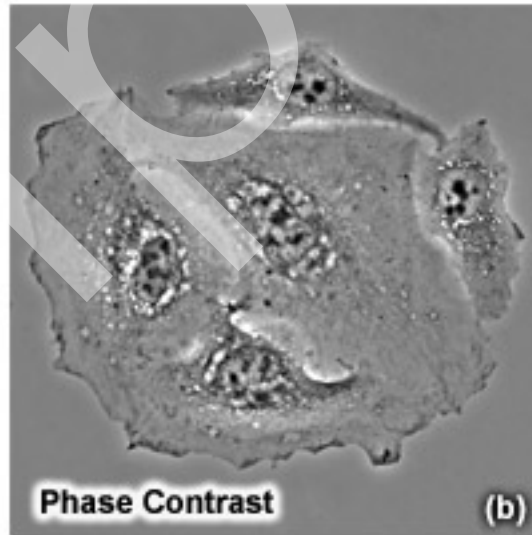
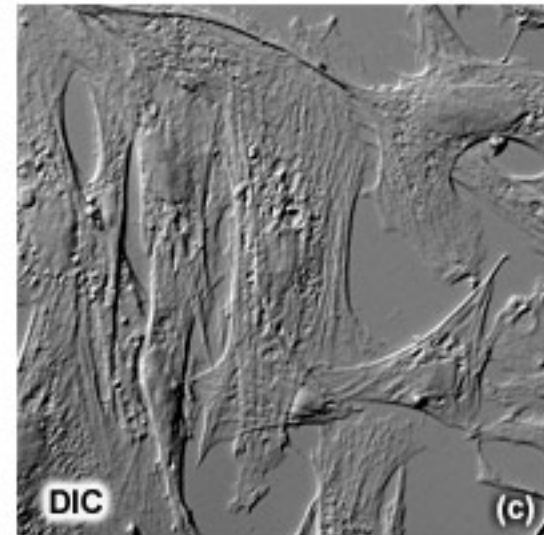
- After passing through another polarizer (analyzer) above the upper Wollaston beam-combining prism, these two beams interfere to translate the path difference introduced by the objects in the sample plane, into intensity difference.
- When a white light source from a lamp is used for imaging, each color will have a different optical path-length difference, thereby producing a color contrast. This results in observing the object details in pseudo-3-D and in color contrast

DIC**Phase****Colour
brightfield**

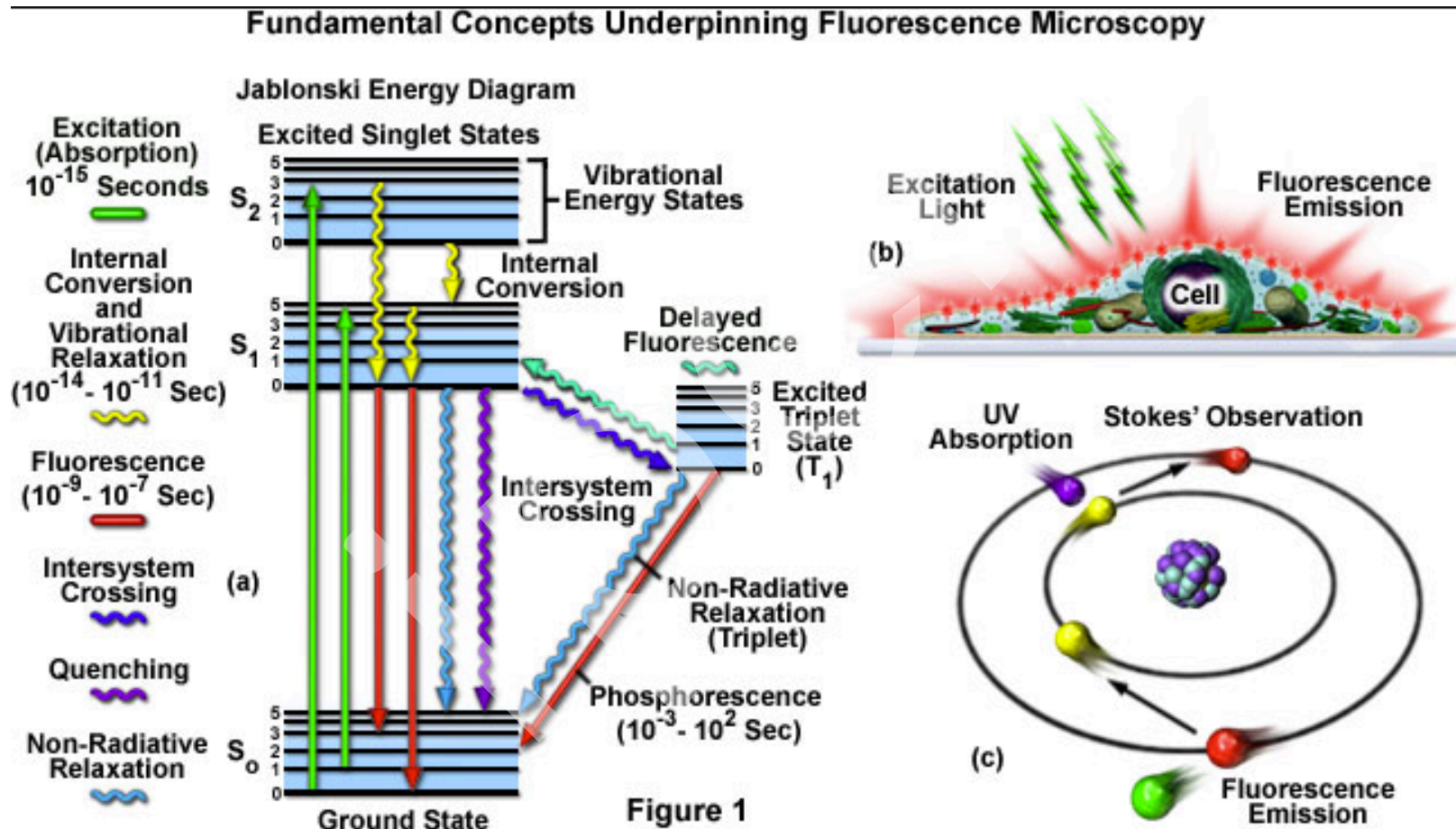
Phase contrast yields image intensity values as a function of specimen optical path length magnitude, with very dense regions (those having large path lengths) appearing darker than the background

In DIC the optical path length gradients are primarily responsible for introducing contrast into specimen images. Steep gradients in path length generate excellent contrast, and images display a pseudo three-dimensional relief shading that is characteristic of the DIC technique. Regions having very shallow optical path slopes, such as those observed in extended, flat specimens, produce insignificant contrast and often appear in the image at the same intensity level as the background.

Contrast-Enhancing Techniques in Optical Microscopy

**(a)****Phase Contrast****(b)****DIC****(c)**

FLUORESCENCE MICROSCOPY



FLUORESCENCE MICROSCOPY

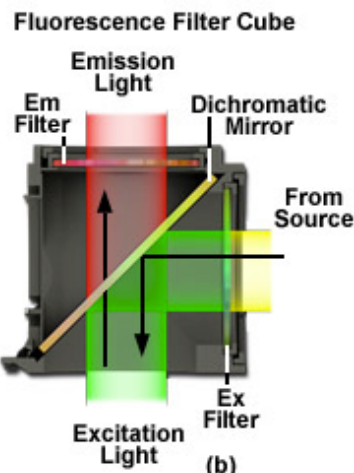


Figure 4

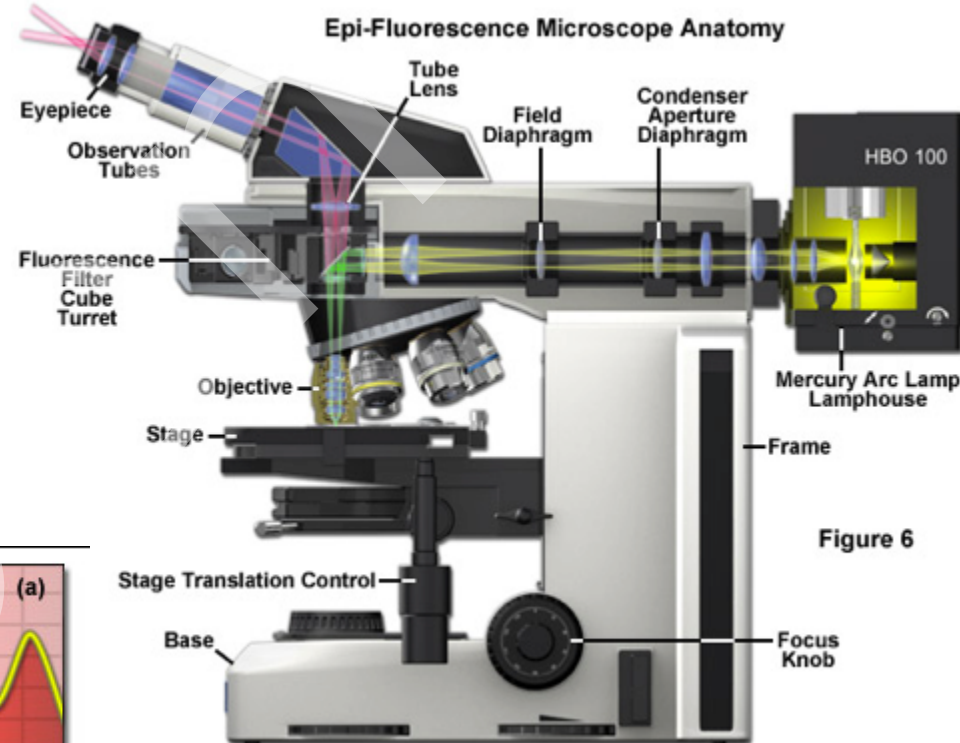
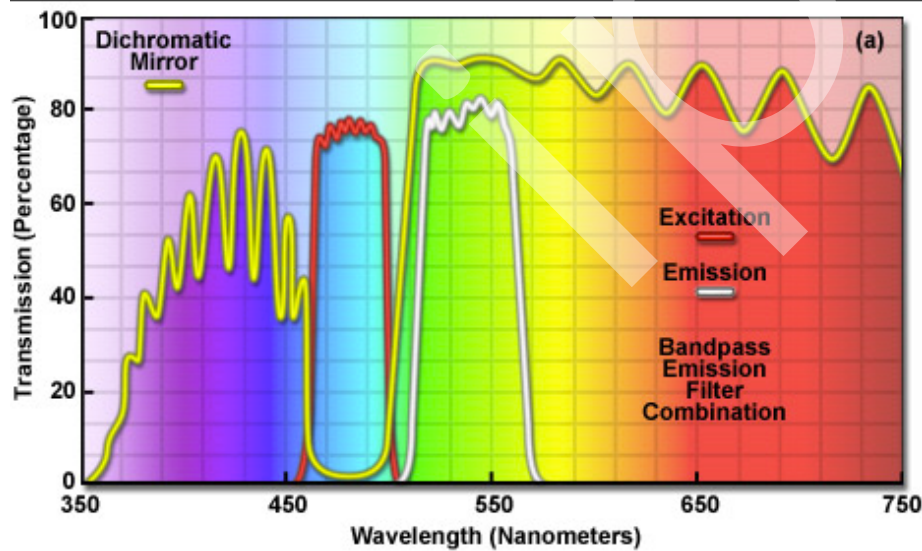
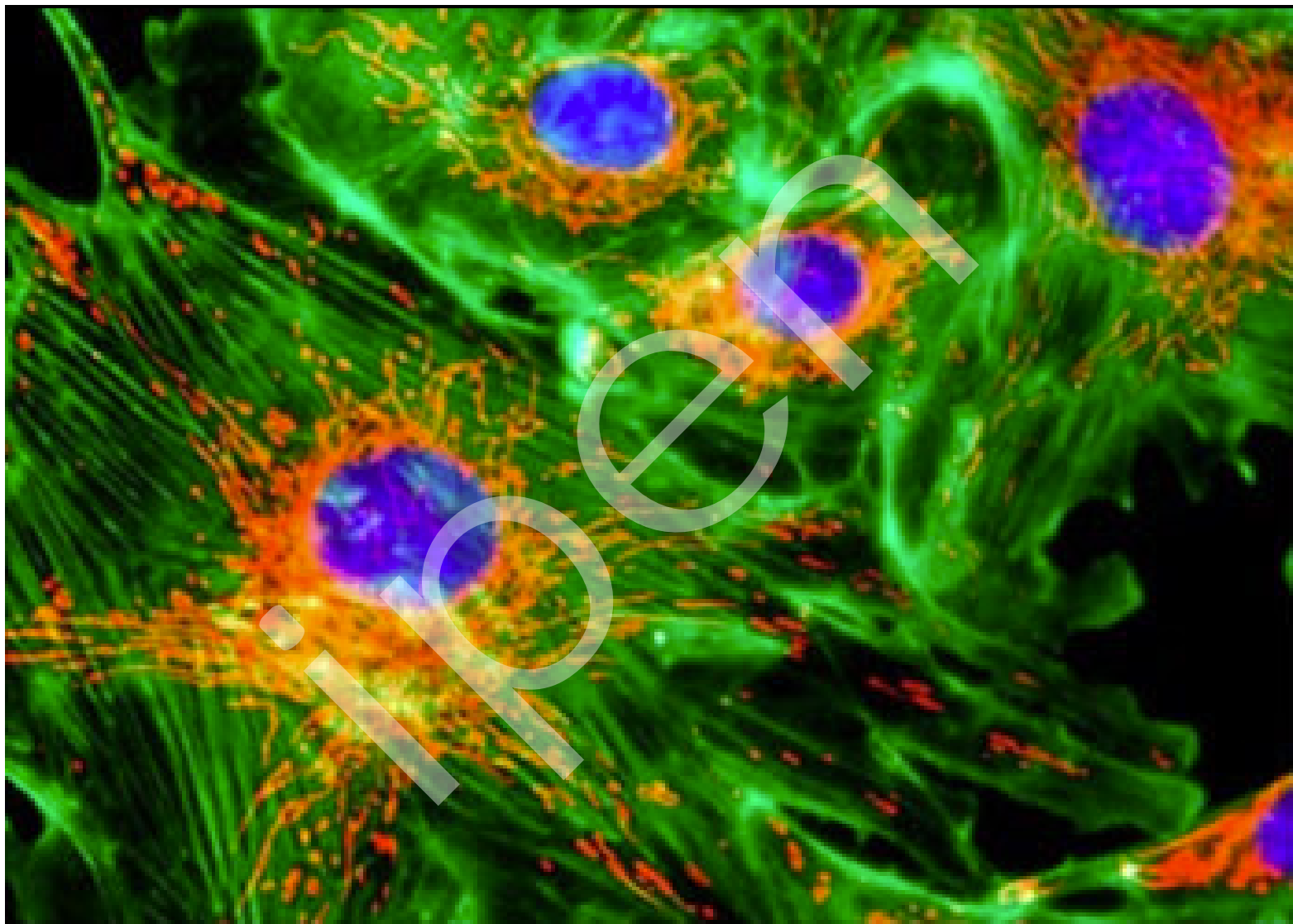
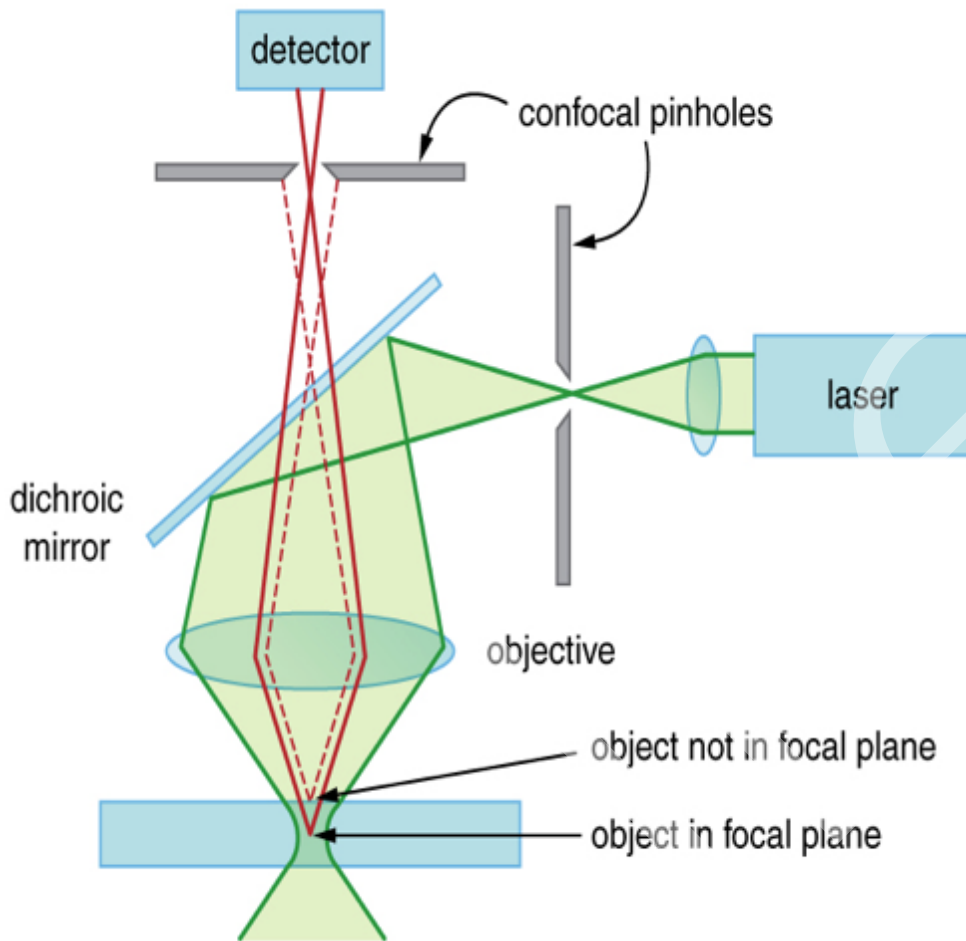


Figure 6



CONFOCAL MICROSCOPY



Pollen Grain Serial Optical Sections by Confocal Microscopy

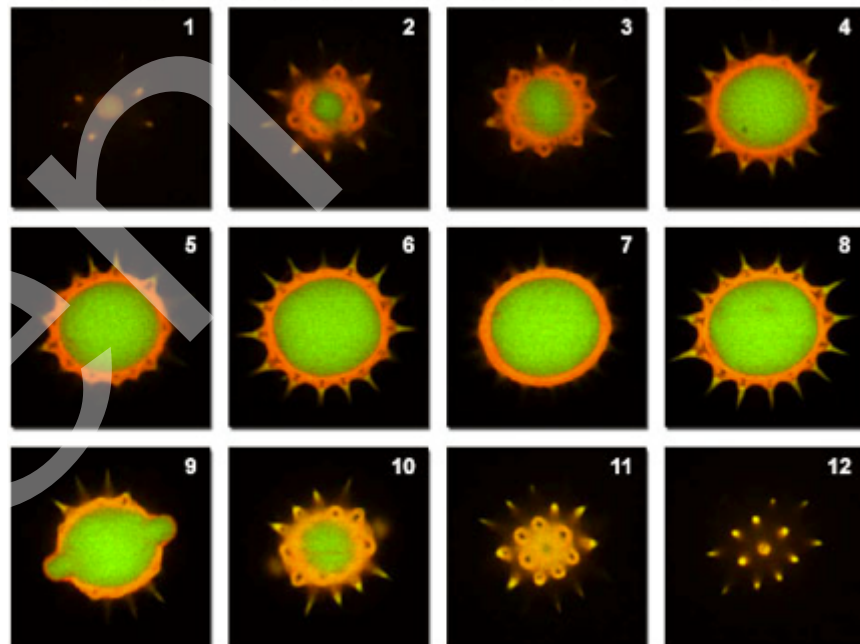
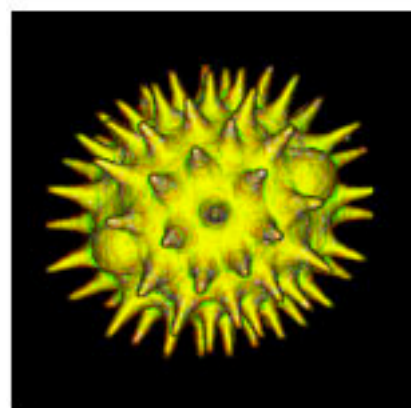


Figure 6



MULTIPHOTON MICROSCOPY

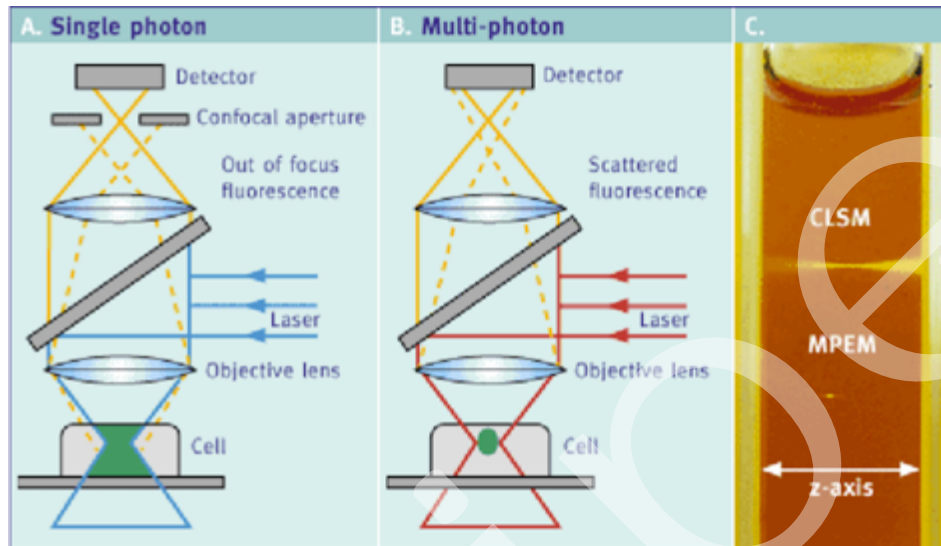
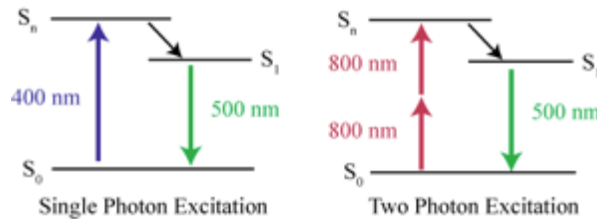
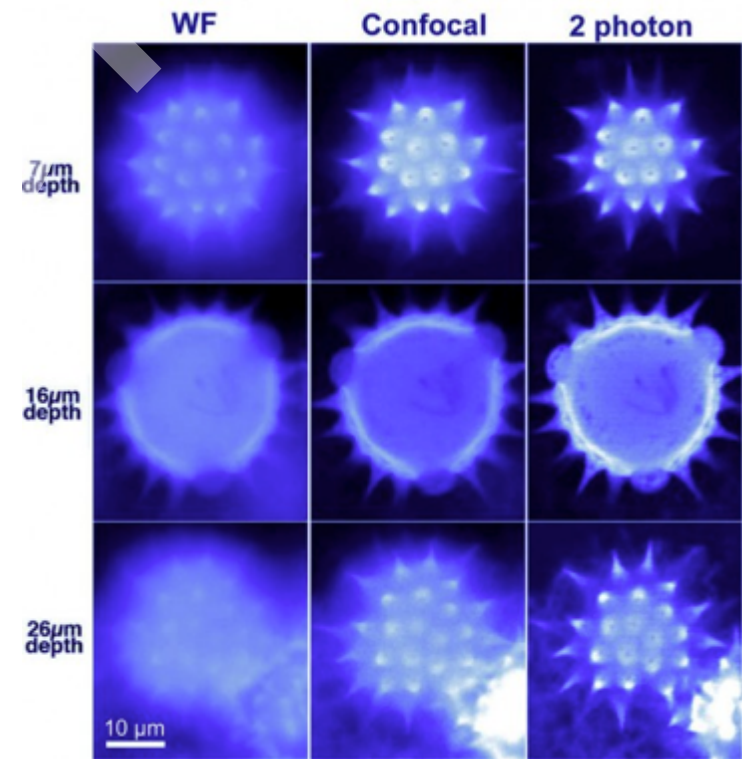
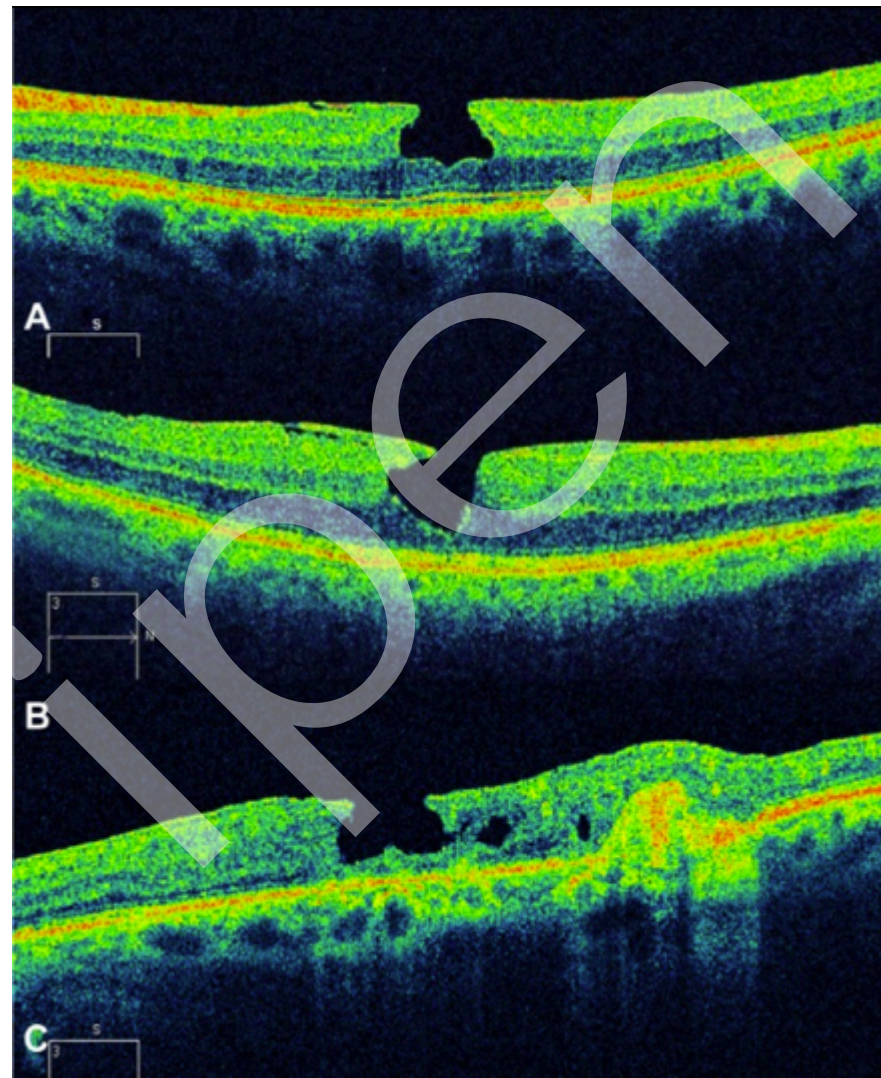


Figure 3: Optical principles of (A) confocal laser scanning microscopy (CLSM) and (B) multi-photon excitation microscopy (MPEM).



OPTICAL COHERENCE TOMOGRAPHY



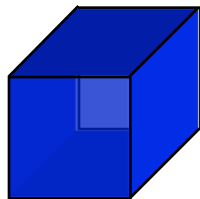
What is a Tomography?



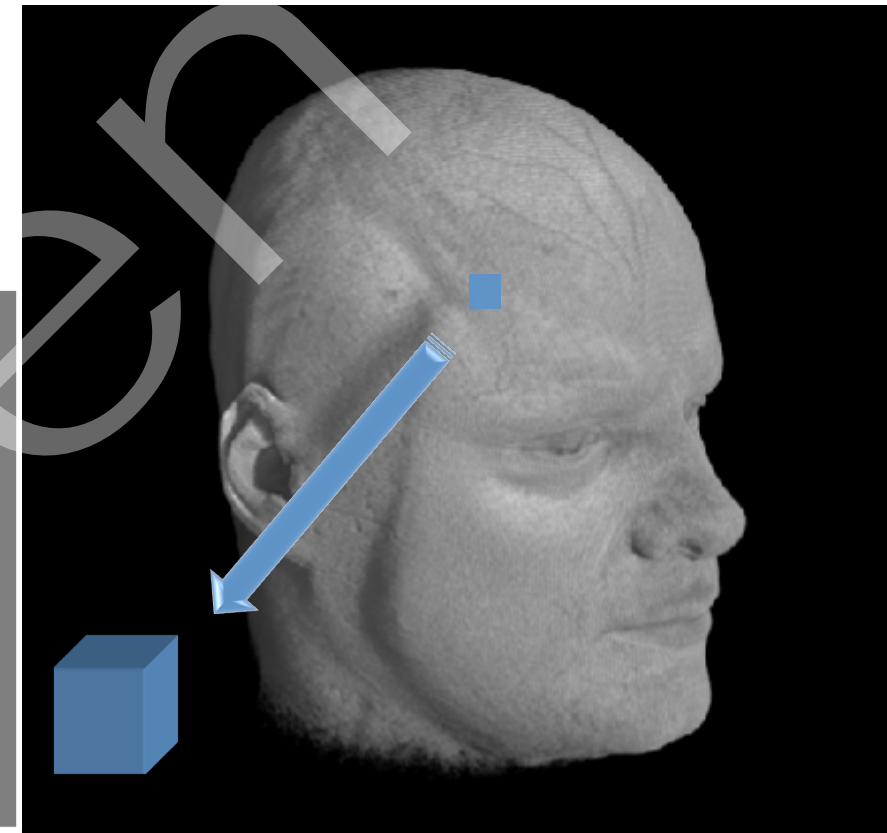
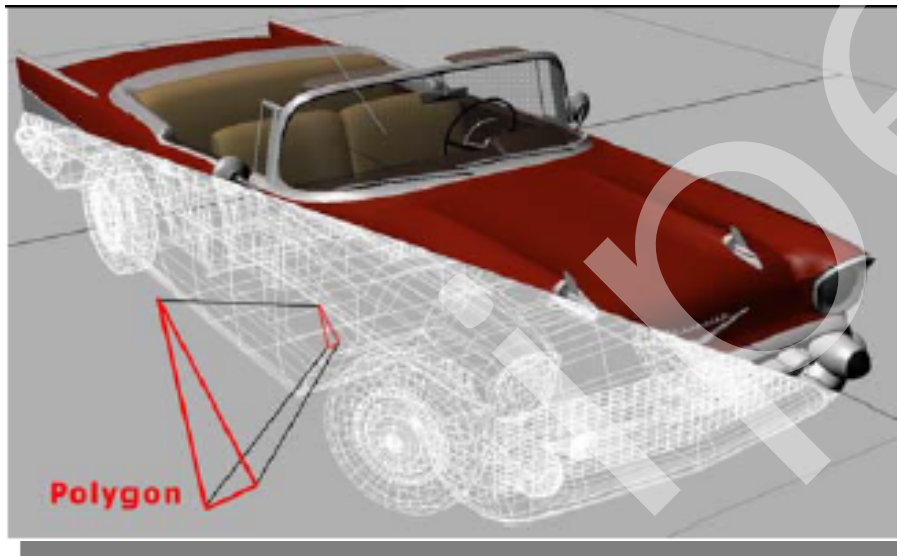
Basic Unit of Image Information



pixel



voxel



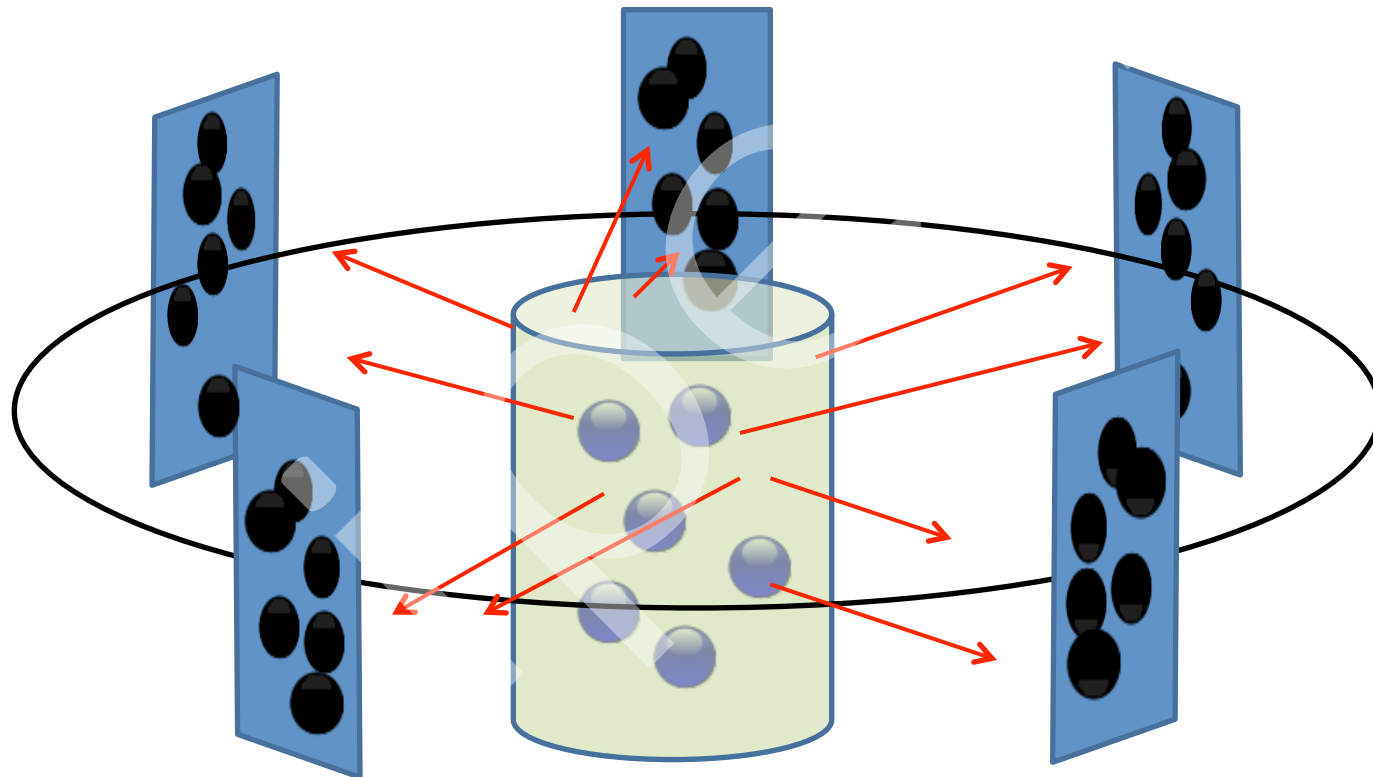
Information about:

- Light and reflectivity of a surface

Information about:

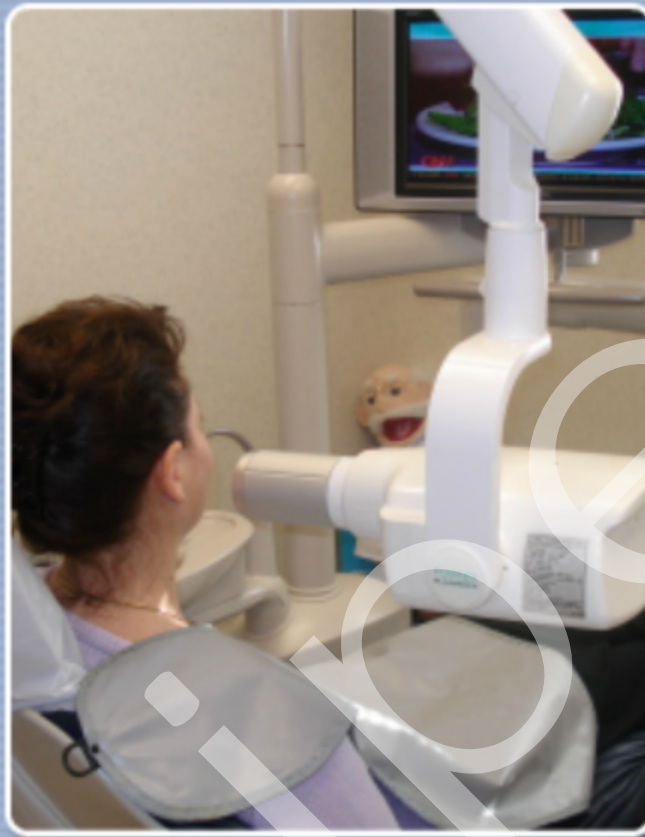
- Light, surface reflectivity and volume transparency

Shadows detection like x-ray tomography



History of Imaging Technology

The 6 Modalities



◀ Prev

◀ Start Over

X-Ray

Emits a beam of radiation to penetrate tissue and gave birth to medical imaging in the late 1800's.

Limitations in dentistry include low resolution and inability to image soft tissue.

1
OCT

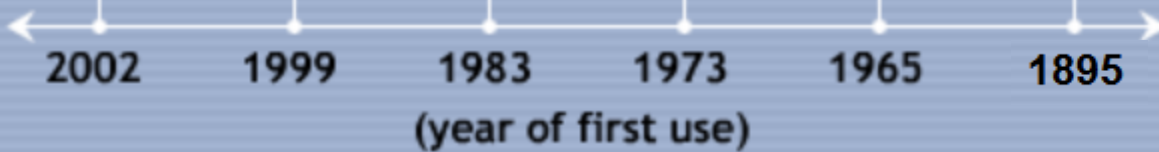
2
PET Scan

3
MRI

4
CT Scan

5
Ultrasound

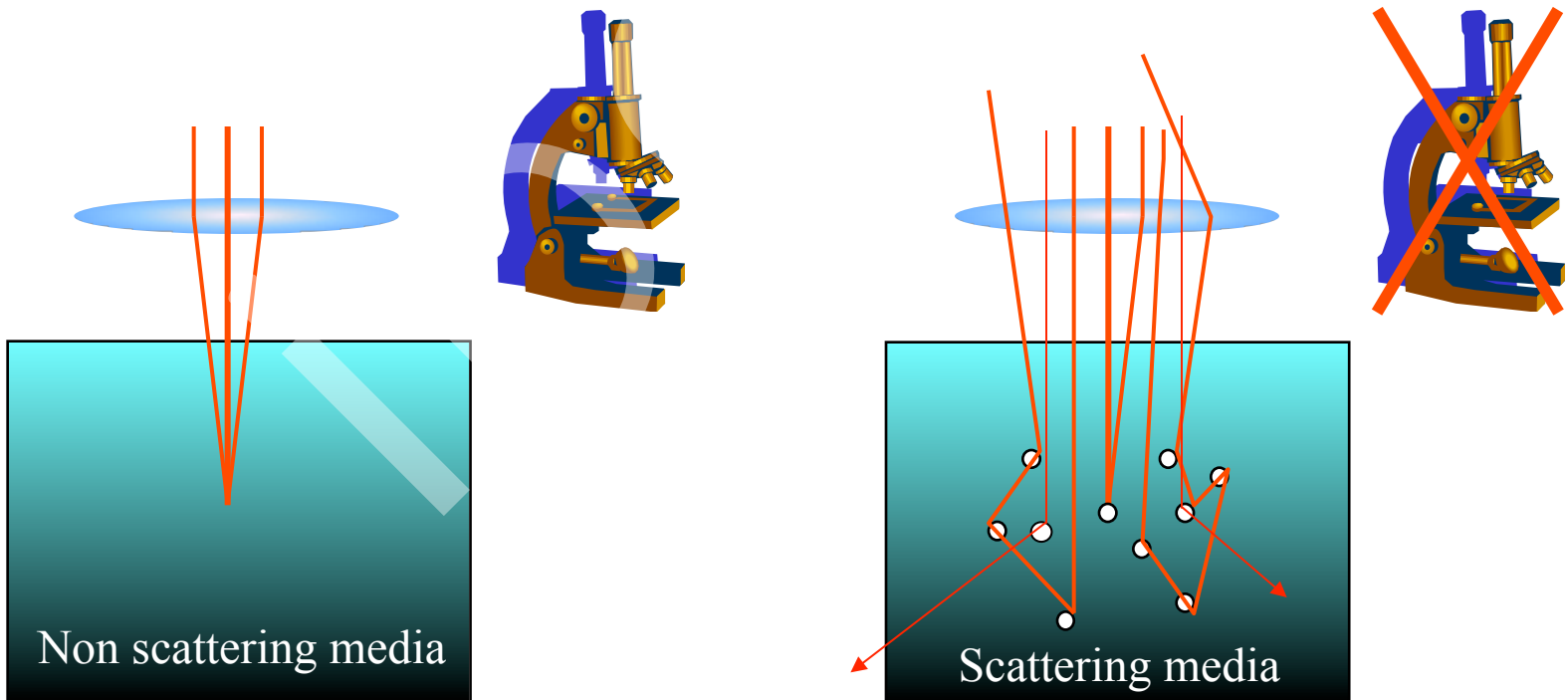
6
X-Ray



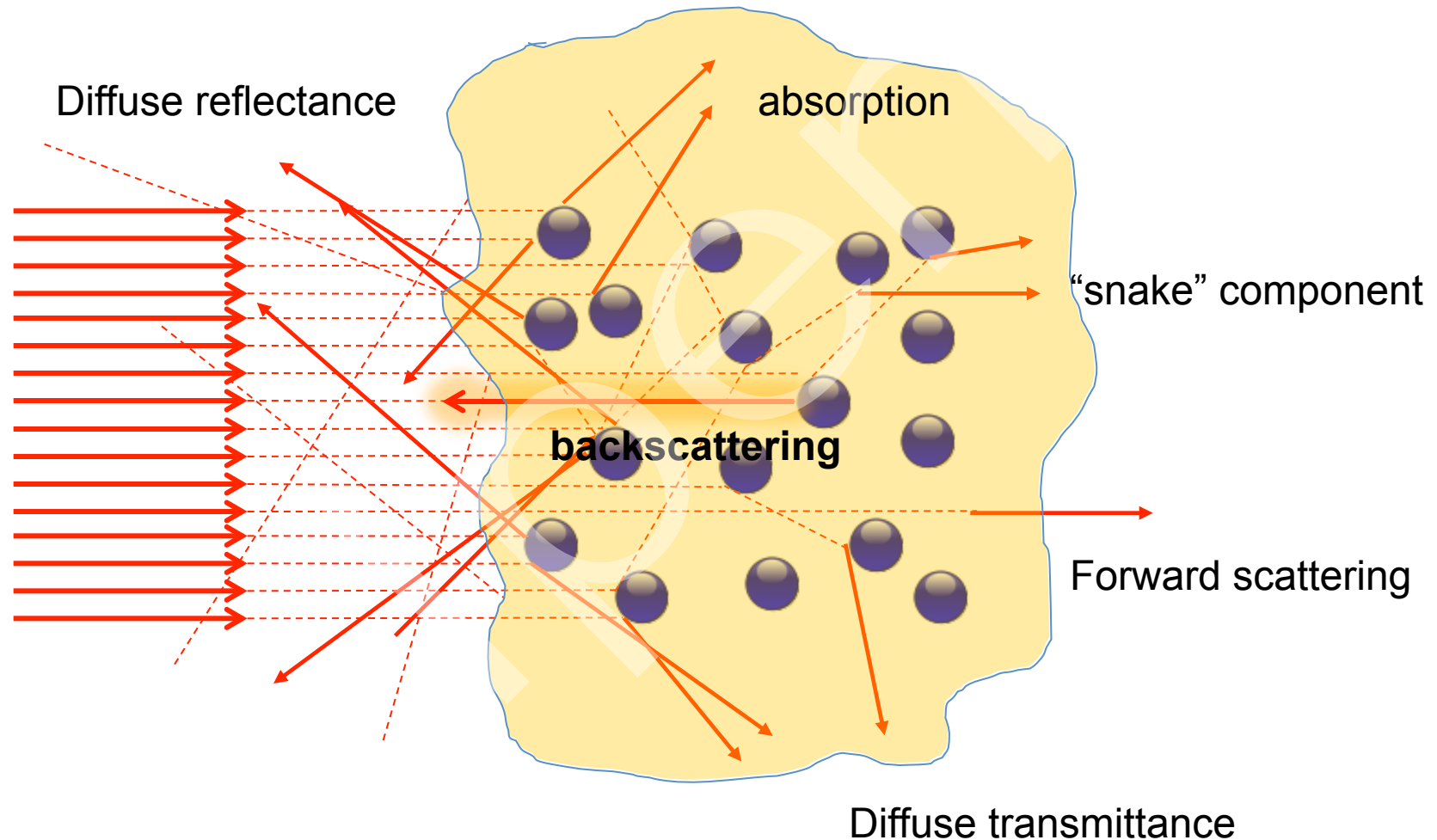
Light Propagation in scattering media

Image a scattering media

Scattering of photons destroys image quality

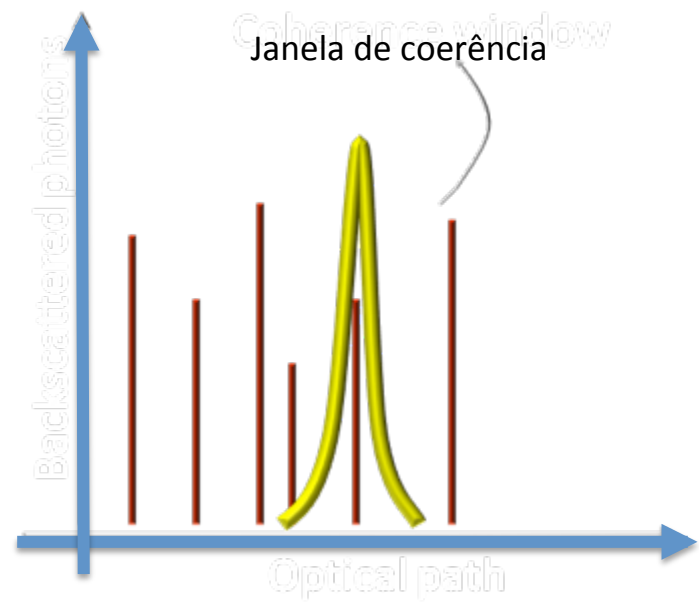
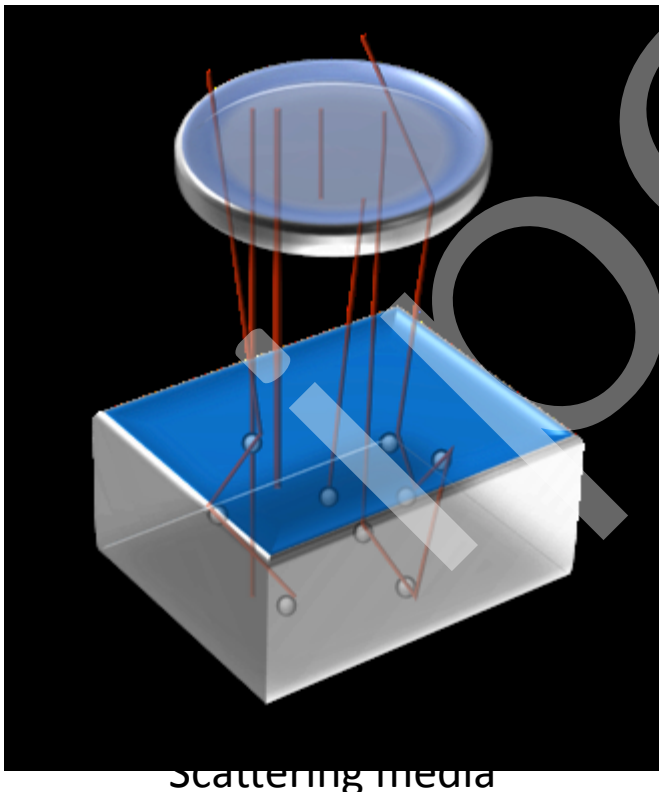


Light Propagation in scattering media

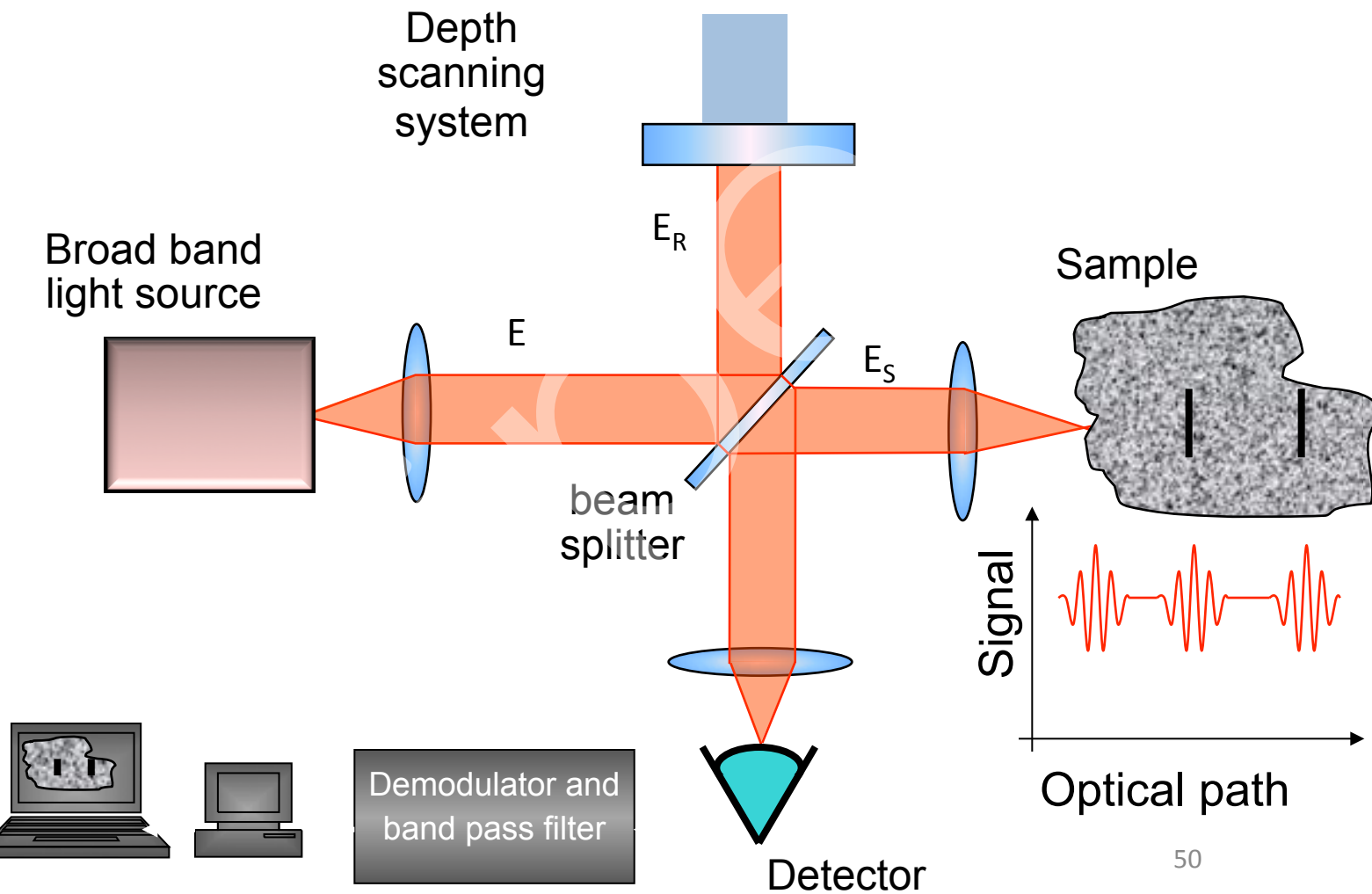


Optical coherence tomography

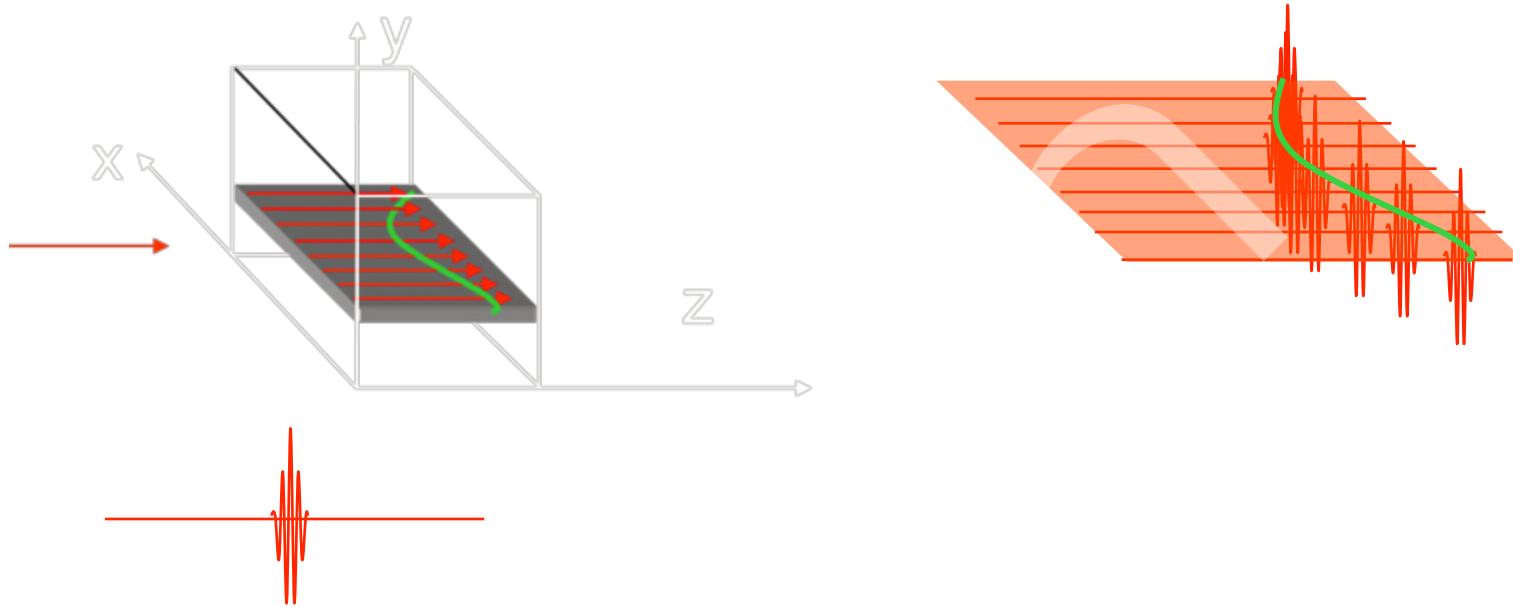
- Noninvasive diagnostic technique
 - coherence window
 - only the ballistic photons are detected



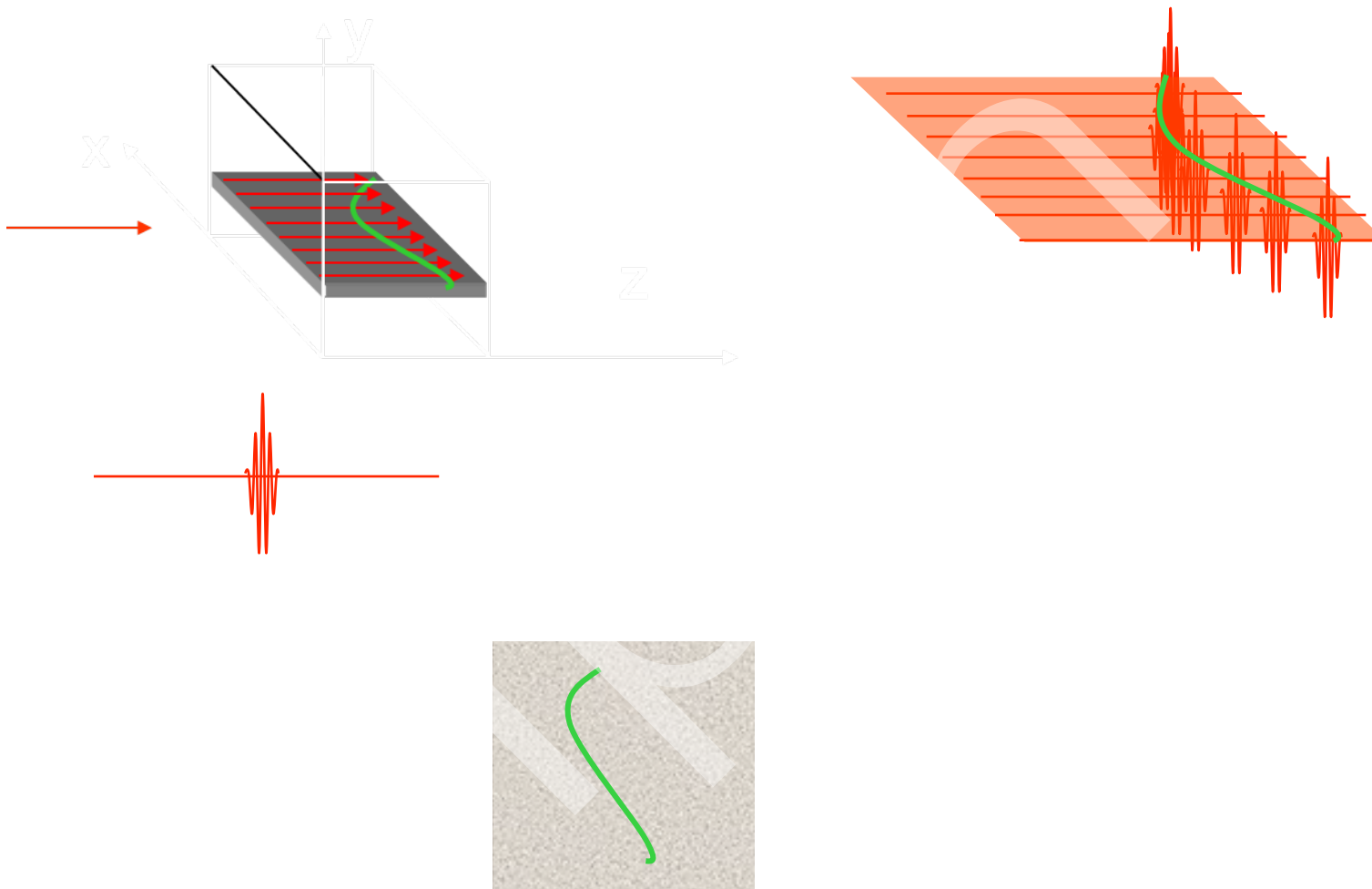
Optical coherence tomography Michelson interferometer



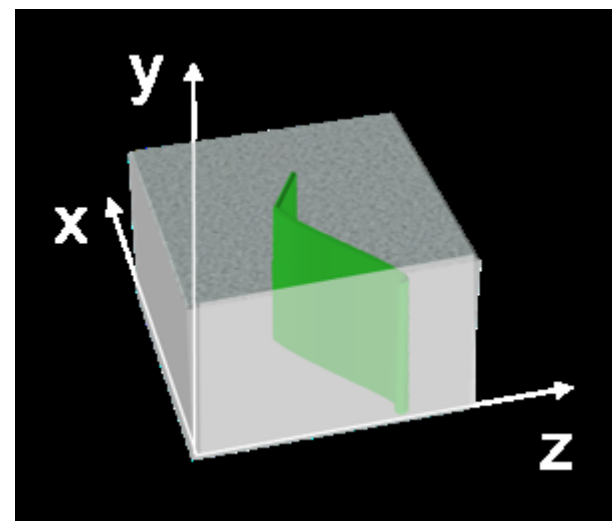
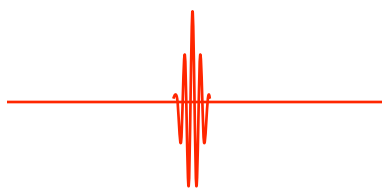
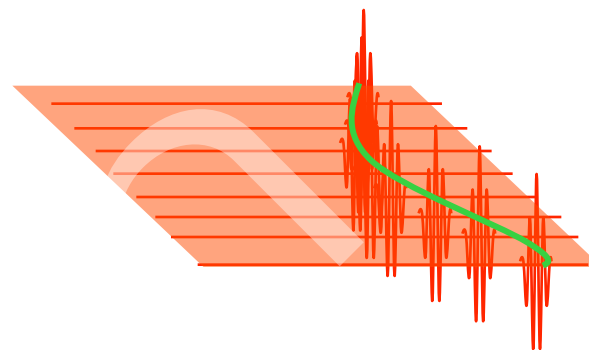
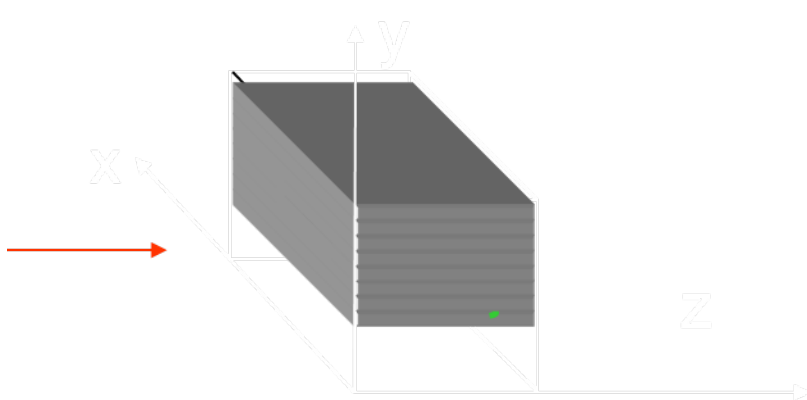
Scanning protocol for OCT imaging



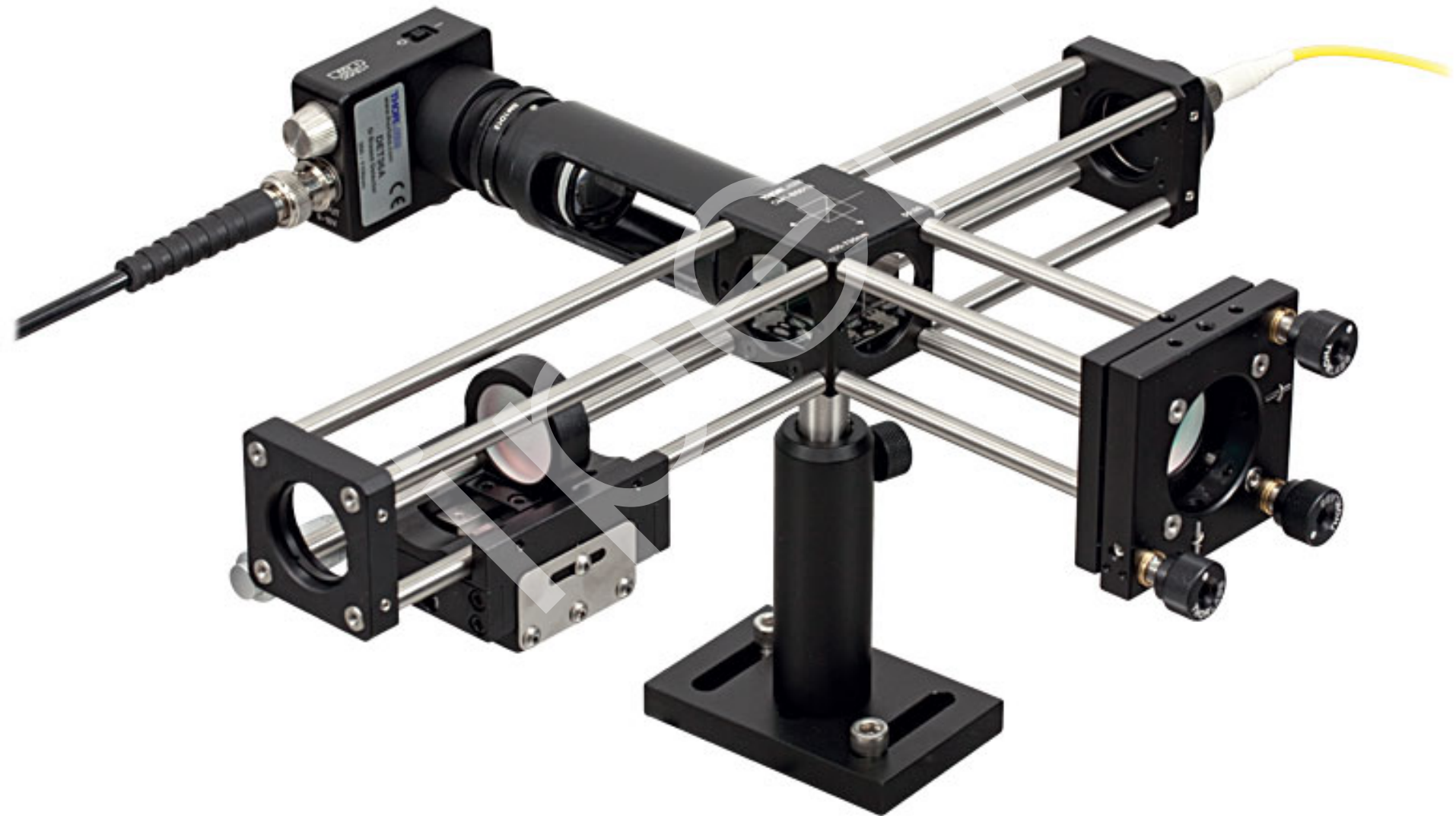
Scanning protocol for OCT imaging



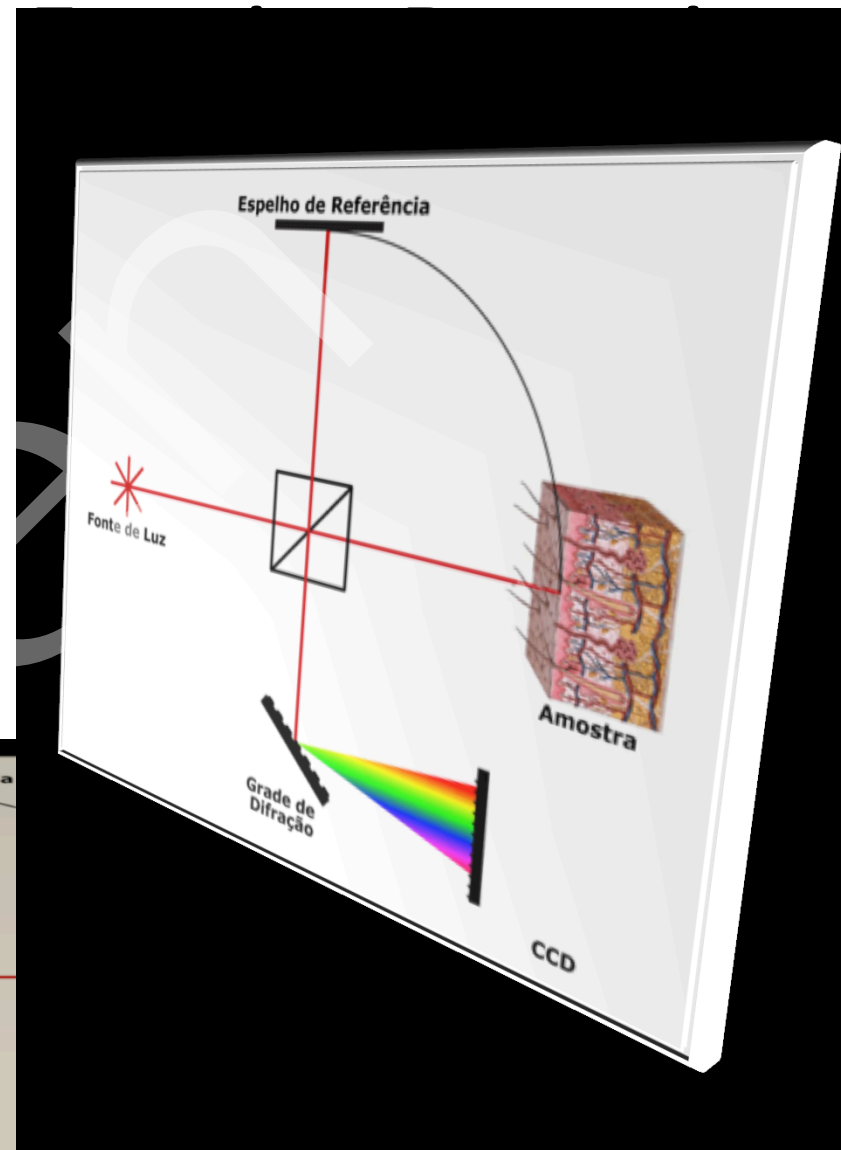
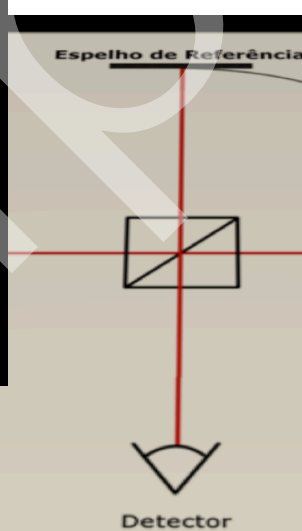
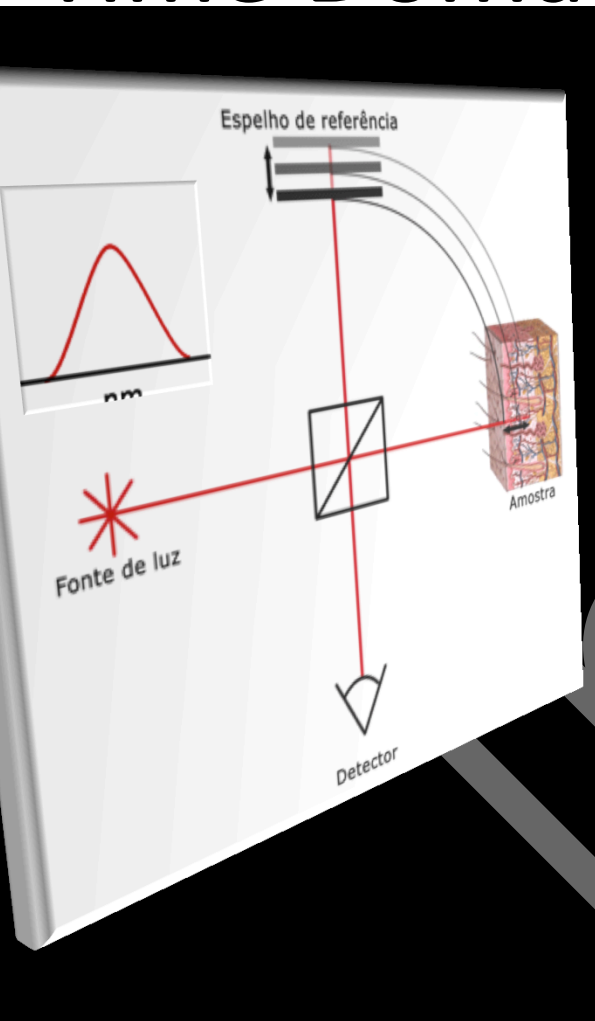
Scanning protocol for OCT imaging



OCT – How it works



Time Domain and



OCT

Systems

Time domain

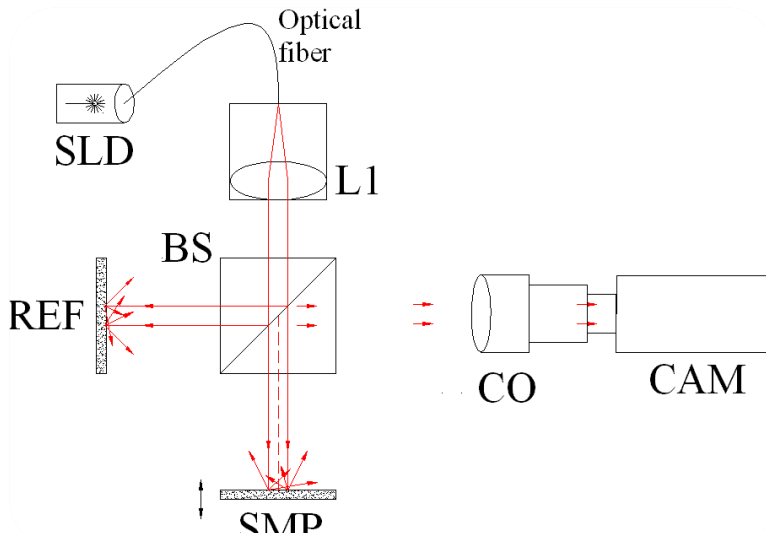


Fig. 1 Full-field OCT optical setup. Components include: super-luminescent diode (SLD), convex lens (L1), 50/50 beamsplitter (BS), camera objective (CO), CMOS-DSP camera (CAM), reference (REF) and sample (SMP). The camera functions as a two-dimensional detector array, and with the OCT technique facilitating scanning in

$$E_i = A_i(\omega) e^{-i(2\beta(\omega)l_{\text{sample}} + \phi(\omega))} = \underbrace{|A_i(\omega)|^2}_{DC \text{ component}} + \underbrace{S(\omega)e^{-\Delta\varphi(\omega)}}_{AC \text{ component}} \frac{d\omega}{2\pi}$$

Axial resolution: $\Delta l_{FWHM} = \frac{2 \ln 2}{\pi} \frac{\lambda_0^2}{\Delta\lambda}$

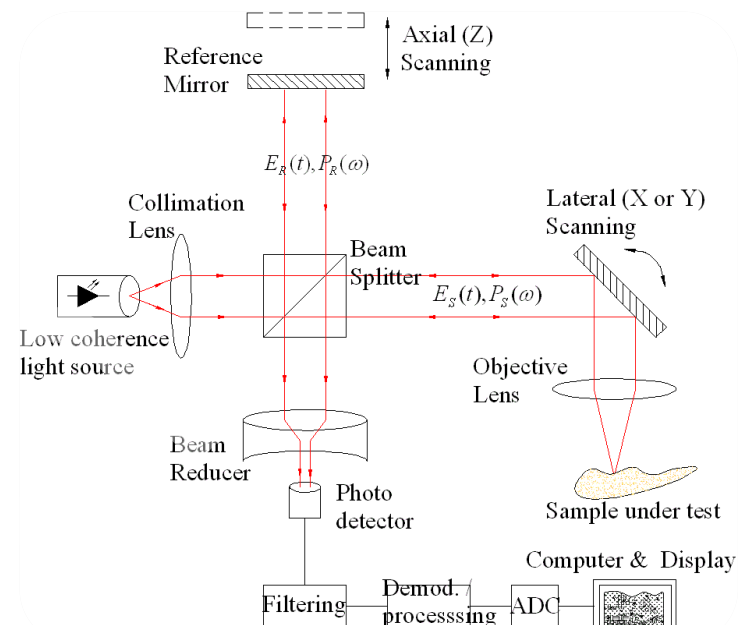
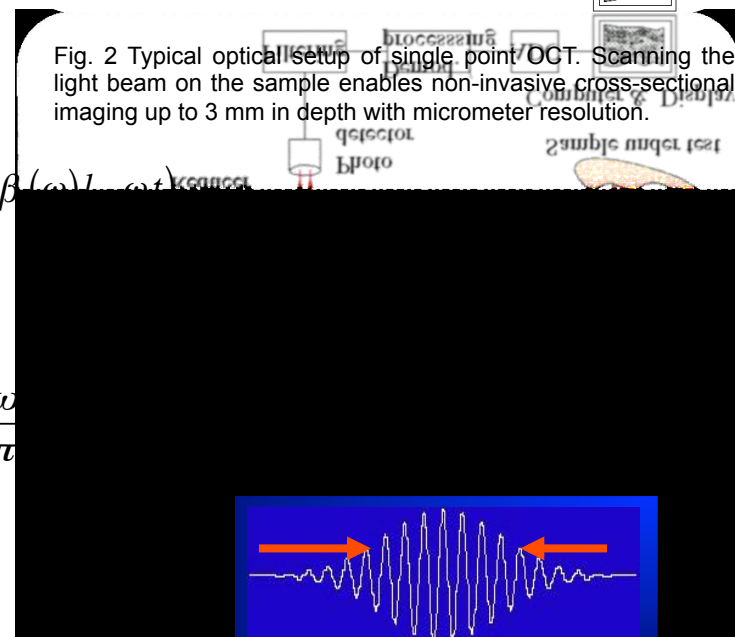


Fig. 2 Typical optical setup of single point OCT. Scanning the light beam on the sample enables non-invasive cross-sectional imaging up to 3 mm in depth with micrometer resolution.



Coherence length

OCT

Systems

Spectral domain

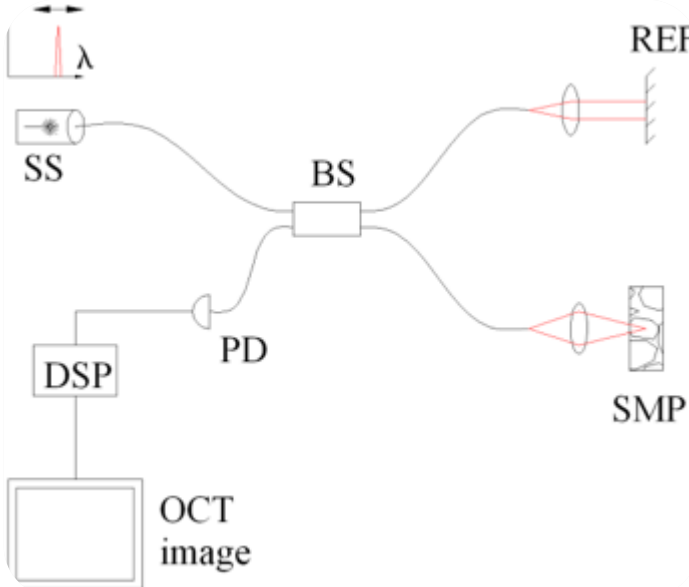


Fig. 3 Spectral discrimination by swept-source OCT. Components include: swept source or tunable laser (SS), beamsplitter (BS), reference mirror (REF), sample (SMP), photodetector (PD), digital signal processing (DSP)

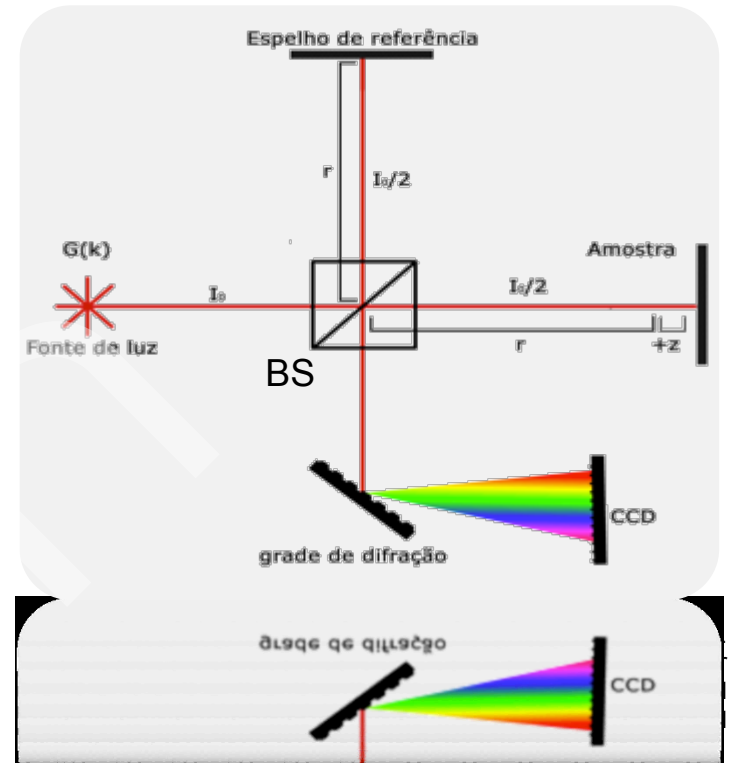
$$I(k) = |A_{r(k,r)} + A_{s(k,r,z)}|^2$$

$$I(k) = \left(\frac{G(k)}{2} \right)^2 \left(1 + 2 \int_{z_0}^{\infty} A_s(z) \cos(2knz) dz + \int_{z_0}^{\infty} \int_{z_0}^{\infty} A_s(z) A_s(z') e^{i2kn(z-z')} dz dz' \right)$$

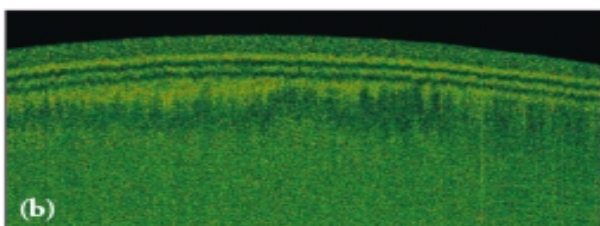
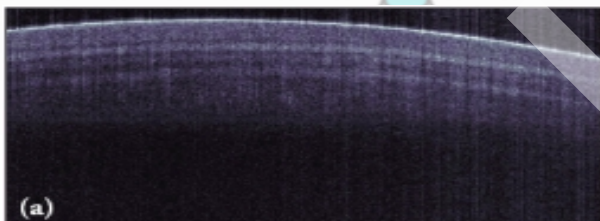
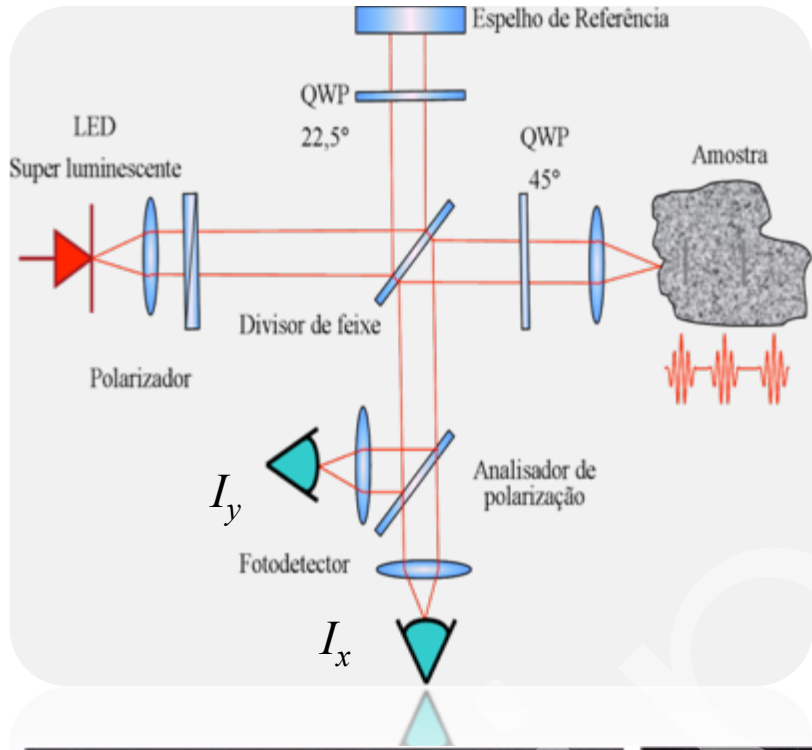
$$A_r(k) =$$

$$A_s(k) =$$

$$\Im_z^{-1}[I(K)] = \Im_z^{-1} \left[\left(\frac{G(k)}{2} \right)^2 \right] \otimes \left([\delta(z)] + \frac{1}{2} \hat{A}_s(z) + \frac{1}{8} AutCorr(\hat{A}_s(z)) \right)$$



PS-OCT



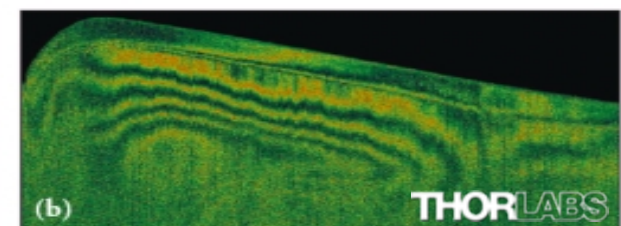
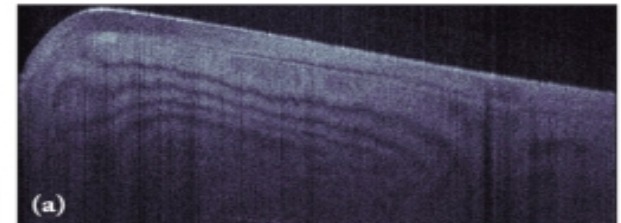
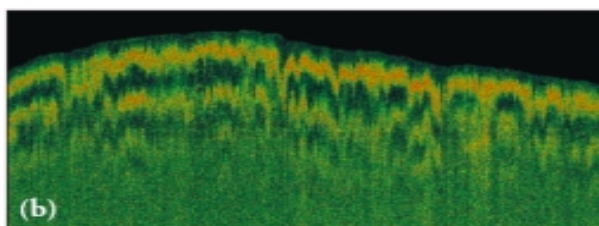
Phase delay
Birefringence media

$$\delta = \frac{2\pi \Delta n z}{\lambda}$$

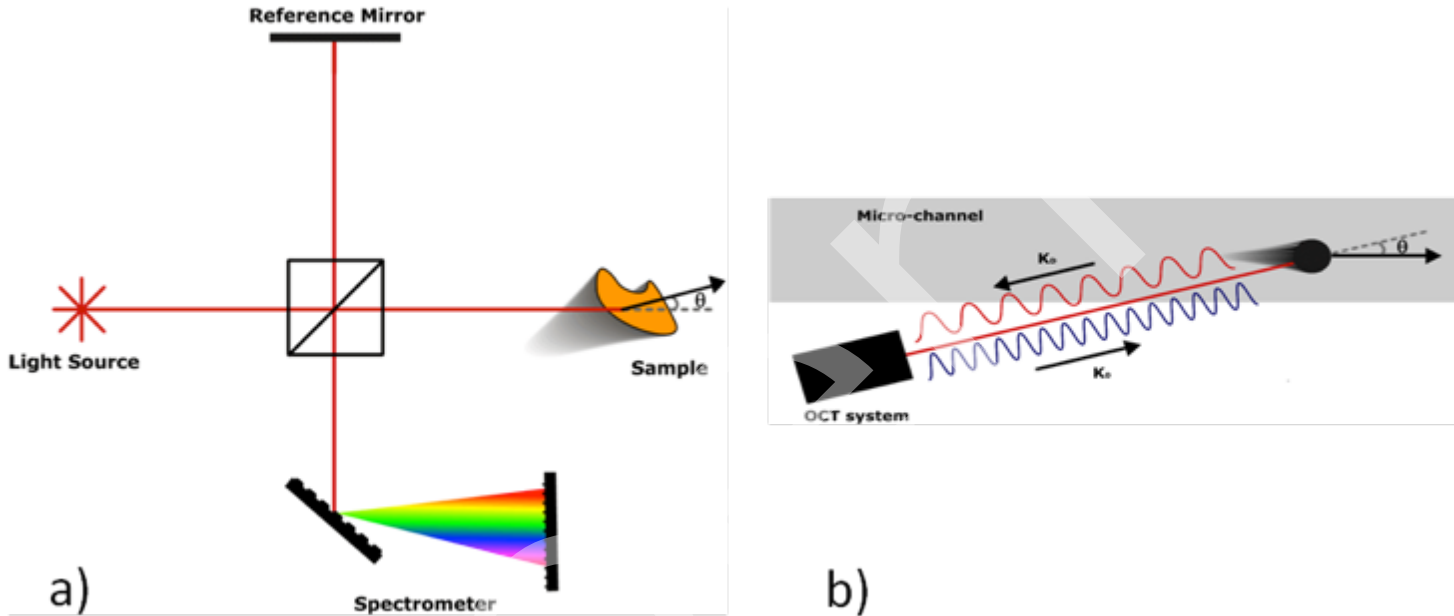
$$\langle \vec{I}(z) \rangle = \left\langle \vec{I}_r \right\rangle + \left\langle \vec{I}_s \right\rangle + \begin{pmatrix} E_{rx}^* E_{sx}(\Delta z) \\ E_{ry}^* E_{sy}(\Delta z) \end{pmatrix} + \begin{pmatrix} E_{rx} E_{sx}^*(\Delta z) \\ E_{ry} E_{sy}^*(\Delta z) \end{pmatrix}$$

$$I_x(z) = R(z) \sin^2 \left(\frac{2\pi}{\lambda_0} z \Delta n \right), \quad I_y(z) = R(z) \cos^2 \left(\frac{2\pi}{\lambda_0} z \Delta n \right)$$

Phase function $\Phi(z) = \arctan \left(\sqrt{\frac{I_x(z)}{I_y(z)}} \right) = \frac{2\pi}{\lambda_0} z \Delta n$



Doppler-OCT



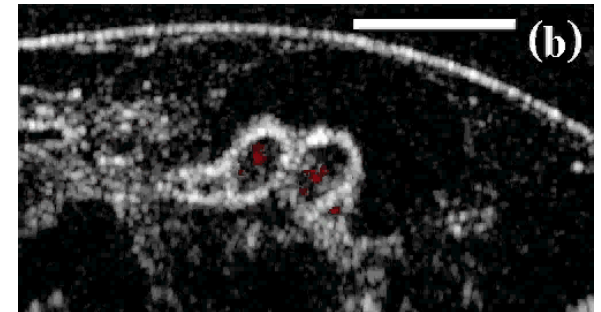
$$\tilde{i}_D(z'') = \text{Re}[\tilde{I}_D(z'')] + i\text{Im}[\tilde{I}_D(z'')] = |\tilde{i}_D(z'')| e^{i\phi(z'')} \quad (30)$$

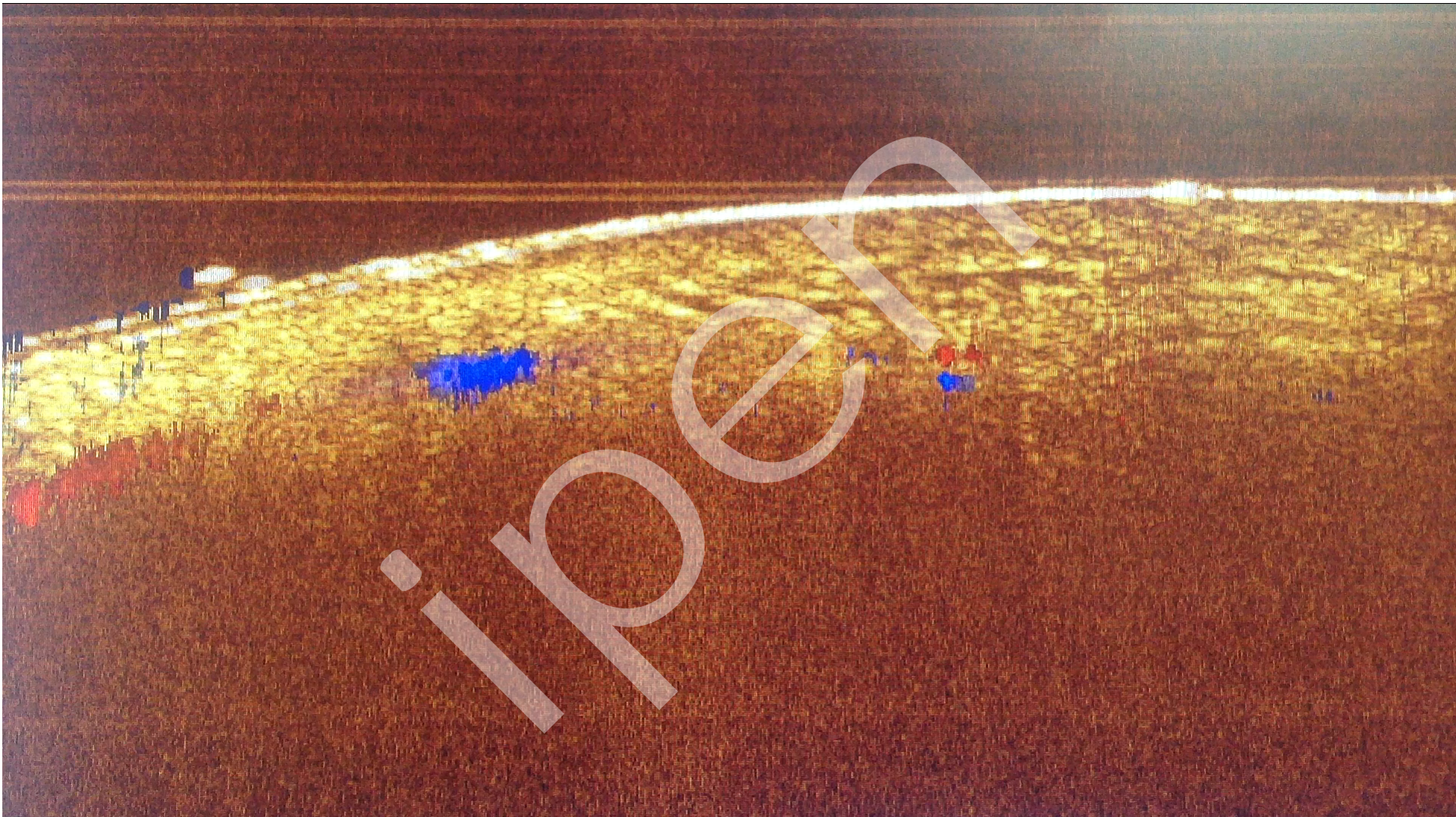
The phase of this complex function is the phase information of each A-scan described as:

$$\phi(z'') = \arctan \left\{ \frac{\text{Im}[\tilde{i}_D(z'')]}{\text{Re}[\tilde{i}_D(z'')]} \right\}$$

the phase shift $\Delta\phi(z'')$ can be used to obtain the Doppler velocity.

$$V_D = \frac{\Delta\phi(z'')}{T 4\pi k_0 n(k_0) \cos\theta}$$





iReer

Ophthalmology

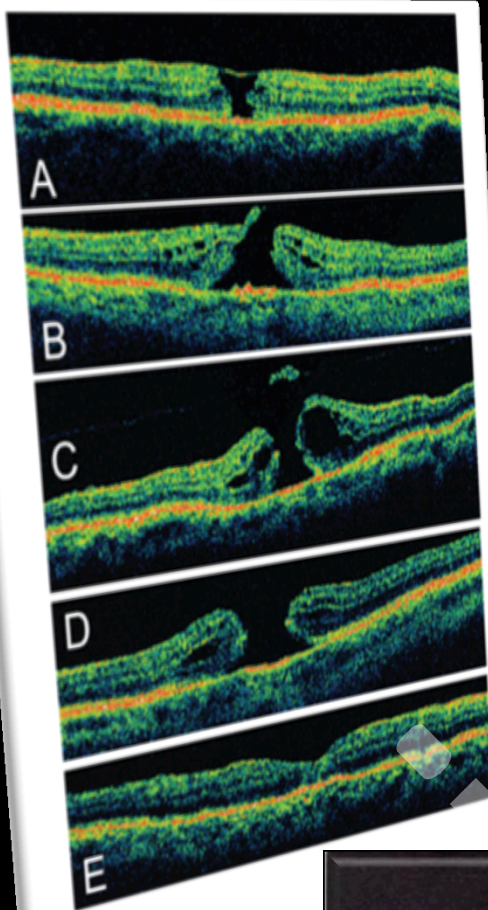
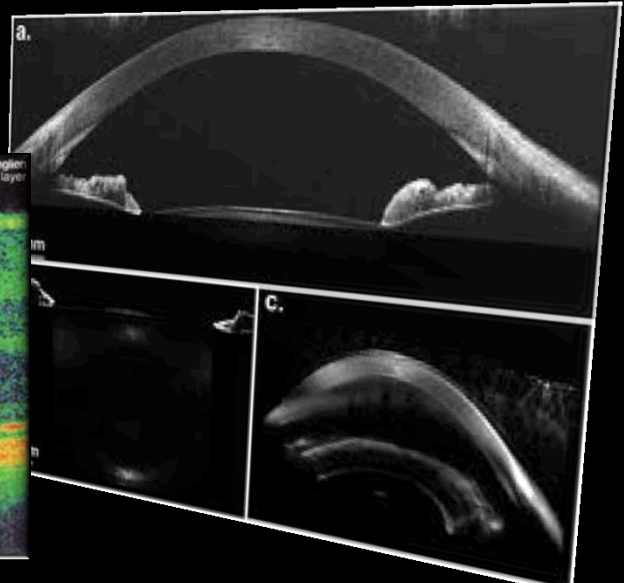
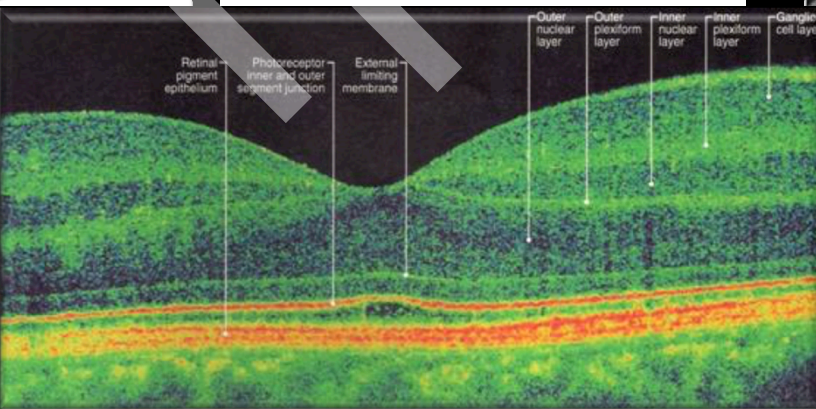


Figure 2. Stages of macular hole as seen on tomography. A) Stage 1B occult hole, visible operculum lifts, the hole goes to stage 2 on clinical examination, vision 20/70. C) The hole is separated from the retina in this stage. D) The macular hole is stage 4 when the vision is 20/200. E) Two months after surgery and face-down positioning, the hole has closed and the vision has improved to 20/30.

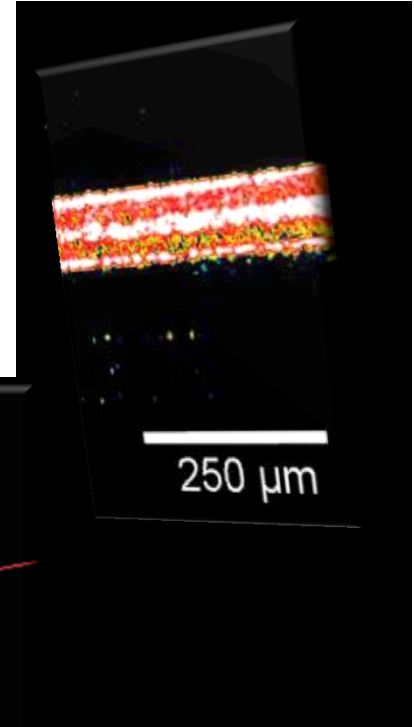
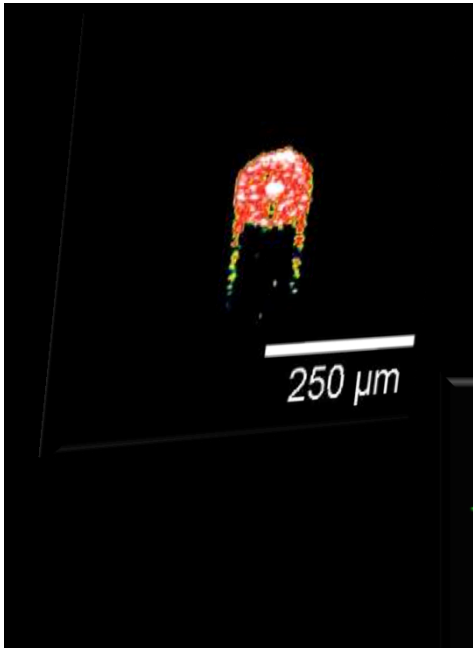


A dark, irregularly shaped object with a mottled texture, appearing to be a piece of debris or a small rock, set against a solid black background.

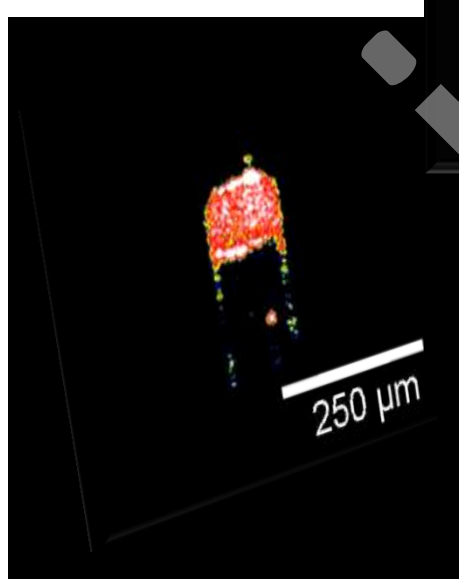
iopen

Hair fiber characteristics and methods to evaluate hair physical and mechanical properties

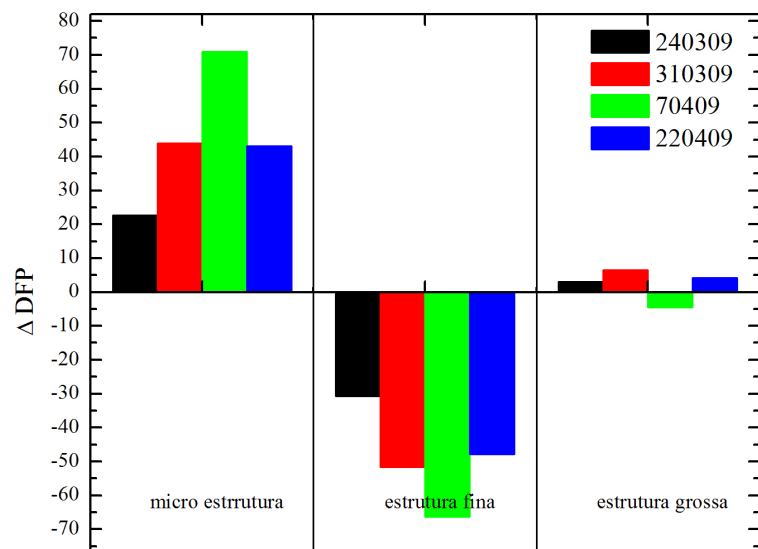
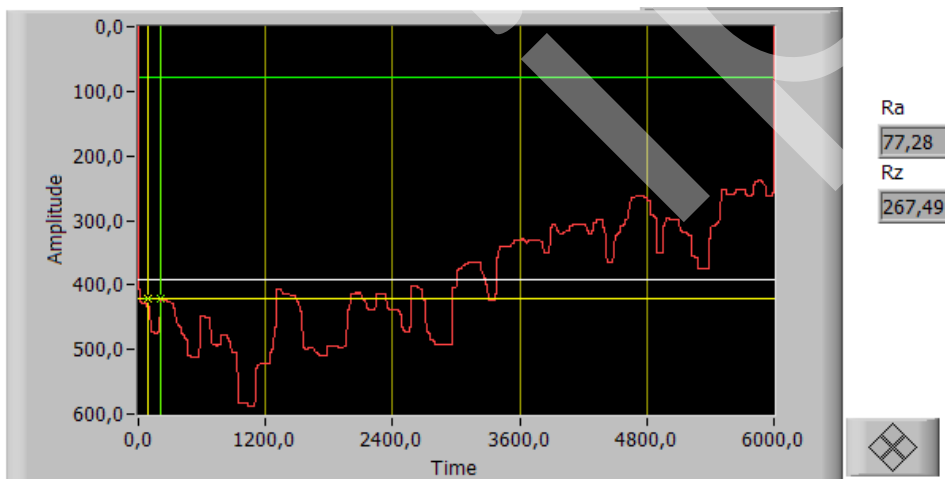
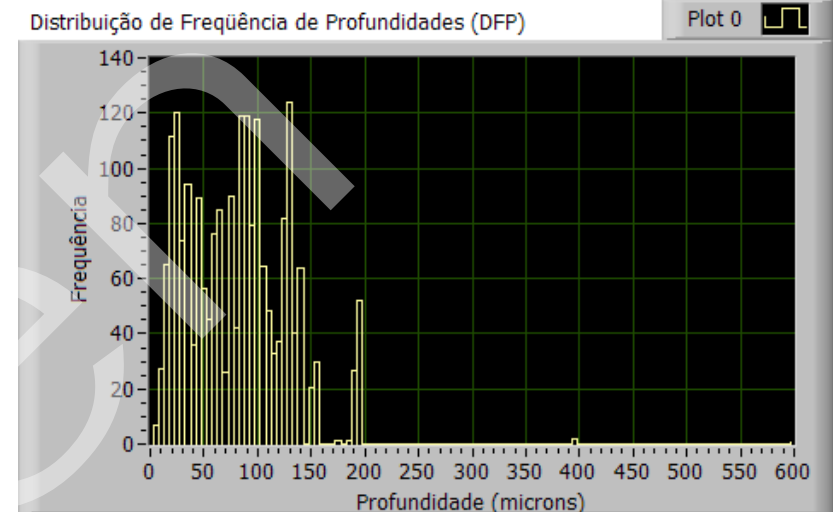
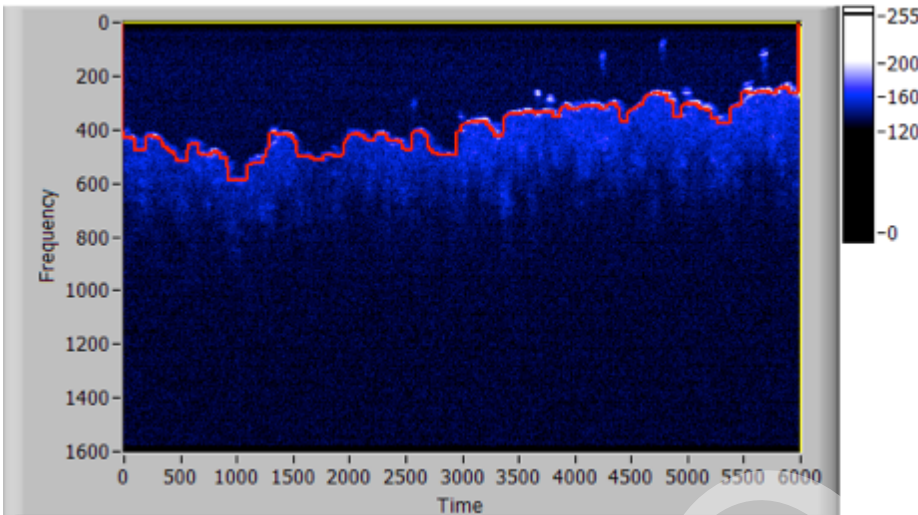
Standard Afro-Ethnic hair



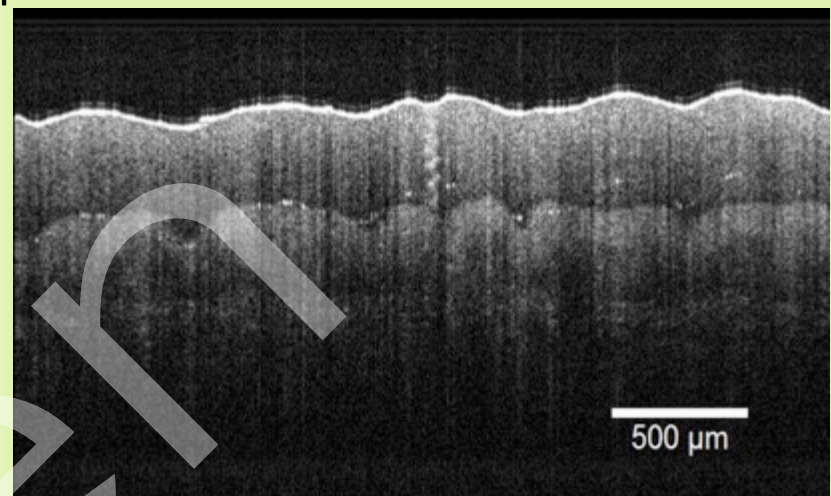
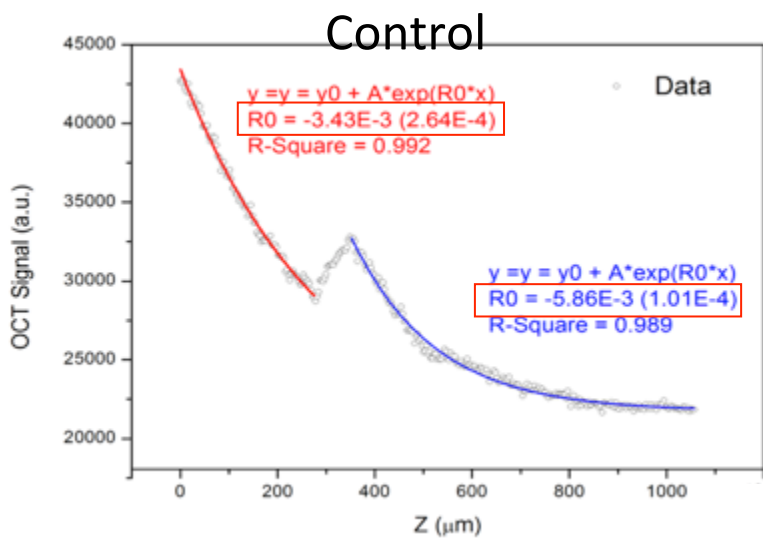
After chemical treatment



Dermatology

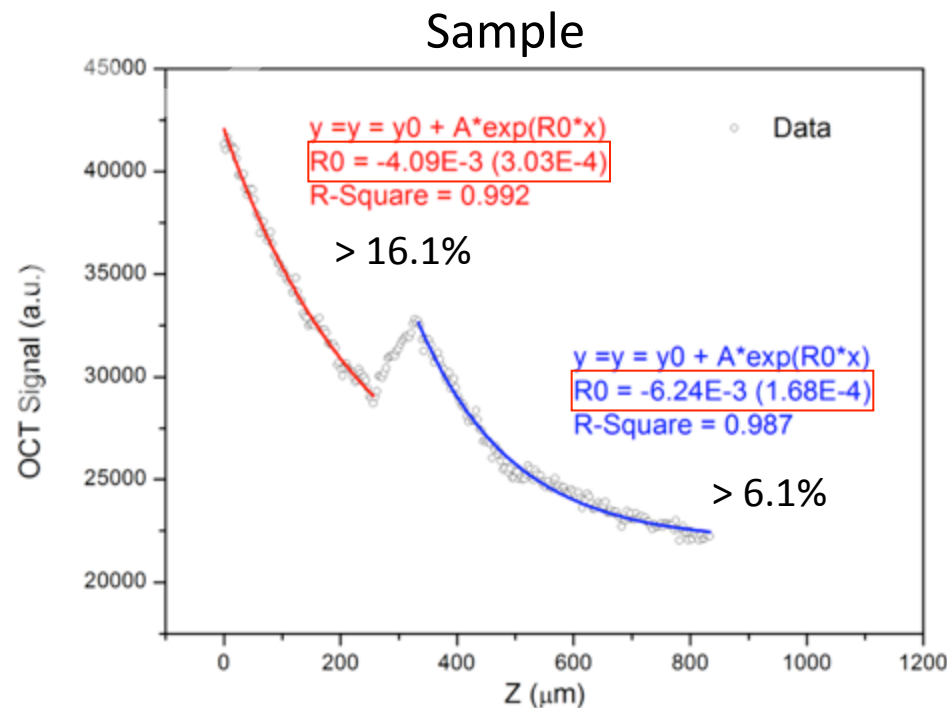
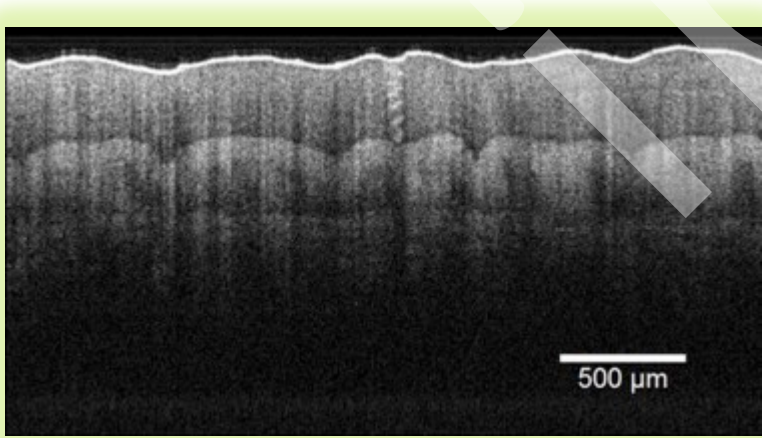


Enhancement of optical coherence tomography images and by gold nanoparticles in skin

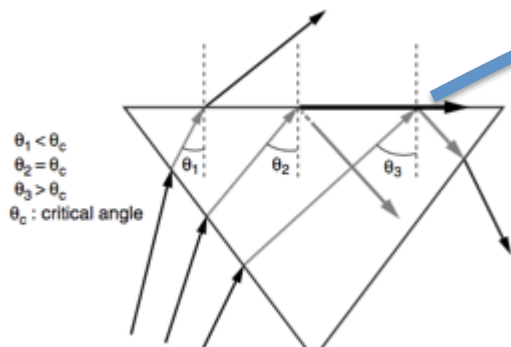


Extinction coefficient

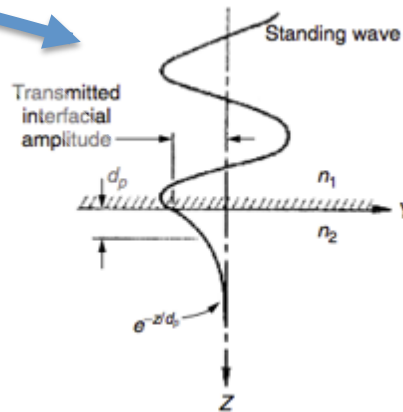
$$\mu_t = \mu_a + \mu_s$$



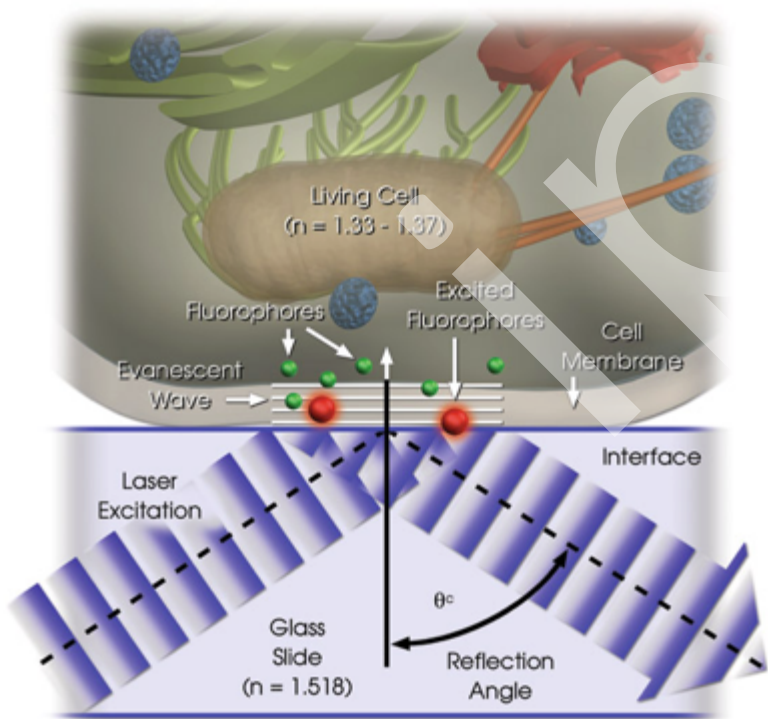
TOTAL INTERNAL REFLECTION FLUORESCENCE MICROSCOPY



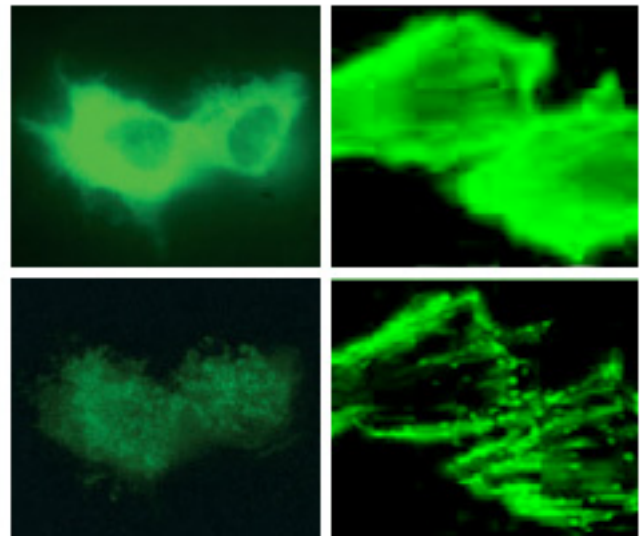
Principles of internal reflection



Total Internal Reflection Fluorescence

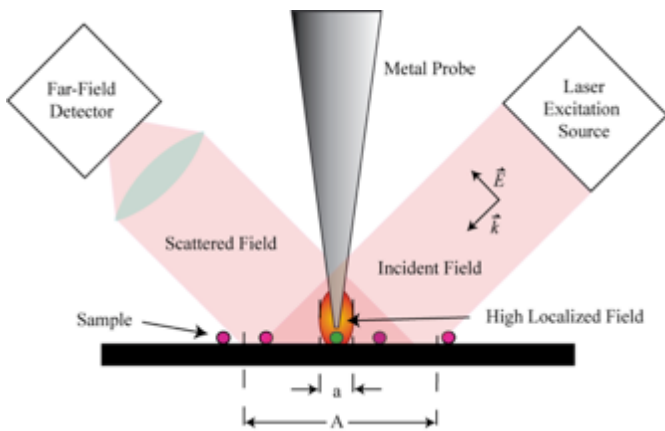
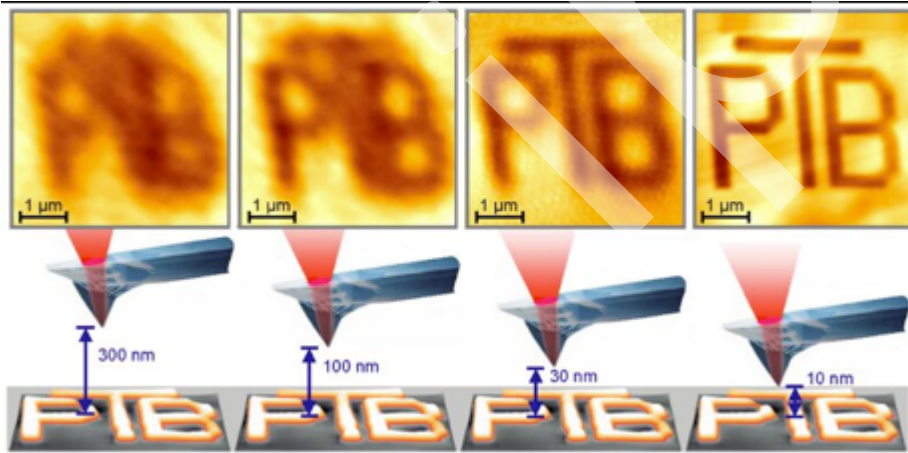
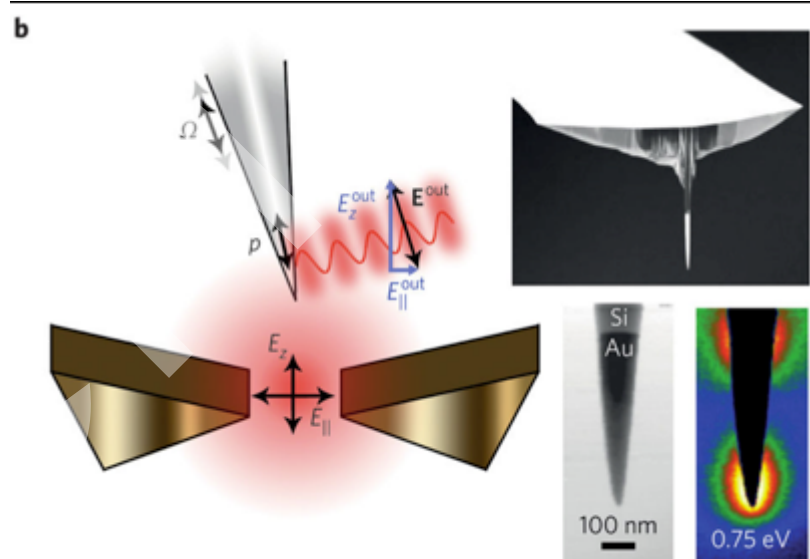
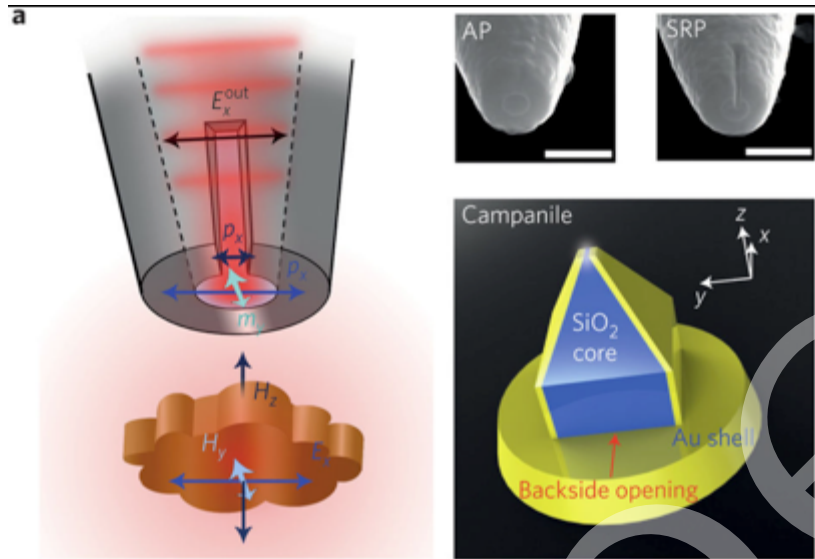


Widefield
Fluorescence



TIRF

NEAR-FIELD OPTICAL MICROSCOPY

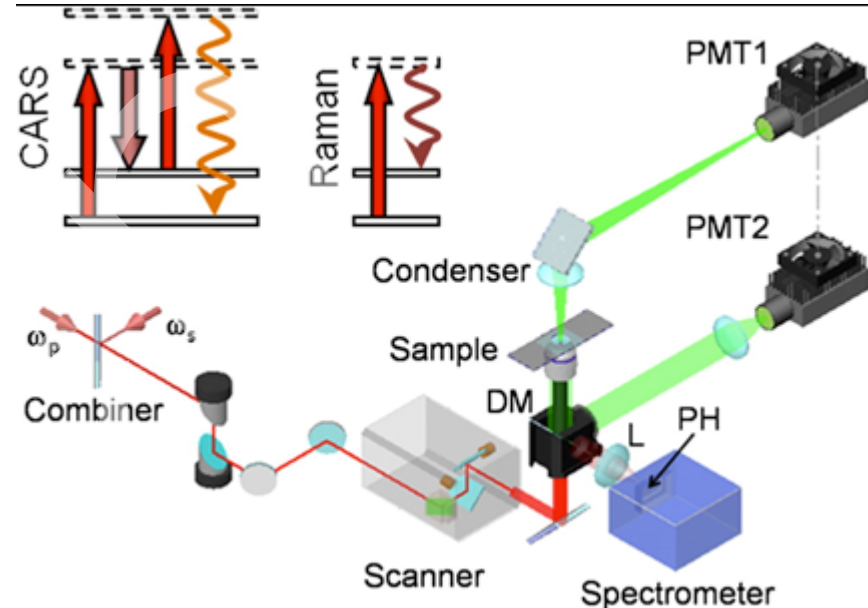
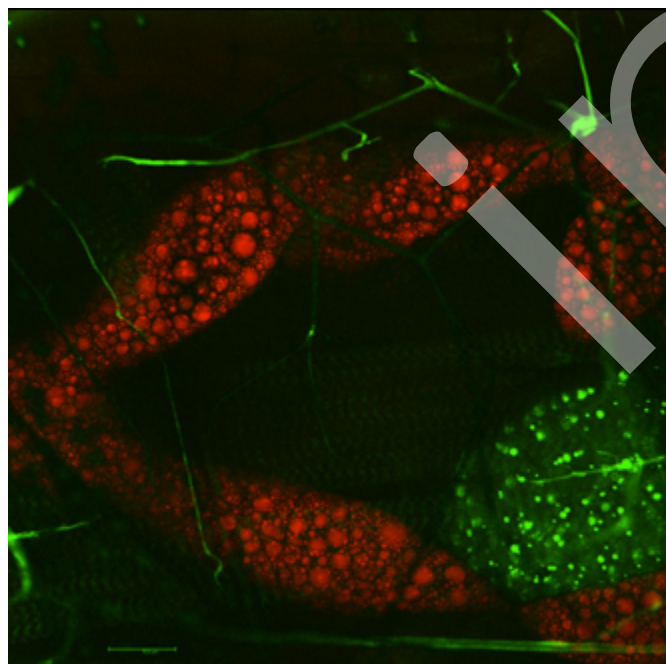


Coherent Anti-Stokes Raman Scattering (CARS) Microscopy

Coherent anti-Stokes Raman scattering (abbreviated as CARS) is a third-order nonlinear optical process that can produce a vibrational transition.

For CARS, two optical beams of frequencies ω_p and ω_s interact in the sample to generate an anti-Stokes optical output at $\omega_c = \omega_p - \omega_s$ in the phase-matched direction (a specific direction). The signal has an electronic contribution (from the electronic third-order nonlinear optical response), but is resonantly enhanced if $\omega_p - \omega_s$ coincides with the frequency of a Raman active molecular vibration (see Chapter 4).

The molecular vibration involved in a CARS signal enhancement can then be used as a contrast mechanism for bioimaging.

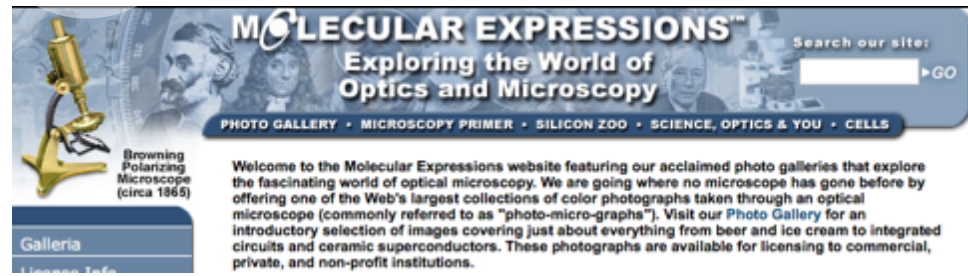
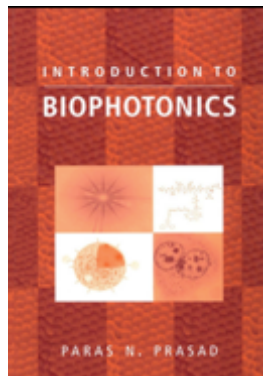


CARS (Coherent Anti-Stokes Raman Scattering) microscopy is a dye-free method which images structures by displaying the characteristic intrinsic vibrational contrast of their molecules. The crucial advantage of this method is that the sample remains almost unaffected.

Thank you

for your attention

freitas.az@ipen.br



<https://micro.magnet.fsu.edu>



MINISTÉRIO DA
CIÊNCIA, TECNOLOGIA,
INOVAÇÕES E COMUNICAÇÕES

